

KINETICS OF THE ADDITION OF HYDROXYL RADICALS TO POLYALKYLATED BENZENES IN THE GAS PHASE

A dissertation submitted to
FACULTY OF BIOLOGY, CHEMISTRY AND GEOSCIENCES
AT THE UNIVERSITY OF BAYREUTH, GERMANY

to attain the academic degree of

DR. RER. NAT.

presented by

PAULO CESAR ALARCON GARCIA

Dipl. Chem.

born 26 March 1982

in Caracas, Venezuela

Bayreuth, Mai 2015

**To my beloved parents:
Pablo Alarcón und Luz de Alarcón**

*„You will teach them to fly, but they won't fly your flight.
You will teach them to dream, but they won't dream your dreams.
You will teach them to live, but they won't live your life.
However, in each flight, in each life, in each dream
the imprint of the path you laid down will last.”*

Mother Teresa of Calcutta

KINETICS OF THE ADDITION OF HYDROXYL RADICALS TO POLYALKYLATED BENZENES IN THE GAS PHASE

Supervisor: Prof. Dr. Cornelius Zetsch

Die vorliegende Arbeit wurde ab März 2009 bis Mai 2015 in Bayreuth an der Forschungsstelle für Atmosphärische Chemie unter Betreuung von Herrn Prof. Dr. Cornelius Zetzsch angefertigt.

Vollständiger Abdruck der von der Fakultät für Biologie, Chemie und Geowissenschaften der Universität Bayreuth genehmigten Dissertation zur Erlangung des akademischen Grades eines Doktors der Naturwissenschaften (Dr. rer. nat).

Dissertation eingereicht am: 08.06.2015

Zulassung durch die Prüfungskommission: 03.07.2015

Wissenschaftliches Kolloquium: 26.01.2016

Amtierender Dekan: Prof. Dr. Stefan Schuster

Prüfungsausschuss:

Prof. Dr. Cornelius Zetzsch (Erstgutachter)

Prof. Dr. Andreas Held (Zweitgutachter)

Prof. Dr. Carl Beierkuhnlein (Vorsitz)

Prof. Dr. Carlo Unverzagt

CONTENTS

DEDICATORY	i
CONTENTS	iv
LIST OF MANUSCRIPTS	v
ACKNOWLEDGMENTS	vi
SUMMARY	vii
ZUSAMMENFASSUNG	viii
1 INTRODUCTION	1
1.1 OH-radical reaction with alkylated aromatic compounds.....	1
1.2 Objectives of the PhD Thesis	3
2. EXPERIMENTAL	4
3. DATA EVALUATION	9
3.1 Reaction mechanisms	9
3.2 Biexponential model ($k_{12a}, k_{12} = 0$)	11
3.2 Triexponential model ($k_{12} = 0$)	15
3.3 Extended triexponential model ($k_{12a} = 0$)	17
4. EXPERIMENTAL RESULTS AND DISCUSSION	19
4.1 Vapour pressure	19
4.2 Goodness of fit.....	20
4.3 Global rate constant (k_{OH}).....	21
4.4 Stability and formation yields of the adducts.	25
4.5 Equilibrium constants and thermodynamics of the adducts.	31
4.6 Dealkylation of OH-aromatic adducts.	36
5 CONCLUSIONS	37
REFERENCES	39
APPENDIX A. Individual contributions to the joint publications.....	42
APPENDIX B. Paper A: Alarcon et al. (2013)	45
APPENDIX C. Paper B: Alarcon et al. (2014)	55
APPENDIX D. Paper C: Alarcon et al. (2015)	67
Erklärung	90

LIST OF MANUSCRIPTS

The thesis is presented in cumulative form consisting of three manuscripts published in peer-reviewed journals.

Published manuscripts:

Paper A: Alarcón, P., Strekowski, R., Zetzsch, C., 2013. Reversible addition of the OH radical to p-cymene in the gas phase: kinetic analysis assuming formation of a single adduct. Part 1. Phys. Chem. Chem. Phys., 15, 20105-20114

Paper B: Alarcón, P., Bohn, B., Zetzsch, C., Rayez, M. T., Rayez, J. C., 2014. Reversible addition of the OH radical to p-cymene in the gas phase: multiple adduct formation. Part 2. Phys. Chem. Chem. Phys., 16, 17315-17326

Paper C: Alarcón, P., Bohn, B., Zetzsch, C., 2015. Kinetic and mechanistic study of the reaction of OH radicals with the methylated benzenes: 1,4- dimethyl-, 1,3,5-trimethyl, 1,2,4,5-, 1,2,3,5-, and 1,2,3,4-tetramethyl-, pentamethyl- and hexamethylbenzene. Phys. Chem. Chem. Phys., 17, 13053-13065

ACKNOWLEDGMENTS

First and foremost, I would like to thank God, whose many blessings and guidance have brought me to this country to accomplish this difficult task.

I am very grateful to my supervisor Prof. Cornelius Zetzsch for his guidance, support, encouragement and the advice he provided throughout these years, and also for his understanding during some difficult personal situations.

I must express my gratitude to Dr. Birger Bohn for his patience, guidance and fruitful discussions during the publication-writing phase.

Furthermore, I am grateful to Dr. Marie- Thérèse Rayez and Dr. Jean-Claude Rayez for expanding my knowledge in theoretical calculations and to Dr. Roger Atkinson for his collaboration with my work by studying the abstraction channel of the p-Cymene reaction and the rate constant of some methylated aromatics.

I would like to thank my co-workers and colleagues from the Atmospheric Chemistry Research Laboratory in Bayreuth for their support during these years: Agnes Bednorz, and Dres. Katharina Kamilli, Matthias Sörgel, Johannes Ofner, Stefan (Nino) Gonser, Sergej Bleicher, Natalja Balzer, Joelle Buxmann, Julian Wittmer and Andreas Held. Furthermore I would like to thank Heinz-Ulrich (Uli) Krüger († Feb. 2012) for his help in the laboratory and for his “crazy” things that made us laugh.

I am also grateful to the deutsche Forschungsgemeinschaft (DFG) under grant ZE 792/6-1, within the French-German CNRS-INSU/DFG bilateral program ATMOCHEM for the financial support of my work

Last but not least, I would like to thank my wife Sandra for complementing my life and for her support during all these years.

SUMMARY

Until a few years ago it was believed that OH radicals would only add to the aromatic molecule at non-substituted sites and that the *ipso* addition (i.e., addition to a substituted site) was unimportant. However, kinetic studies on hexamethylbenzene indicated that the *ipso* addition was not only possible but can occur much faster than what could be explained by the H-atom abstraction alone. In this work, we investigated a series of alkylated benzenes with two to five substituents, using flash photolysis of water vapour for production of OH radicals and resonance fluorescence for their time resolved detection. Among these methylated compounds there are three that can form only 2 adducts (ortho at an unoccupied site and ipso at an occupied site): 1,4-dimethylbenzene, 1,3,5-trimethylbenzene, and 1,2,4,5-tetramethylbenzene. For these compounds two different mechanisms were investigated: (i) formation of two adducts by direct addition and (ii) formation of a second adduct by isomerization of the first adduct. For the other methylated compounds: 1,2,3,4-, 1,2,3,5-tetramethylbenzene, and pentamethylbenzene, several adducts are expected, and therefore only the rate constants for the overall reaction were investigated. Moreover, the mechanism for the reaction of the aromatic biogenic p-cymene (4-isopropyl-toluene) with OH radicals was investigated. In this case, theoretical predictions helped to reduce the number of possible adducts from four to two, which allowed applying the two-adduct-formation model. OH rate constants for all the studied aromatics at temperatures between 300 K and 340-360 K, equilibrium constants and formation yields for each adduct, as well as formation entropies and enthalpies were determined. Formed adducts were identified based on thermodynamic data and comparison with published theoretical predictions and experimental results. Nevertheless, it was not possible to determine if the formation of both adducts occurs via direct formation or via isomerization, being more likely that the real mechanism lies between these two extremes.

ZUSAMMENFASSUNG

Addition von OH radikale an aromatischen Moleküle ist seit mehrere Jahrzehnten untersucht worden. Es wurde angenommen dass die Addition nur an freien Stellen des Aromaten stattfindet und die *ipso* Addition (d.h., OH Addition an einer bereits besetzten Stelle) wurde immer vernachlässigt. Jahre später, kinetische Untersuchung des voll besetzten Aromat Hexamethylbenzol haben bewiesen dass die *ipso* Addition nicht nur möglich ist sondern viel schneller verläuft als erwartet nur von der H-atom Abstraktion. Eine Folge von alkylierten Benzolen mit zwischen zwei und fünf Substituenten wurde für diese Arbeit untersucht. OH Radikale wurden mit Wasserdampfphotolyse erzeugt und ihre relative Konzentration wurde mit Resonanzfluoreszenz zeitlich verfolgt. Drei der untersuchten Aromaten können nur zwei Addukte bilden (jeweils ein *ortho* and ein *ipso*): 1,4-Dimethylbenzol, 1,3,5-Trimethylbenzol und 1,2,4,5-Tetramethylbenzol. Für diese drei Substanzen zwei Mechanismen wurden untersucht: (i) Bildung von zwei Addukte aus der direkten Addition und (ii) Bildung von zwei Addukte mit Isomerisierung von einem Addukt in das Andere. Für die Aromaten: 1,2,3,4-, 1,2,3,5-Tetramethylbenzol, and Pentamethylbenzol erwartet man die Bildung mehrerer Addukte und deswegen nur die gesamte Geschwindigkeitskonstante (Abstraktion + Addition) wurde bestimmt. Außerdem, der Mechanismus der Reaktion von OH radikale mit der biogenen Molekül p-Cymol (4-isopropyl-toluol) wurde untersucht. In diesem Fall, theoretische Berechnungen haben ergeben dass nur zwei Addukte eine Rolle spielen und dementsprechend das zwei-Addukte-Modell konnte angewendet werden. OH Geschwindigkeitskonstanten zwischen 300 und 340-360K wurden gemessen, und Gleichgewichtskonstanten und Ausbeuten für jedes Addukt, sowie Entropien und Enthalpien wurden bestimmt. Addukte wurden identifiziert mit Hilfe ihre thermodynamische Eigenschaften und Vergleich mit, in der Literatur verfügbare, theoretischen Berechnungen und experimentellen Ergebnisse. Dennoch, war es unmöglich zu bestimmen welche der zwei Mechanismen von den untersuchten Reaktionen verfolgt wird, und wahrscheinlich der wahre Mechanismus liegt dazwischen.

1 INTRODUCTION

Volatile organic compounds (hereafter referred to as VOCs) are carbon-containing gases present in the troposphere at mixing ratios of some 10 parts per billion (ppb) in polluted air down to less than one ppb in remote areas.¹⁻³ They are released by either anthropogenic or biogenic sources. Biogenic VOC emissions, on a global scale, equal or exceed anthropogenic sources, although the latter are more important in urban areas, contributing to photochemical smog formation.⁴ Aromatic hydrocarbons, an important subclass of VOCs, react promptly with OH radicals in the gas phase at rates which depend on the quantity and properties of the substituent group(s) attached to the aromatic ring.⁵ These rate constants have been extensively studied for the aromatics benzene,⁶⁻¹⁸ toluene,^{7-11, 17-25} 1,2-dimethylbenzene (o-xylene),^{7-9, 20-22, 26, 27} 1,3-dimethylbenzene (m-xylene),^{7-10, 18, 20-22, 25-28} 1,4-dimethylbenzene (p-xylene),^{7-9, 18, 20-22, 26, 27, 29} 1,2,3-trimethylbenzene, 1,2,4-trimethylbenzene and 1,3,5-trimethylbenzene,^{7-9, 20, 22, 30} while for aromatics with higher methylation either only a few studies (1,2,4,5-tetramethylbenzene³¹, pentamethylbenzene³¹ and hexamethylbenzene^{32, 33}) or no studies at all have been carried out (1,2,3,5- and 1,2,3,4-tetramethylbenzene). After this high number of studies, comprising not only room-temperature measurements but also temperature and pressure dependence, using absolute and relative studies, little is known about the mechanism after the initial OH-radical attack in the absence of oxygen. These rate constants are important to understand the local, regional or long-range effects of their oxidation products. Moreover, a good understanding of these rate constants can improve the results obtained from the application of the master chemical mechanism (MCM) for environmental chamber studies.³⁴⁻³⁹

1.1 OH-radical reaction with alkylated aromatic compounds

OH radicals react very readily with aromatic compounds. OH addition to a non-substituted site, H atom abstraction from the aromatic ring and reaction at the substituent group attached to the aromatic ring have been investigated and discussed.⁵ OH-rate constants at low temperatures (<325K) have slightly negative activation energies (i.e., they decrease with increasing temperatures) while at high temperatures (>400 K), the OH rate constants increase rapidly with increasing temperatures.⁴⁰ At intermediate temperatures, non-exponential decays of OH radicals have been observed, caused by the combination of OH addition and H-atom abstraction,^{9, 11, 13, 15, 27} and depending on the experimental conditions.⁴¹ Until a few years ago, OH addition to a substituted site (*ipso* addition) was considered to be

unimportant in the gas phase, and it gained significance after the investigation of the reaction of OH radicals with hexamethylbenzene (HMB) by Berndt and Böge⁴² using a relative rate technique with 1,3,5-trimethylbenzene as reference. They detected hexamethyl-2,4-cyclohexadienone as a product of consecutive reactions with NO₂, and the OH+HMB-rate constant, $(1.13 \pm 0.11) \times 10^{-10} \text{ cm}^3 \text{ s}^{-1}$ at 295 K,⁴² was found to be approximately 20 times higher than the respective rate constant for the reaction of OH with toluene,^{7-11, 17-25} a molecule in which the majority of its sites are unsubstituted and no steric hindrance is expected, and also 30 times more reactive than the expected rate constant for the H abstraction from a total of six methyl groups alone,⁴⁰ indicating that an *ipso* addition can occur at room temperature. It is therefore interesting to elucidate the mechanism for the OH radical addition to methylated compounds. Soon after, Koch and Zetzsch⁴³ observed biexponential decays of OH from the reaction with HMB at elevated temperatures, indicating the formation of an HMB-OH adduct in equilibrium with the reactants. Later on, these investigators inspected archived digital files of previously published data and detected deviations from the biexponential behaviour for 1,3,5-trimethylbenzene, supporting the idea of the formation of *ipso* adducts.⁴⁴ More recently Bohn and Zetzsch³⁰ published a detailed analysis of the reversible reaction of OH radicals with 1,3,5-trimethylbenzene (135-TMB), a highly symmetric molecule which could form only two types of OH-(135-TMB)-adducts after the OH radical addition at either an occupied (*ipso*) or at a free (*ortho*) position (at three equivalent positions each). Bohn and Zetzsch (2012)³⁰ re-evaluated the triexponential OH-decay curves which corresponded to the formation of two energetically different adducts by solving the corresponding system of differential equations, and they developed two reaction mechanisms assuming: a) direct formation of both adducts and b) the direct formation of one adduct with subsequent isomerization into the other. These authors concluded that the formation of *ipso* adducts was possible and tentatively identified the observed adducts.

During my PhD work, I investigated the possible formation of *ipso* adducts from the OH reaction with the biogenic aromatic molecule 4-isopropyltoluene (p-cymene) and the influence of two non-equivalent alkyl groups on the reaction mechanism. The preliminary experimental results presented before³³ for hexamethylbenzene (HMB) were re-evaluated using an improved fitting analysis, and the possible formation of *ipso* adducts from the reaction with OH radicals was investigated for 1,4-dimethylbenzene (14-DMB), 1,3,5-trimethylbenzene (135-TMB), 1,2,3,4-tetramethylbenzene (1234-TeMB) as ideal model

molecules and finally accomplished for 1,2,3,5-tetramethylbenzene (1235-TeMB), 1,2,4,5-tetramethylbenzene (1245-TeMB) and pentamethylbenzene (PMB) as well.

1.2 Objectives of the PhD Thesis

The main goal of my thesis is to improve the understanding of the OH-initiated degradation of aromatic hydrocarbons by investigating the possible formation of ipso adducts from the reaction of OH radicals with p-cymene and polymethylated benzenes at various temperatures. Rate constants for the global reaction and for individual reaction channels were determined, as well as the yield in cases where more than one adduct was formed. Thermodynamic data (entropy and enthalpy) were determined, facilitating in some cases the identification of the formed adducts.

The manuscripts presented on page *iv* contribute to this research as follows:

- i. Alarcón et al. (2013) present the application of a known, widely used model^{13, 45-47} to the reaction of OH radicals with p-cymene. In the paper, it becomes clear that the mechanism is more complex than expected and that a new model has to be developed in order to elucidate the reaction mechanism.
- ii. Alarcón et al. (2014), published as a continuation of the previous paper, present a re-evaluation of the measurements, performed using an extended mechanism to understand the fate of the OH reaction with p-cymene. The extended model served to determine global and separate reaction rate constants assuming the formation of two adducts. Quantum chemical calculations and numerical simulations, performed by colleagues at Bordeaux and Jülich, demonstrated the predominant formation of two adducts from the four possible adducts.
- iii. Alarcón et al. (2015) present the application of the triexponential model (i.e., formation of two adducts) and the extended triexponential model (i.e., direct formation of each adduct and isomerization of one adduct into the other) to a series of polymethylated aromatic compounds: 14-DMB, 135-TMB and 1245-TeMB which, by symmetry, can form two adducts alone (*ipso* and *ortho*). OH-rate constants, adduct-formation yields, formation entropies and enthalpies and equilibrium constants were determined for the direct addition of OH to these compounds and for the isomerization of the OH-adducts. Formed adducts were tentatively identified by comparison with published thermodynamic data on benzene and a re-evaluation of former experimental data with HMB. Furthermore, total OH rate constants were determined for the aromatic compounds which

could form more than two adducts (and for which the triexponential models do not apply): 1234-TeMB, 1235-TeMB and PMB.

2. EXPERIMENTAL

The experimental methodology was originally developed by Stuhl and Niki,⁴⁸ and consists of OH radical production by vacuum UV flash photolysis of water vapour and time resolved detection of OH radicals using resonance fluorescence. The apparatus used in this work was originally built by Witte et al.¹⁵, a temperature-controlled further developed version of the apparatus built by Wahner and Zetzsch.¹³ The saturator system for the correct dosage of reactants and water, as well as the software for automatic control of the experiments were developed by Rinke and Zetzsch,¹⁴ and Koch et al.,^{46, 47} respectively. A detailed description of the experimental setup used during my PhD work has also been presented in Alarcon et al.⁴⁹. Briefly, gaseous mixtures of aromatic-He-H₂O and He-H₂O were prepared by passing the carrier gas (He) through vessels (saturator) at a given mass flow rate, one of them containing water and another containing the compound (solid or liquid) to be studied. The temperature of the saturators was kept constant by circulating water through the glass mantle at a temperature at which the vapour pressure of the substances was known. Concentrations of H₂O and aromatics were calculated from vapour pressures at the saturator temperature, ambient and reaction cell temperatures, mass-flow rates through both saturators and total pressure on the reaction cell. Gas mixtures containing either He-H₂O or aromatic-He-H₂O flow into the reaction cell under slow flow conditions to avoid accumulation of reaction products. To avoid condensation of compounds with low vapour pressure, the glass tubing from the saturators to the reaction cell was heated using a resistance-heating wire. An important improvement to the already built apparatus was a commercial Perkin Elmer FX1165 short arc xenon flash lamp with a MgF₂ window was used in the experiments as VUV source, typically using a flash energy of 540 mJ. This new lamp has proven to be very reliable, with increased signal and trigger stability. Experiments, accomplished before my arrival, were performed using a home-made flash lamp with spark discharge in N₂ (flash energy = 600 mJ). This lamp has been used for the study of HMB³³ and for the first experiments with p-cymene presented in Alarcon et al.⁴⁹ Results obtained with the N₂-spark lamp in the p-cymene study did not agree with later results, showing an increased OH reactivity in comparison to those obtained with the Xe-flash lamp. This higher reactivity is assumed to be caused by impurities with higher vapour

pressure in the p-cymene sample, which were slowly stripped from the reactant in the saturator.

The initial OH concentration, produced by VUV photolysis of $1.5 \times 10^{15} \text{ cm}^{-3}$ of H_2O , was determined by Zhang et al.,⁵⁰⁻⁵² using the same flash lamp with a flash-photolysis resonance fluorescence system of similar geometry,¹³ obtaining a value of $2 \times 10^{10} \text{ cm}^{-3}$ under the experimental conditions employed. This initial concentration is at least 10 times smaller than the lowest aromatic concentration used in our experiments, ensuring pseudo first order conditions. The resonance lamp operated with a slow flow of a gas mixture of He and water vapour at a constant pressure of 130 mbar. The microwave power was supplied by a microwave generator (Muegge, Reichelsheim, MW-GPRYJ1511-300-01, 2.45 GHz, 300 W) via a water-cooled circulator (Philips, Type 2722 163 02071) and operated at 30% of the maximum power. The microwave discharge dissociates the water vapour, contained in the gas mixture, to produce OH radicals that are then electronically excited by colliding with excited He or free electrons. Excited OH radicals decay to the ground state by fluorescence, and this emitted radiation is focused into the reaction cell (see f in fig. 1), exciting the OH radicals produced by VUV photolysis. The resonance lamp is equipped with a concave mirror at the top (see q in fig. 1) that captures the emitted radiation and resends it to the reaction cell through the focusing lenses, increasing by this manner the total fluorescence intensity. Excited OH radicals in the reaction cell decay to the ground state, and the emitted radiation passes through an interference filter (308 nm) to block impurity emissions from the resonance lamp, and later is focused onto the photocathode of a photomultiplier (Thorn-EMI, 9789QB) placed at right angles to the Xe flash lamp and the resonance lamp. The output pulses from the photomultiplier were processed by a home-made discriminator and accumulated in a multichannel-scaling card (EG&G Ortec, model ACE MCS) at a dwelltime of 0.98 ms and saved in a PC. Koch et al.⁴⁶ compressed the data points from the 4096 channels of the multichannel scaling card into 62 values, by doubling the time interval width after every 6 intervals.⁴⁶ This compression of the data needs less memory space and decreases the data noise toward longer times, and it has been demonstrated that its use does not lead to systematic deviations.⁴⁶

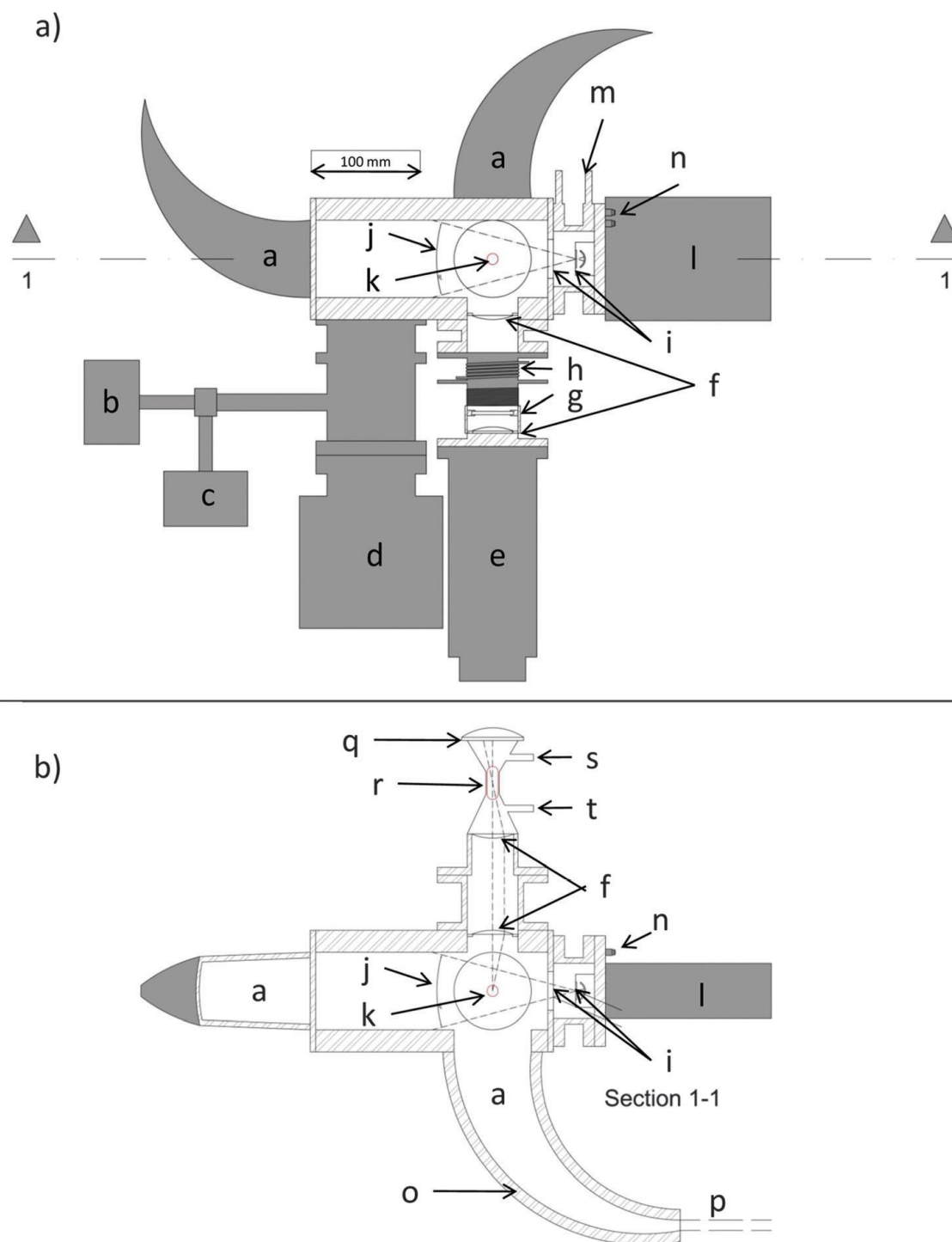


Fig. 1 Top (a) and side (b) views of the flash photolysis resonance fluorescence (FR-RF) system used in this work. (a) Wood's horn; (b) pressure gauge (10 Torr); (c) pressure gauge (1000 Torr); (d) vacuum valve; (e) photomultiplier; (f) focusing lenses; (g) interference filter (308 nm); (h) focusing screw; (i) MgF_2 windows; (j) 60% intensity compared to the central beam; (k) observation zone; (l) lamp power supply; (m) N_2 purge gas inlet; (n) lamp water cooling; (o) mantle with silicon oil circulating from a thermostat; (p) gas mixture inlet; (q) concave mirror; (r) microwave discharge; (s) resonance lamp He– H_2O mixture outlet and (t) inlet. Taken from Alarcon et al.,⁴⁹

The temperatures in both saturators, of the reaction cell and in the laboratory were measured using platinum resistance thermometers, PT100. The pressure in the cell and in the saturator system was determined using pressure transducers type 222B of 1000 mbar range (MKS Instruments). The He flows through both saturators and for dilution were controlled using mass flow controllers (MFCs) ranging from 5 to 2000 sccm (Wagner Mess- und Regeltechnik). Each MFC was calibrated using soap-bubble flowmeters, and the resulting parameters of second-order polynomials were saved into a calibration data file (calibr.dat) which was called by the program to interpolate the flow rates. Using the calculated flow rates, vapour pressures, temperatures, and pressures, concentration of water and reactants were determined in real-time. All this information was saved in a protocol file (*.prt) for each measurement that was created in parallel to the file containing the raw data of the decays (*.dec), and it has proven to be very helpful in the search for the causes of some problems detected after the automatically obtained data was processed.

Typically, an experimental series was performed in the following way:

- a) The saturators were emptied and flushed several times using high-purity hexane (sample saturator) and deionized water (water saturator).
- b) The saturator used for the aromatics was heated to 80 to 90 °C, and the He flow through it was at its maximum (10 sccm) to assure that neither the previous compound used nor hexane could contaminate the new compound to be measured.
- c) The glass tubing was heated to around 50°C to avoid condensation of compounds with low vapour pressure.
- d) The temperature of the reaction cell was set at 350 – 360 K and the pressure was kept at 50 – 80 mbar to remove as much impurity as possible.
- e) Blank experiments were performed under typical experimental conditions (water concentration = $1.5 \times 10^{15} \text{ cm}^{-3}$, temperature in the cell = 300 K, total pressure = 200 mbar), with the exception that the saturator for the aromatic was kept at 80 to 90°C and maximum He flow (10 sccm), until the OH-radical decay rates decreased to less than $2 - 4 \text{ s}^{-1}$.
- f) In cases where the biexponential behaviour of the OH radical decays did not disappear after the treatment from steps a) to d), an intense cleaning of the reaction cell was

performed: the cell was again heated and evacuated using a diffusion pump and kept in this configuration for several hours (typically during the whole night).

- g) After the system was clean, a new compound was transferred into the reactant saturator. Vapour pressure data was searched in the literature for the temperature at which the saturator was kept during the experiments (between 275 and 370 K when using water as circulating liquid). If no Clausius-Clapeyron/Antoine coefficients were found for the studied compounds, these were calculated in the required range from measurements in the literature, using the same temperature range as the authors in their experiments. These Antoine coefficients, either obtained or directly used from literature data, were saved in a file containing vapour pressure coefficients (antoine.dat).
- h) If for the compound to be measured there were no rate constants for the reaction of OH radicals available in the literature, a series of experiments with increasing concentrations of the aromatic was performed until the first OH decay became faster than 300 s^{-1} . The concentration, at which this decay was found, was then used as maximum in the forthcoming experiments.
- i) The minimum aromatic concentration used was dependent on the minimum setting of the mass flow controller used for the aromatic saturator (10 % of the full range) and the saturator temperature. When a minimum was found, at least 10 aromatic concentrations were selected between the minimum and maximum.
- j) The experiments were designed such that for each temperature the aromatic concentration was increased systematically until the maximum was reached and then decreased again back to the minimum concentration. In this manner it could be observed if the results were the same independent if the concentrations were being increased or decreased and therefore an interfering ad-/ desorption of the aromatic in the cell could be detected.
- k) The temperature in the reaction cell was varied from 300 K up to around 380 – 400 K, typically increasing and decreasing systematically and then picking some random temperatures in between to confirm the obtained results, thus checking the long-term stability of the purity of the sample.

3. DATA EVALUATION

Exponential functions (bi- and triexponential) were fitted to obtained raw data using two approaches. The first, so called “e-fit”⁴⁶ (from the German word “Einzel” which means individual), was only used to get an overview of the data or to detect problems with specific measurements. Moreover, this overview can show deviations from the linear dependence of the OH-decay rate on the aromatic concentration caused by low equilibration times (time needed for the concentration of the studied substance to become stable and constant in the reaction cell after being set by the software). However, no rate constants were calculated from the e-fit mainly because at some temperatures/concentrations of aromatic, the intensity ratios (i.e., I_1/I_2 . See eq. 10) might become too large or too small, or the rates of both exponential decays become similar (i.e., $\tau_1^{-1} \approx \tau_2^{-2}$. See eq. 10) and the fitting routine cannot determine these parameters correctly. The second approach, so called “k-fit” or simultaneous fit, was developed by the former co-worker Koch⁴⁷ in order to minimize those problems, being applied to sets of decays at various reactant concentrations and the same temperature. Both, e-fit and k-fits were performed in this work using fitting routines written with the IDL software (Interactive Data Language, Research Systems Inc.). Uncertainties of the fitted parameters were estimated by increasing and decreasing the value of each parameter and fixing it (while other parameters are allowed to vary) until the measured χ^2 was increased by a given factor.^{30,49} This factor was calculated for each set of curves for the degrees of freedom (DOF) given to obtain a probability of 0.68, which corresponds to 1σ uncertainty. Uncertainties of enthalpies and entropies were estimated applying the Bootstrap method. For this method, applied when the uncertainty of the single data points are poorly known, the data sets were repeatedly resampled using N randomly selected data points from the original set. The standard deviations of the fitted parameters define their estimated uncertainty.⁵³

3.1 Reaction mechanisms

As mentioned above in section 1.1, OH radicals react with aromatic molecules following mainly two pathways: OH-radical addition and H-atom abstraction. OH radical addition could occur in all positions; however the reactivity of some positions might be affected by inductive or resonance effects of the substituents (alkyl groups are ortho/para directing) and/or by steric hindrance. Generally, numerous adducts should be expected from the reaction of OH radicals with alkylated aromatics (see table 1), but the ability of detecting them experimentally depends on the differences of the thermodynamic properties of the

adducts (entropy and enthalpy of formation), subsequent reaction of the adducts, time resolution of the experiments, among others. Nevertheless, even if the adducts were distinguishable and measurable, a numerical solution for the differential equation system of $n+1$ equations and $3n+2$ variables (with n =number of distinguishable adducts) needs to be found. These numerical solutions are available for the formation of one^{13, 46} and two adducts,³⁰ and they were applied to the measured data as will be shown below.

Tab. 1. Adducts expected from the reaction of the given aromatic compounds with OH radicals.

Aromatic	<i>ipso</i> adducts	<i>non-ipso</i> adducts	Total adducts
Benzene	0	1	1
Toluene	1	3	4
12DMB	1	2	3
13DMB	1	3	4
14DMB*	1	1	2
123TMB	2	2	4
124TMB	3	3	6
135TMB*	1	1	2
1234TeMB*	2	1	3
1235TeMB*	3	1	4
1245TeMB*	1	1	2
PMB*	3	1	4
HMB*	1	0	1
p-cymene*	2	2	4

*aromatic compounds studied for this dissertation

OH-decay curves were observed to become bi- or triexponential, depending on the studied aromatic. A fourth exponential decay term was beyond the capabilities of our experimental setup, and our study was therefore limited to three reaction mechanisms: formation of one adduct (biexponential model), direct formation of two adducts (triexponential model) and direct formation of one adduct and isomerization into the other (extended triexponential model). A diagram with all possible reactions is shown in fig. 2.

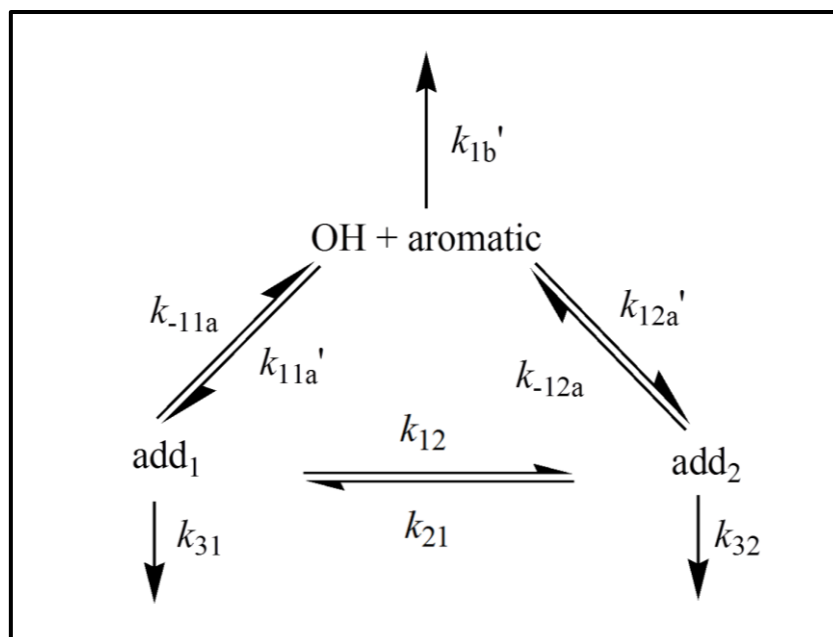


Fig 2. Schematic diagram with all possible reactions. The $k_i' = k_i \times [\text{aromatic}]$ denote pseudo first-order rate constants of bimolecular reactions. Adapted from Alarcón et al (2015)⁵⁴

3.2 Biexponential model ($k_{12a}, k_{12} = 0$)

The biexponential model (mod-1) applies strictly to molecules which can form one adduct alone from the reaction with OH radicals (benzene and HMB). The incorrect use of this model, applied to p-cymene⁵⁵ and 135-TMB,³⁰ has shown large underestimation of the OH rate constants at temperatures higher than room temperature. The reaction mechanism used in this model can be obtained from the global scheme (fig. 2) when suppressing the formation of a second adduct ($k_{12a}=0$), as well as the isomerization of the adduct formed ($k_{12}=0$). The mechanism involves the reversible addition of OH radicals to the aromatic ring (k_{11a}, k_{-11a}), H-atom abstraction (k_{1b}), OH radical losses (k_2) and adduct losses (k_{31}), leading to a system of two differential equations (Eq. 1 and 2)

$$\frac{d[OH]}{dt} = -a [OH] + b[adduct] \quad 1$$

$$\frac{d[adduct]}{dt} = c [OH] - d[adduct] \quad 2$$

The general solution for the system of differential equations (eq. 1 and 2) is expressed by eq. 3 and leads to biexponential OH-decay curves characterized by a first fast decay due to the OH addition to the aromatic ring and abstraction (k_{11a} and k_{1b}) and a second slow decay

due to the equilibrium reached between the OH addition (k_{11a}) and the unimolecular decay of the adduct (k_{11a} , k_{-11a}) with a subsequent loss of the adduct without regeneration of OH (k_{31}) that cannot be distinguished from abstraction (k_{1b}).⁴⁶ Example-fits of the biexponential model to data from measurements with 1,4-dimethylbenzene are shown in fig. 3.

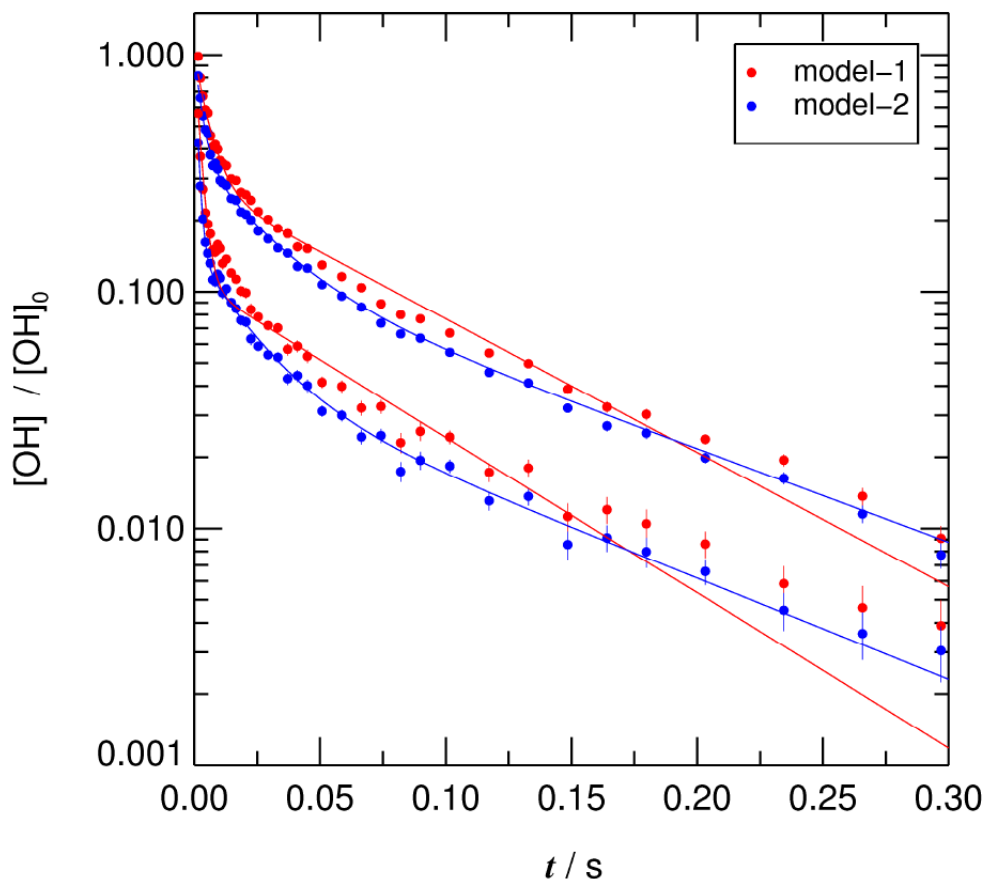


Fig. 3. Examples of OH decay curves in a semilogarithmic plot. Two from a total of eleven decay curves of the experiments with 1,4-DMB at 334 K are shown. 1,4-DMB concentrations were $1.7 \times 10^{13} \text{ cm}^{-3}$ (top) and $5.0 \times 10^{13} \text{ cm}^{-3}$ (bottom). Full lines show the results of fits to all eleven decay curves simultaneously according to model-1 (red) and model-2 (blue). The data points were calculated from photon counts divided by interval widths and assigned to the middle of the intervals. Fitted backgrounds were subtracted and data then normalized to the fitted starting count rates. For that reason, model-1 and model-2 data points are different even though they represent the same experimental decay curve. Only a small fraction of the total measurement time of 4 s is shown. Taken from Alarcon et al.⁵⁴

$$[OH] = I_1 \exp(-t/\tau_1) + I_2 \exp(-t/\tau_2) \quad 3$$

Parameters a, b, c and d are related to the rate constants in the following way (Eq. 4 - 7):

$$a = k_2 + (k_{11a} + k_{1b})[\text{aromatic}] \quad 4$$

$$b = k_{-11a} \quad 5$$

$$c = k_{11a}[\textit{aromatic}] \quad 6$$

$$d = k_{-11a} + k_{31} \quad 7$$

Parameters a and d are obtained directly from simultaneous fit of isothermal sets of OH decay curves, from which the global rate constant $k_{\text{OH}} (= k_{11a} + k_{1b})$ and the unimolecular decay of the adduct are calculated. The analytical solution of the differential equation system does not allow us to separate parameters b and c (obtained as a product), limiting its use mostly to the determination of the equilibrium constant using either eq. 8 or 9, given the H atom abstraction rate constant (k_{1b}) or the adduct losses (k_{31}), respectively. Rate constants for elementary reactions cannot be directly fitted due to a degeneracy problem (i.e., there are more variables than equations). In order to partially solve this problem, limiting cases are studied. At low temperatures, the abstraction plays a minor role a_r (slope of a vs [aromatic]) and $a_r = k_{11a}$. On the other hand, at high temperatures, the unimolecular decay of the adduct plays a major role in the adduct-losses term d , resulting in $d=k_{-11a}$.^{46, 47}

$$K_{eq}(\textit{biex}) = \frac{(k_{\text{OH}} - k_{1b})^2}{bc} = \frac{k_{11a}^2}{k_{11a}k_{-11a}} = \frac{k_{11a}}{k_{-11a}} \quad 8$$

$$K_{eq}(\textit{biex}) = \frac{bc}{(d - k_{31})^2} = \frac{k_{11a}k_{-11a}}{k_{-11a}^2} = \frac{k_{11a}}{k_{-11a}} \quad 9$$

H-atom abstraction can be estimated using the expression recommended by Atkinson⁴⁰ based on high-temperature (>450K) rate constants for the reaction of OH radicals with toluene and the xylenes. H-atom abstraction (per methyl group) is expressed by the modified Arrhenius expression $k_{1b}=8.07 \times 10^{-18} T^2 \exp(-38/T) \text{ cm}^3 \text{ s}^{-1}$ over the temperature range 470 – 1046 K, and an extrapolation to room temperature yields a rate constant of $6.3 \times 10^{-13} \text{ cm}^3 \text{ s}^{-1}$ for each methyl group⁴⁰. While the abstraction for the methylated benzenes can be estimated by this approximation, this approach should not be used for aromatics with alkyl groups other than CH₃; for example p-cymene. In this case, a different approach was needed. Upon our request, Aschmann et al.,⁵⁶ measured the formation yields of the major products expected after the H-atom abstraction from the isopropyl group from the reaction of OH radicals with p-cymene in a Teflon chamber at 297 ± 2 K. These authors determined that the H-atom abstraction from the methyl and isopropyl groups represented $20 \pm 4\%$ of the total rate

constant at room temperature (much larger than expected for the methylated aromatics of 10% for p-xylene at room temperature and becoming less important with increasing methylation). The temperature dependence of the H-atom abstraction for p-cymene was estimated on a first approximation by structure activity relationship (SAR).⁵⁷ This method requires the knowledge of so-called “substituent factors” i.e., empirical factors related to the identity of substituent groups attached to the primary, secondary or tertiary carbons suffering the H-atom abstraction. These factors were not available for the compounds formed after the H-atom abstraction from the methyl group or from the three carbon atoms of the isopropyl group. Assuming, by simplicity, that these substituent factors had the same value and that the estimation must yield the experimental value at room temperature ($3.1 \pm 0.7 \times 10^{-12} \text{ cm}^3 \text{ s}^{-1}$), an expression for the H-atom abstraction was estimated. Nevertheless, this expression seemed to underestimate the abstraction at high temperatures, and another approach was needed. As it is expected that the abstraction will be the major reaction path for reaction with OH radicals at high temperatures, the modified Arrhenius equation: $k = A (T/K)^2 \exp(-E/RT)$ was fitted to data at these temperatures (>380K) and the experimental value at room temperature. In the present work, values for A of $2 \times 10^{-17} \text{ cm}^3 \text{ s}^{-1}$ and $-E/R$ of 170K for p-cymene were determined.

The adduct-loss rate constant, k_{31} , can be directly estimated from parameter d since the unimolecular decay rate constant, k_{-11a} , depends strongly on the temperature, while the adduct-loss rate constant, k_{31} , is assumed to be constant over the studied temperature range. Fitting the parameter d to an expression of the form: $A \exp(-B/T) + C$ allow us to determine both rate constants.

The equilibrium constants, estimated by equation 8 and 9, are not different, but each equation has its advantages and drawbacks at different temperatures. At low temperatures, the abstraction does not play a major role in the overall rate constant (i.e., $k_{OH} \gg k_{1b}$), and the equilibrium constant is well described by eq. 8. On the other hand, at these temperatures, the parameter d is comparable with the adduct-loss rate constant k_{31} (i.e., the unimolecular decay of the adduct, k_{-11a} , is very small), and small deviations in the determinations of the latter increase the uncertainties of the equilibrium constant estimated by eq. 9. With increasing temperatures, the abstraction becomes more important, increasing the uncertainties of the estimated equilibrium constant using eq. 8; the adduct-loss rate constant then becomes negligible against the parameter d , and the equilibrium constant at these temperatures can be well estimated by eq. 9.

In order to determine equilibrium constants valid over the studied temperature range, equations 8 and 9 were combined into equation 10. Optimized values for k_{31} were estimated by fitting the concentration-dependent term of parameter a , parameters bc and d to equation 10, using as k_{1b} the recommendation from the literature^{30, 40} for the methylated aromatics or the expression determined for p-cymene.⁴⁹

$$k_{OH} - k_{1b} = k_{11a} = \frac{k_{11a}k_{-11a}}{k_{-11a}} = \frac{bc}{d - k_{31}} \quad 10$$

3.2 Triexponential model ($k_{12} = 0$)

Triexponential decays of OH in presence of aromatics were first overlooked several years ago when studying trimethylbenzenes.^{46, 58} Application of the biexponential model to the obtained data was not satisfactory but, as *ipso* adducts had been considered to be unimportant in the gas phase and only one adduct was expected, no explanations were found for the deviation of the curves from biexponential decays. It should be mentioned here that Uc et al.,⁵⁹ predicted high statistical occurrence of the *ipso* adduct from the reaction of OH radicals with toluene from theoretical calculations, as well as higher stability compared to the other adducts. Furthermore, the experimental determination of a very fast rate constant for the reaction of OH with HMB at 296 K by Berndt and Böge⁴² showed the importance of the *ipso* addition in the gas phase. Deviations from the biexponential model were also observed with p-cymene, increasing the need for the analytical solution of the reaction mechanism for the formation of two distinguishable adducts.

The reaction mechanism (fig. 2) contains now, additional to the biexponential model, the direct formation of a second adduct (isomerization was suppressed; $k_{12} = 0$). The solution for the differential equation system given by eq. 11 – 13 was found by Bohn and Zetzsch³⁰ and was used for the determination of the rate constants using the triexponential model (mod-2).

$$\frac{d[OH]}{dt} = -a [OH] + b[adduct_1] + e [adduct_2] \quad 11$$

$$\frac{d[\text{adduct}_1]}{dt} = c [\text{OH}] - d[\text{adduct}_1] \quad 12$$

$$\frac{d[\text{adduct}_2]}{dt} = f [\text{OH}] - g[\text{adduct}_2] \quad 13$$

The general solution for the system of differential equations (eq. 11 - 13) is expressed by eq. 14 and leads to triexponential OH-decay curves, characterized by a first fast decay due to the OH addition to the aromatic ring, a second slow decay due to the equilibrium established between the OH addition and the unimolecular decay of the more unstable adduct and a third decay due to the equilibrium reached between the OH addition and the unimolecular decay of the more stable adduct. Data fitted to the triexponential model is shown in fig. 3, and the improvement is obvious, as compared to the biexponential model.

$$[\text{OH}] = I_1 \exp(-t/\tau_1) + I_2 \exp(-t/\tau_2) + I_3 \exp(-t/\tau_3) \quad 14$$

Analogous to the biexponential model, rate constants are contained in the parameters a-g as shown in eq. 15–21.

$$a = k_2 + (k_{11a} + k_{12a} + k_{1b})[\text{aromatic}] \quad 15$$

$$b = k_{-11a} \quad 16$$

$$c = k_{11a}[\text{aromatic}] \quad 17$$

$$d = k_{-11a} + k_{31} \quad 18$$

$$e = k_{-12a} \quad 19$$

$$f = k_{12a}[\text{aromatic}] \quad 20$$

$$g = k_{-12a} + k_{32} \quad 21$$

Parameters *a*, *d* and now *g* are obtained directly from the simultaneous fits of triexponential functions to isothermal sets of decays, from which the global rate constant k_{OH} ($= k_{11a} + k_{12a} + k_{1b}$) and the unimolecular decay of each adduct are calculated. Parameters *bc*, and now *ef* cannot be separated, and they are used mainly for the determination of the equilibrium constant using equations 22 and 23, given the losses for each adduct (k_{31} and k_{32}

for adduct 1 and 2, respectively). Despite the fact that these equilibrium constants can be determined for each temperature from the fitted parameters, we preferred to adapt the fit routines to obtain directly the equilibrium constants. Direct results obtained by this way are the same as with eq. 22 and 23, but the uncertainties of these values can be determined by the method described at the beginning of this section and they are helpful in order to weight data for the determination of entropies and enthalpies.

$$K_{eq}^1 = \frac{bc}{(d - k_{31})^2} = \frac{k_{11a}k_{-11a}}{k_{-11a}^2} = \frac{k_{11a}}{k_{-11a}} \quad 22$$

$$K_{eq}^2 = \frac{ef}{(g - k_{32})^2} = \frac{k_{12a}k_{-12a}}{k_{-12a}^2} = \frac{k_{12a}}{k_{-12a}} \quad 23$$

Analogous to the biexponential model, optimized adduct loss rate constants k_{31} and k_{32} were estimated by fitting eq. 25 simultaneously at all temperatures, given the H atom abstraction rate constant k_{1b} from literature data.

$$k_{OH} - k_{1b} = k_{11a} + k_{12a} = \frac{k_{11a}k_{-11a}}{k_{-11a}} + \frac{k_{12a}k_{-12a}}{k_{-12a}} \quad 24$$

$$k_{OH} - k_{1b} = \frac{bc}{d - k_{31}} + \frac{ef}{g - k_{32}} \quad 25$$

3.3 Extended triexponential model ($k_{12a} = 0$)

Bohn and Zetzsch³⁰ proposed a variation of the triexponential model, taking the possible isomerization of the adducts one into the other into account. They studied the limiting case with no direct formation of adduct 2 ($k_{12a} = 0$) but via isomerization of adduct 1. The extended triexponential model (mod-3), as its name implies, presents only minor variations from the triexponential model. The differential equation system is described by eq. 26 - 28. Direct formation of adduct 2 is suppressed, i.e., $k_{12a} = 0$, and a new reaction is added for the isomerization of the adducts (k_{12} and k_{21}), the parameters d and g from the triexponential model are redefined (eq. 29 - 30) and the product of the two new parameters hi , that (similar to bc and ef) cannot be separated, is added (eq. 31 and 32).

$$\frac{d[OH]}{dt} = -a [OH] + b[adduct_1] + e [adduct_2] \quad 26$$

$$\frac{d[adduct_1]}{dt} = c [OH] - d[adduct_1] + h[adduct_2] \quad 27$$

$$\frac{d[adduct_2]}{dt} = f [OH] + i[adduct_1] - g[adduct_2] \quad 28$$

$$d = k_{-11a} + k_{12} + k_{31} \quad 29$$

$$g = k_{21} + k_{32} \quad 30$$

$$h = k_{12} \quad 31$$

$$i = k_{21}[aromatic] \quad 32$$

The general solution for the system of differential equations (eq. 26-28) is given by eq. 14. Equilibrium constants for the formation of the adduct 1 and for the isomerization into adduct 2 can be calculated using eq. 33 and 34, respectively. Similar to the previous models, it is necessary to determine the adduct loss rate constants k_{31} and k_{32} , as well as the isomerization rate constant k_{12} . Initially, adduct loss rate constants k_{31} and k_{32} are determined by a simultaneous fit of eq. 36 at all temperatures. Finally, k_{12} is determined after rearrangement of eq. 35 and 36 as shown by eq. 37.

$$K_{eq_isom}^1 = \frac{bc}{(d - k_{12} - k_{31})^2} = \frac{k_{11a}k_{-11a}}{k_{-11a}^2} = \frac{k_{11a}}{k_{-11a}} \quad 33$$

$$K_{eq_isom}^3 = \frac{hi}{(g - k_{32})^2} = \frac{k_{12}k_{21}}{k_{21}^2} = \frac{k_{12}}{k_{21}} \quad 34$$

$$k_{OH} - k_{1b} = k_{11a} = \frac{k_{11a}k_{-11a}}{k_{-11a}} = \frac{bc}{d - k_{12} - k_{31}} \quad 35$$

$$= \frac{bc(g - k_{32})}{(d - k_{31})(g - k_{32}) - hi} \quad 36$$

$$k_{12} = (d - k_{31}) - \frac{(d - k_{31})(g - k_{32}) - hi}{(g - k_{32})} \quad 37$$

4. EXPERIMENTAL RESULTS AND DISCUSSION

4.1 Vapour pressure

Parameters a , bc , ef and hi are directly related to the aromatic concentration (Eq. 4, 6, 15, 17, 20 and 32); thus for an accurate determination of the global rate constant (k_{OH}) and equilibrium constants this concentration must be well known. Concentrations are calculated from the saturated vapour pressure of the compound at the employed saturator temperature (accuracy: ± 1 K), the He flow through the saturator, and taking and the He flows used for controlling water vapour and dilution into account. The critical part is to find reliable vapour pressure measurements in the desired range for which either well-characterized Antoine parameters are available or can be calculated from the published data. Values obtained from the suppliers were not used in this work because usually further information regarding experimental conditions, error margins and determination procedure (direct measurements, calculation from thermodynamic data, etc.) are not available.

The vapour pressure of the studied substances in the indicated phase (l=liquid, s=solid) has been summarized by Alarcon et al.:^{49, 54} Vapour pressures for 14-DMB, 135-TMB and HMB have been widely studied and are in good agreement with each other in the temperature ranges 247-453 K, 223-373K and 223-363 K, respectively. In the case of 14-DMB, the saturator temperature was set during the experiments accidentally at 284 K (i.e., 2 K below its melting point), but no freezing was observed during the experiments. Hence, estimation of the 14-DMB concentrations was done using the parameterisations for the liquid phase, and in the case that the sample was solid, the vapour pressure would be lower by 5%, increasing in the same manner the OH rate constants. Antoine coefficients for 14-DMB, 135-TMB and HMB were obtained from the tables published by Stephenson et al.⁶⁰ Vapour pressure data for the tetramethylbenzenes and p-cymene at the saturator temperature was not found in the available literature. For 1245-TeMB, the low temperature data of Colomina et al.,⁶¹ was used to determine Antoine coefficients and extrapolate the vapour pressure to the saturator temperature. Vapour pressure data for the other tetramethylbenzenes (1234-TeMB and 1235-TeMB) is found for temperatures much higher than those used in this study and therefore an extrapolation would be too uncertain. In the case of p-cymene, vapour pressure measurements at temperatures higher and lower than the saturator temperature are available in the literature. In these cases, the vapour pressure was estimated using the recommendation of Ruzicka et al.⁶² These authors reviewed high-temperature vapour pressures and thermodynamic data for some high boiling alkylbenzenes and recommended Cox equation parameters for the estimation of the vapour pressures at temperatures between 223 and 323 K. In summary, we

estimate maximum uncertainties of the reactant concentrations of around 10% for 14-DMB, 135-TMB, PMB, HMB and p-cymene and 20% for the three tetramethylbenzenes.⁵⁴

4.2 Goodness of fit.

Bi- and triexponential models were fitted to decay curves in the presence of the studied aromatics. The fitted sum of squared residuals divided by the degrees of freedom (χ^2/DOF) was determined for each temperature. The degrees of freedom (DOF) are given by the total number of data points minus the number of parameters fitted according to the model. A χ^2/DOF value around unity indicates that the applied model is appropriate to describe the data, while deviations from unity indicate over- or underestimation of the fitted parameters as shown for p-cymene^{49, 55} and 135-TMB.³⁰

Fig. 4 shows obtained values for χ^2/DOF from the bi- and triexponential models for the studied polymethylated benzenes. It is evident that the triexponential model describes the OH-decay curves in the studied temperature range much better than the biexponential model, except in the case of HMB, which can react only to form one adduct and where pure biexponential curves were expected. Outliers observed for HMB were caused by trigger problems (the lamp triggered several times during single recordings of the OH decay by multichannel scaling) and therefore, some accumulated curves had to be deleted. Nevertheless, this plot shows that both models return similar values. For the other compounds, at room temperature, differences between the bi- and triexponential models are small, indicating the formation of one adduct with high stability. With increasing temperatures, this adduct becomes less stable, and large deviations from the biexponential model are observed. A similar behaviour of χ^2/DOF has been observed for the reaction of OH radicals with the trimethylbenzenes.³⁰ At temperatures much higher, the decomposition rate of the less stable adduct is large; the terms for the first and second decay rate become comparable, turning the curves biexponential. This limit was reached for the aromatics presented in this work around 340 – 360 K. Results presented in this work have been restricted to this temperature limit.

From the substances studied in this work, only for HMB, 14-DMB, 135-TMB, and 1245-TeMB either the bi- or the triexponential model applies strictly and can be used for the determination of rate and equilibrium constants. For substances for which more than two adducts are expected: p-cymene, 1234-TeMB, 1235-TeMB and PMB, the triexponential model represents merely an approximation. In the case of p-cymene, theoretical calculations predicted the formation of only two adducts contributing to the OH decays⁵⁵ as will be shown

in section 4.4, and consequently the determination of the rate and equilibrium constants was possible. For the other compounds, no such calculations have been performed yet and therefore only global rate constants will be presented. For 14-DMB, 135-TMB and 1245-TeMB, isomerization of the adducts was investigated based on the reaction mechanism shown in section 3.3. Values obtained for χ^2/DOF using the extended triexponential model were exactly the same as the ones obtained by the triexponential model, indicating that both, the direct formation of the adducts or the isomerization of one adduct into the other, could explain the experimental results.

4.3 Global rate constant (k_{OH})

Global rate constants (k_{OH}), i.e., the sum of OH radical addition and H-atom abstraction, for the aromatics presented in this work are shown in table 2 together with rate constants found in the literature. OH rate constants for the aromatics studied in this work are in good agreement with the available literature, except perhaps to a lesser extent for 135-TMB and HMB.

135-TMB has been widely studied, but in spite of the large number of publications available in the literature, there is still high uncertainty on the k_{OH} at room temperature, ranging from $(40.9 \pm 5.6) \times 10^{12} \text{ cm}^3 \text{ s}^{-1}$ up to $(62.4 \pm 7.5) \times 10^{12} \text{ cm}^3 \text{ s}^{-1}$.^{7, 9} The room-temperature k_{OH} determined in this study is higher than all the rate constants measured before, but still in agreement with some of the studies (table 2), mostly where FP-RF was employed. Nevertheless, the Arrhenius coefficients of the present work are in good agreement with all previous temperature dependence studies within the indicated uncertainties.^{9, 30, 63}

The rate constant determined for the reaction of OH radicals with HMB is, as expected from a re-evaluation of the same raw data, in good agreement with the preliminary value of von Buttlar et al.,³³ but almost 1.5 times larger than the value determined by Berndt and Böge.⁴² Since our rate constants are directly related to the vapour pressure data of the aromatic used, one might prefer results determined by a relative rate technique. Nevertheless, as shown in section 4.1, the vapour pressure for HMB has been very well investigated around the temperature at which the saturator was kept and the agreement between the authors^{60, 61, 64, 65} is excellent as shown in fig. S1 in Alarcon et al., (ESI).⁵⁴

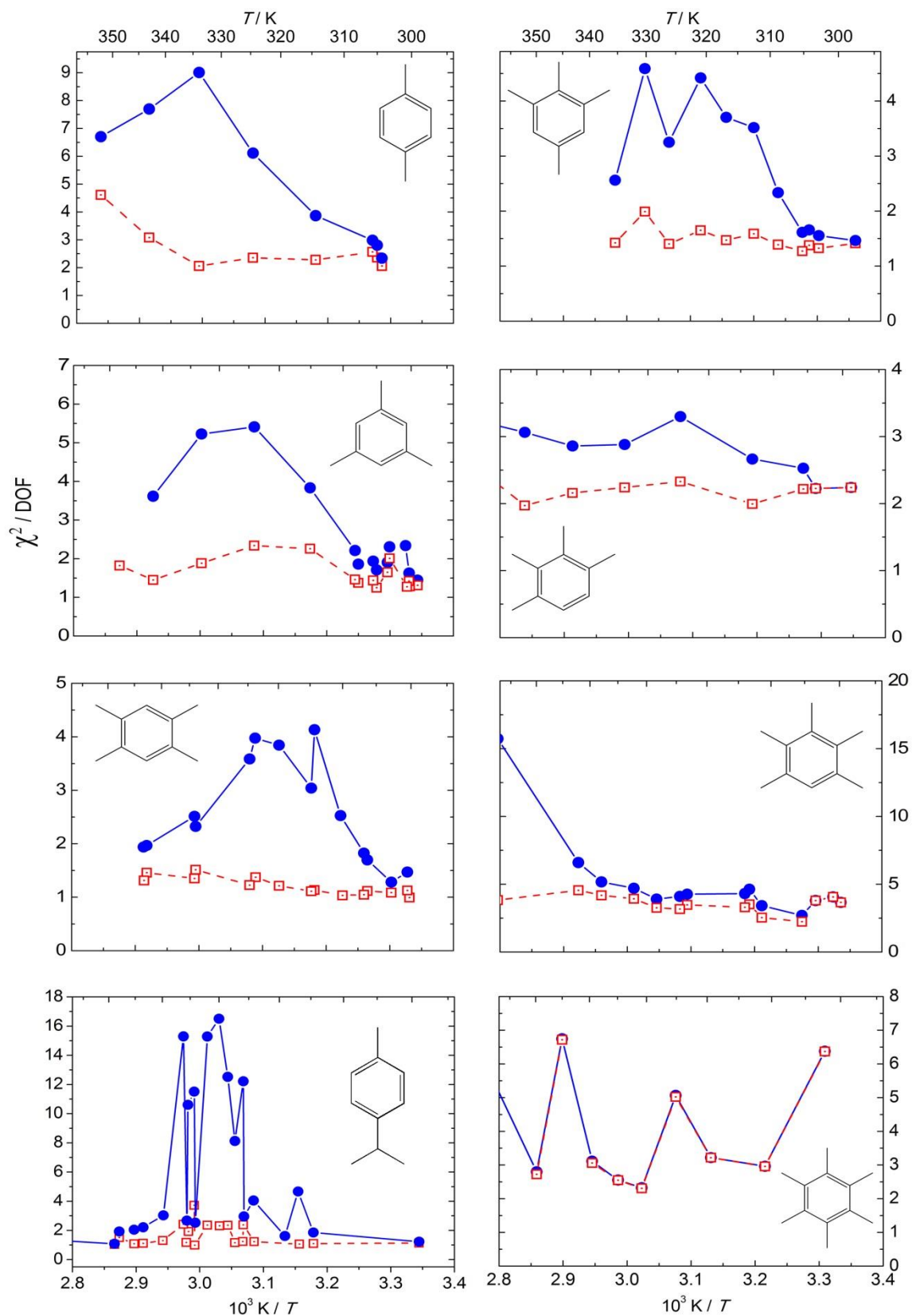


Fig 4. Estimated χ^2 / DOF for the alkylated benzenes of this study. Filled circles and open squares indicate values obtained from the application of the bi- and triexponential models, respectively.

EXPERIMENTAL RESULTS AND DISCUSSION

Tab. 2 Arrhenius parameters of the total rate constant (k_{OH}) for the reaction OH + Aromatic. $k_{\text{OH}} = A \exp(-B/T)$

	$\ln(A/\text{cm}^3\text{s}^{-1})$	B/K	$k_{\text{OH}}(298\text{ K}) / 10^{-12} \text{ cm}^3\text{s}^{-1}$	Experimental Technique ^j
14-DMB (<i>p</i> -xylene)			12.2 ± 1.2^8	FP-RF
			10.7 ± 2.4^{20}	RR $k(\text{n-butane})=2.99$
	-25.8 ± 1.6	-300 ± 500	15.3 ± 1.7^9	FP-RF
			10.5 ± 1.0^{26}	FP-RF
			13.5 ± 1.4^{27}	FP-RF
			13.6 ± 0.6^7	RR $k(\text{hexane})=5.9$
			13.6^{21}	RR $k(\text{cyclohexane})=7.34$
			13.0 ± 2.0^{22}	RR $k(\text{propene})=26.6$
			14.7 ± 3.0^{18}	RR $k(\text{n-hexane})=5.55$
	-25.7^a	-150^a	11.9 ± 0.7^{29}	RR $k(1,4\text{-dioxane})=10.9$
	-25.6 ± 0.3^b	-160 ± 90^b	13.1 ± 0.3^{54}	FP-RF
135-TMB (mesitylene)			47.2 ± 4.8^8	FP-RF
			44.4 ± 5.3^{20}	RR $k(\text{n-butane})=2.99$
	-26.2 ± 3.2	-860 ± 1010	62.4 ± 7.5^9	FP-RF
			40.9 ± 5.6^7	RR $k(\text{hexane})=5.9$
			57.5 ± 9.2^{22}	RR $k(\text{propene})=2.66$
			57.3 ± 5.3^{25}	RR (several)
			59.1 ± 1.1^{66}	RR $k(\alpha\text{-pinene})=52.8$
	-26.1	-740 ± 180	51.7 ± 1.1^{63}	RR $k(\alpha\text{-pinene})=1.21 \times 10^{-11} \exp(436/T)$
	-25.1	-450 ± 50	59.5 ± 2.0^{30}	FP-RF
	-25.3 ± 0.6^c	-550 ± 180^c	68.4 ± 0.9^{54}	FP-RF
1245-TeMB (durene)			55.5 ± 3.4^{31}	RR $k(135\text{TMB})=56.7$
	-27.3 ± 0.3^d	-1120 ± 90^d	57.8 ± 0.6^{54}	FP-RF
1235-TeMB (isodurene)	-24.6 ± 0.3^e	-330 ± 100^e	62.4 ± 0.8^{54}	FP-RF
1234-TeMB (prehnitene)	-26.2 ± 0.4^f	-820 ± 100^f	66.4 ± 1.8^{54}	FP-RF
PMB			103 ± 8.0^{31}	RR $k(135\text{TMB})=56.7$
	-26.2 ± 0.4^g	-980 ± 130^g	110 ± 4^{54}	FP-RF
HMB (mellitene)			113 ± 11^{42}	RR $k(135\text{TMB})=57.3$
	-24.3	-498	149^{33}	FP-RF
	-24.5 ± 0.2^h	-570 ± 40^h	$153 \pm 2^{33, 54}$	FP-RF
<i>p</i> -cymene			15.1 ± 4.1^{67}	RR $k(\text{cyclohexane})=7.43$
	-27.0	-612 ± 210^i	$14.9 \pm 0.8^{49, 55}$	FP-RF

^aArrhenius parameter calculated from k_{OH} of indicated reference (240 -340 K). Arrhenius parameter for the following temperature ranges (K): 304-352^b; 299-348^c; 300-343^d; 297-335^e; 298-362^f; 299-362^g; 311-370^h; 299-349^j. 295ⁱ K.FP-RF: Flash photolysis –resonance fluorescence technique. RR: relative rate technique. ^jReference substance and the used rate constant are indicated for results with relative rate technique. Units are $10^{-12} \text{ cm}^3\text{s}^{-1}$. Adapted from Alarcon et al. ⁵⁴. Values in bold were determined in this work.

Rate constants for 1235-TeMB and 1234-TeMB have not been measured before, and they were found to be slightly higher than for 135-TMB, but lower than for PMB. Overall, determined room temperature k_{OH} increase with increasing methylation, as shown in fig. 5, with 14-DMB reacting about 15 times slower than HMB. Room-temperature k_{OH} for the biogenic *p*-cymene was found to be comparable to the one obtained for the similar *p*-dialkylated aromatic 14-DMB (table 2), but about 2.5 times larger than the value measured for the reaction of isopropylbenzene with OH radicals^{7,26}, consistent with the activating effect of the additional methyl group in *para* position⁶⁸ and according to the Hammett equation.

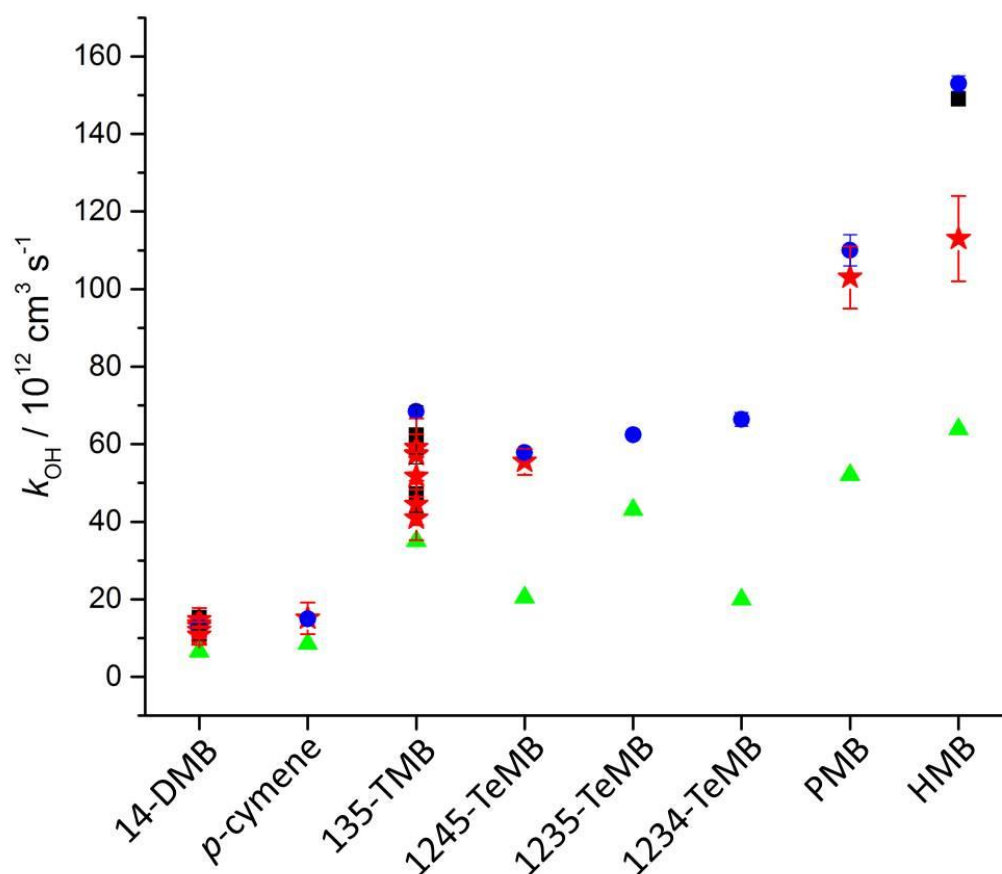


Fig. 5. Global rate constant k_{OH} at room temperature measured in this work (blue circles) compared to the available literature obtained by the relative-rate method (red stars), FP-RF (black squares and blue circles) and estimated by the AOPWIN software of the EPI Suite (green triangles).⁶⁹ References and exact experimental values are shown in table 2

Arrhenius parameters have been determined previously only for 14-DMB, 135-TMB, and HMB and are in agreement with the parameters estimated in this study. Negative activation energies ($E_a = B \times R$; $R =$ gas constant), observed for all the aromatics studied in this work, are in agreement with the formation of a pre-reactive π complex as predicted by several authors.^{9, 32, 55, 59, 70, 71} Theoretical studies on the reaction of OH radicals with 14-DMB⁷² predicted a total rate constant of $10 \times 10^{-12} \text{ cm}^3 \text{ s}^{-1}$ in reasonable agreement with the rate constant determined in this work and with the available literature. Estimations obtained from the EPI-Suite⁶⁹ (AOPWIN Module)⁶⁹ according to the procedure proposed by Zetzsch⁶⁸ employing the Hammett equation for electrophilic addition are also plotted in fig. 5. With increasing methylation, the disagreement between the estimations and measurements increases. The disagreement is about factor of two for 14-DMB, p-cymene, 135-TMB (our work), PMB and HMB⁴², a factor of three for 1234-TeMB, 1245-TMB and HMB (our work), and only a factor of 1.5 for 1235-TMB. These results demonstrate that the EPI-Suite⁶⁹ underestimates the OH rate constants of aromatic compounds and should be improved.

4.4 Stability and formation yields of the adducts.

Another parameter, obtained directly from the bi- and triexponential models, is the sum of rate constants for adduct losses ($k_{Li} = k_{-1ia} + k_{3i}$ for adduct i). Decomposition rate constants of the adducts (k_{-11a} , k_{-12a}) as well as their formation yields ($\Phi_1 = k_{11a} / k_{OH}$; $\Phi_2 = k_{12a} / k_{OH}$) can be easily determined from the fitted parameters, but these rate constants and their corresponding thermodynamic values (enthalpies, entropies, activation energy, etc.) are only valid if the applied mechanistic model (bi- or triexponential) corresponds to the studied compound. While the HMB+OH reaction (1 adduct) can be described by the biexponential model and 14-DMB+OH, 135-TMB+OH, and 1245-TeMB+OH (2 adducts) by the triexponential model, further complications arise for the reaction p-cymene+OH (4 distinguishable adducts).

Theoretical calculations, performed by our collaboration partners from the University of Bordeaux, are presented in detail in Alarcon et al.,⁵⁵ and the results obtained will be explained briefly here. A very minor formation (3%) of the *ipso* adduct formed from the OH radical addition to the position occupied by the methyl group (*ipso*-CH₃), a major formation of ortho adducts (24% *ortho*-CH₃ and 55% *ortho*-C₃H₇) and a considerable contribution from the other *ipso* adduct (18% *ipso*-C₃H₇) were predicted. Additionally, the dealkylation of the *ipso* adducts to form *p*-cresol and 4-isopropyl-phenol was investigated using theoretical calculations. For both dealkylation pathways, overall reaction energies were found to be

exothermic by 38 kJ mol^{-1} and 52 kJ mol^{-1} . The low activation energy at room temperature for *ipso*- C_3H_7 indicates that dealkylation of this adduct to form *p*-cresol is very likely. Based on these theoretical predictions, the reaction $\text{OH} + \text{p-cymene}$ would produce primarily two distinguishable *ortho* adducts and *ipso*- C_3H_7 ; but the latter would react further by dealkylation to form *p*-cresol. To determine if these predicted values would yield triexponential decay curves as observed experimentally, decay curves of OH were simulated using the values obtained by the theoretical calculations and experimental conditions (details can be found in Alarcon et al.⁵⁵). Simulated decays of OH were treated like the experimental data by fitting them to the triexponential model, but no deviation from this model was observed, confirming the major contribution of only two adducts to the regeneration of OH radicals. Results obtained from the simulated OH decay curves will be shown for comparison in the plots below. Recently, Dash and Rajakumar⁷³ calculated rate constants for the reaction of p-cymene with OH radicals in the temperature range between 200-400 K at the M06-2X/6-31+G(d,p) levels of theory. These authors determined a pre-reactive complex below the energy of the reactants, a small energy barrier at the transition state and similar energy for the adducts formed, ranging between 73 and 82 kJ mol^{-1} . Even though the relative stability of the adducts formed does not correspond to the values estimated by Alarcon et al.,⁵⁵ the energy range is too narrow for these disagreements to be important. Furthermore, Dash and Rajakumar⁷³ estimated a total rate constant of $0.82 \times 10^{-12} \text{ cm}^3 \text{ s}^{-1}$ and a portion for H-atom abstraction of $0.79 \times 10^{-12} \text{ cm}^3 \text{ s}^{-1}$ (96% of their estimated total rate constant) at 298 K in large disagreement with the measurements.^{49, 55, 56, 67} On the other hand, the ratio of H-atom abstraction from the methyl group, divided by the abstraction from the isopropyl group from the theoretical calculations⁷³ ($0.69 \times 10^{-12} \text{ cm}^3 \text{ s}^{-1} / (1.79 + 4.51) \times 10^{-12} \text{ cm}^3 \text{ s}^{-1} = 0.15$), is in good agreement with the experimental values ($2.7 \% / 17.6 \% = 0.15$).⁵⁶

It was found for all aromatics studied that the unimolecular decay of the adducts increased with increasing temperature (fig.6). In all cases, the decomposition of adduct 2 was much slower than for adduct 1, with rates increasing from about $2\text{-}6 \text{ s}^{-1}$ at room temperature to 30 s^{-1} , 33 s^{-1} , 26 s^{-1} , and 51 s^{-1} for p-cymene, 14-DMB, 135-TMB and 1245-TeMB at around 343 K. These rate constants are slightly higher but are still in agreement with the decomposition rate constants of the HMB (*ipso*) adduct, which increased from 8 s^{-1} at 320K to 16 s^{-1} at 345K, which could lead to the preliminary identification of adduct number 2 as the *ipso* adduct. In the case of p-cymene, the theory does not predict any formation of a significant amount of *ipso* adduct, and adduct 2 therefore represents one very stable *ortho*

adduct. The less stable adduct 1 was found to decompose ten times faster than adduct 2 and to be even slightly more unstable than the benzene-OH (*ortho*) adduct.⁷⁴

Overall adduct loss rate constants are described by a modified Arrhenius equation: $k_L = A \times \exp(-B/T) + C$. Parameters A , B , C are presented in table 3. Pre-exponential factors range between 1 and $60 \times 10^{12} \text{ s}^{-1}$ for adduct 1, 10^7 - 10^{12} for adduct 2 and 10^6 - 10^{11} for adduct 2 using the extended triexponential model. These are in reasonable agreement with the expected ones for unimolecular reactions.⁷⁵ Activation energies for the adducts can be obtained directly from parameter B ($E_a = B \times R$). Activation energies for adduct 1 and adduct 2 are rather similar, with values for adduct 1 slightly larger than for adduct 2 in the cases of 14-DMB and 135-TMB, and the opposite for p-cymene and 1245-TMB. Activation energies for 135-TMB are in good agreement, within experimental uncertainties, with previous measurements from Bohn and Zetzsch³⁰ using the triexponential model (81 ± 9 and $42 \pm 8 \text{ kJ mol}^{-1}$ for adduct 1 and 2 respectively) and using the extended triexponential model ($80 \pm 7 \text{ kJ mol}^{-1}$ and $62 \pm 27 \text{ kJ mol}^{-1}$ for adduct 1 and 2 respectively).

Similar to the work of Bohn and Zetzsch,³⁰ the agreement found between the decomposition rates for adduct 1 and for the benzene-OH adduct¹⁷ as well as for adduct 2 and for the HMB-OH adduct,^{33, 54} cannot be reproduced for 135-TMB, comparing the activation energies. The activation energy for the unimolecular decay of HMB is the largest measured for the methylated aromatics ($86 \pm 2 \text{ kJ mol}^{-1}$), but the E_a estimated for the other adducts in this work is rather similar to that determined for the benzene-OH adduct by Perry et al.,⁹ ($78 \pm 8 \text{ kJ mol}^{-1}$) and Knispel et al.¹⁷ ($72 \pm 2 \text{ kJ mol}^{-1}$). Hence, an identification of the adducts formed, based only on the activation energies for the decomposition of the adducts, is not possible. On the other hand, theoretical studies on the reaction of OH radicals with 14-DMB⁷² predicted that the *ortho* adduct would decompose much faster than the *ipso* adduct, in agreement with an identification of adduct 1 as *ortho* and adduct 2 as *ipso*.

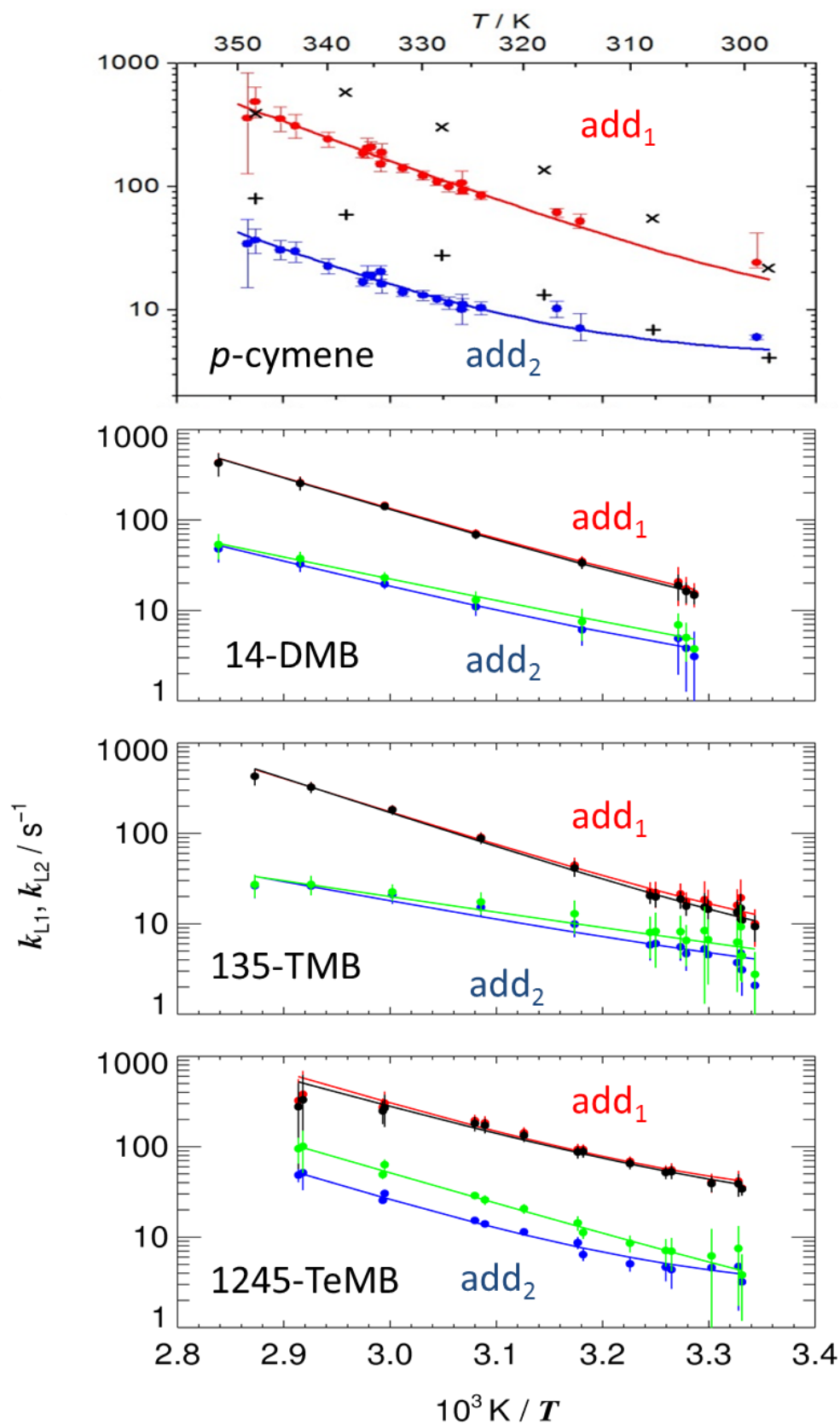


Fig. 6 Arrhenius plots of loss rate constants k_{L1} and k_{L2} of add_1 and add_2 for *p*-cymene, 14-DMB, 135-TMB and 1245-TeMB. Exes and crosses show simulated results from a combined theoretical/experimental approach for *p*-cymene (top). Red: k_{L1} of model-2, black: k_{L1} of model-3, blue: k_{L2} of model-2, and green: k_{L2} of model-3.^{54,55}

EXPERIMENTAL RESULTS AND DISCUSSION

Tab 3 Arrhenius parameters A and B of total adduct loss rate constants according to the equation: $k_L = A \times \exp(-B/T) + C$ of add₁ (left), and add₂ (right). The C parameters were held fixed. They correspond to optimized values according to equations (9), (25) and (37) for model-1, model-2 and model-3, respectively. Error limits do not include potential systematic effects caused by deficiencies of reaction models.

	add ₁			add ₂		
	$\ln(A / \text{s}^{-1})$	$B / 10^3 \text{ K}$	C / s^{-1}	$\ln(A / \text{s}^{-1})$	$B / 10^3 \text{ K}$	C / s^{-1}
model-2						
p-cymene	27.6 ± 0.7	7.6 ± 0.8	7.5	26.4 ± 1.2	8.0 ± 0.3	4.1
14-DMB	29.0 ± 0.5	8.0 ± 0.2	4.1	23.0 ± 0.8	6.7 ± 0.3	1.3
135-TMB	31.0 ± 0.9	8.6 ± 0.3	3.9	18.3 ± 1.4	5.1 ± 0.4	1.2
1245-TeMB	30.1 ± 1.5	8.2 ± 0.5	22.8	28.5 ± 1.5	8.4 ± 0.5	2.5
model-3						
14-DMB	29.3 ± 0.5	8.2 ± 0.2	3.5	20.1 ± 1.1	5.7 ± 0.3	0.5
135-TMB	31.7 ± 0.8	8.9 ± 0.2	2.8	15.3 ± 1.3	4.1 ± 0.4	0.5
1245-TeMB	28.2 ± 1.2	7.5 ± 0.4	16.3	27.5 ± 1.3	7.9 ± 0.4	0.5
model-1						
benzene ^a	29.8 ± 0.8	8.6 ± 0.3	0.0	–	–	–
HMB	32.3 ± 0.5	10.4 ± 0.2	8.7	–	–	–

^a Evaluated from k_R data by Knispel et al.,¹⁷ $k_L = k_R + \text{adduct background loss rate constant}$.

Parameter C represents irreversible losses of the adducts without formation of OH radicals (similar to the H-atom abstraction). These values were optimized using eqns. 9, 25 and 37 for the biexponential, triexponential and extended triexponential model, respectively, and were found to be in reasonable agreement among them ($<7\text{s}^{-1}$), except in the case of 1245-TeMB with extremely large adduct loss rates for adduct 1. We speculate that the high losses observed for adduct 1 for 1245-TeMB could be explained by an unknown unimolecular loss reaction (rearrangement or dealkylation).

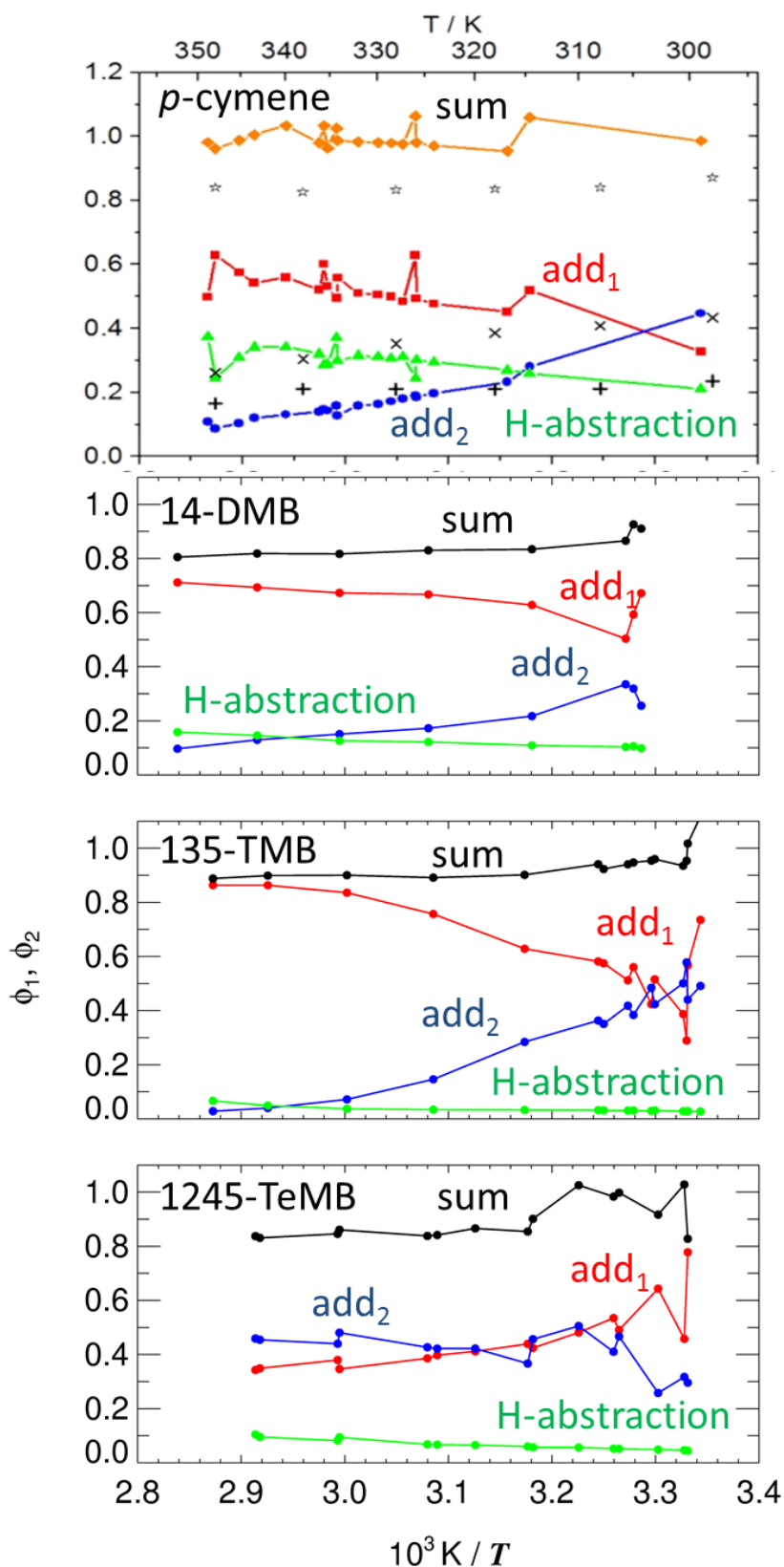


Fig. 7 Formation yields for add_1 (red), add_2 (blue), H-atom abstraction (green) and sum (orange for *p*-cymene and black for the rest) after optimization of k_{31} and k_{32} for *p*-cymene, 14-DMB, 135-TMB and 1245-TeMB. Exes (add_2), crosses (add_1) and stars ($\text{add}_1+\text{add}_2$) show simulated results from a combined theoretical/experimental approach for *p*-cymene (top).

Estimated formation yields for both adducts (Φ_1 and Φ_2) are shown in fig. 7. At room temperature, Φ_1 and Φ_2 are relatively similar for p-cymene and 135-TMB, while for 14-DMB and 1245-TeMB adduct 1 was predominantly formed. Nevertheless, for all studied compounds, formation yield for one adduct increased with temperature (Φ_1 for p-cymene, 14-DMB, 135-TMB and Φ_2 for 1245-TeMB), while for the other adduct the opposite behaviour was observed. Small values of Φ_2 at high temperatures explain why the OH decays turned biexponential with increasing temperatures. After subtraction of the abstraction contribution, the experimental formation yields at room temperature for 14-DMB are in good agreement with the theoretically predicted values by Fan and Zhang⁷² of about 20:80 *ipso:ortho* branching ratio.

Rate constants for unimolecular decays and formation yields, estimated from the simulated OH decays for the OH+p-cymene reaction, are not in disagreement with the experimental values; however, contrary to the experimentally observed ones, about 10% of the sum of formation yields from the simulated decays are missing. These are attributed to the dealkylation of the *ipso*-C₃H₇ adduct.

4.5 Equilibrium constants and thermodynamics of the adducts.

Equilibrium constants, as mentioned in section 3, can be estimated from the fitted parameters bc, d, ef and g, provided that the adduct background losses are known. Equilibrium constants for p-cymene and the methylated aromatics (fig. 8) are located between the equilibrium constants for the reaction of benzene and HMB with OH radicals, represented as dotted and dashed lines, respectively. These two aromatics react with OH radicals to form one adduct alone, with the first being a model compound for non-*ipso* OH addition and the latter being for pure *ipso* addition. Therefore, model-1 (the biexponential model) is sufficient to describe the measurements. Equilibrium constants for benzene were estimated from the results of Knispel et al.,¹⁷ while equilibrium constants for HMB were determined by re-evaluation of the measurements by von Buttlar et al.³³ Entropies of formation for the reaction of both aromatics with OH radicals are similar, as expected from association reactions, while the enthalpy for the HMB reaction is 26 kJmol⁻¹ larger than the respective enthalpy for benzene (tab.7).

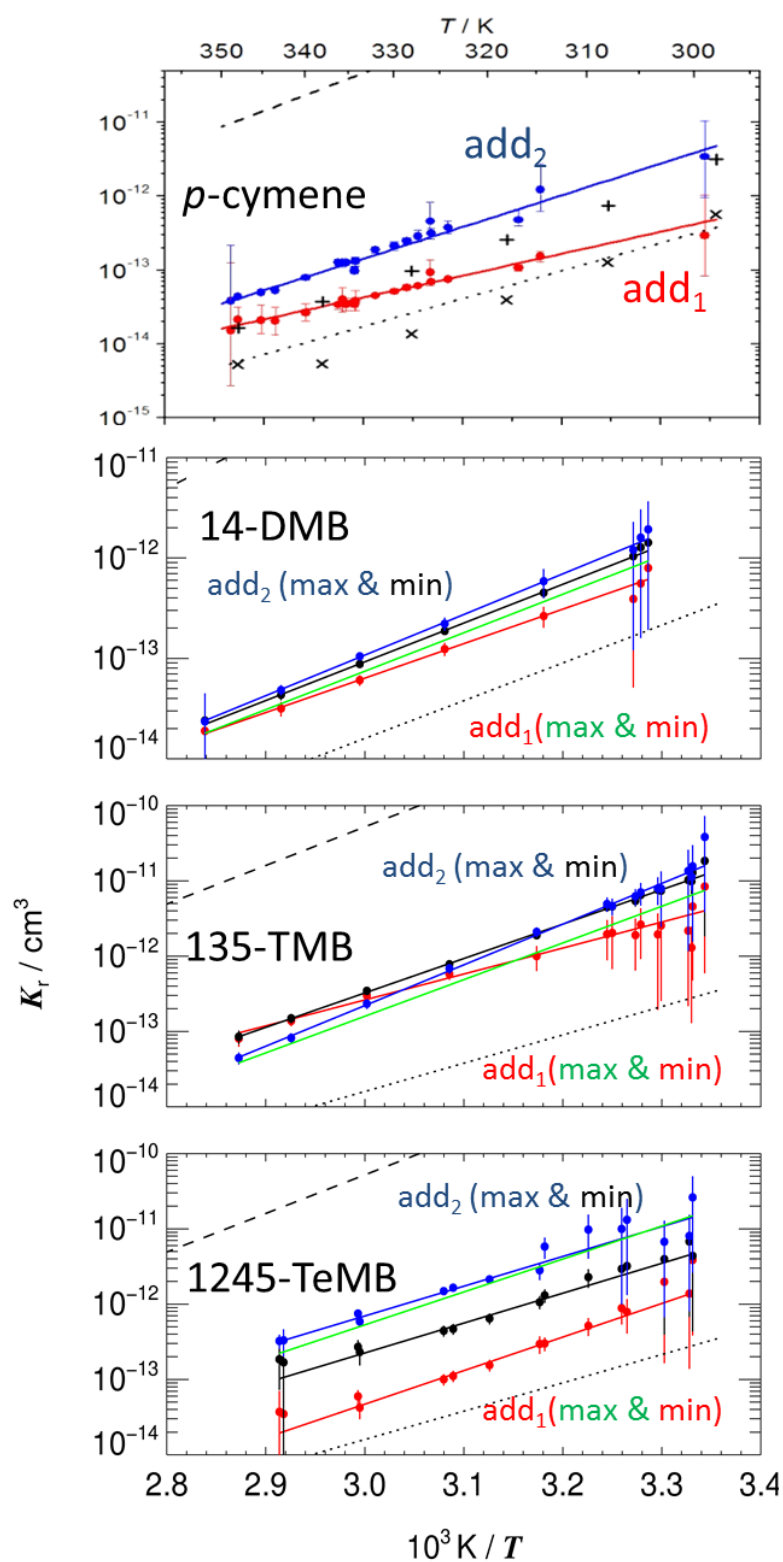


Fig. 8. Van't Hoff plots of equilibrium constants for *p*-cymene, 14-DMB, 135-TMB and 1245-TeMB. Exes and crosses show the simulated results from a combined theoretical/experimental approach for add_1 and add_2 of *p*-cymene. Red: $K_{c1} = k_{11a}/k_{-11a}$ of model-2, blue: $K_{c2} = k_{12a}/k_{-12a}$ of model-2, and black: $K_{c1} = k_{11a}/k_{-11a}$ of model-3. Green lines show the limiting K_{c2} of model-3 according to equation (40), dotted, and dashed lines show model-1 results for benzene and HMB for comparison.

Equilibrium constants for adduct 1, determined by model-2 and model-3 for 14-DMB, 135-TMB and 1245-TeMB, show large differences with a maximum K_c given by model-3 and a minimum given by model-2. Furthermore, equilibrium constants for adduct 2 are higher than the upper limit of adduct 1 (model-3), except in the case of 135-TMB where the equilibrium constants for both adducts crossed each other. This behaviour can be attributed to some discrepancies observed for adduct 2 for this compound in this work and in agreement with a previous work³⁰: while for both adducts of all studied compounds the slope in the Arrhenius plots of $k_f \times k_r$ was negative (i.e., sum of activation energies for the forward and backward reaction was positive), the opposite behaviour was observed for adduct 2 of 135-TMB (fig. 9). This seems very unlikely, as the OH radical addition is expected to have a negative activation energy and moreover, the activation energy of the unimolecular decay was estimated in this work to be also negative. Furthermore, formation enthalpy for adduct 2 (Tab.4) is very large, while the activation energy for the decomposition of the adduct is low. For the other aromatics, no such discrepancies were observed. Hence, in the specific case of 135-TMB, results obtained with model-3 are expected to be more reliable than those obtained with model-2.

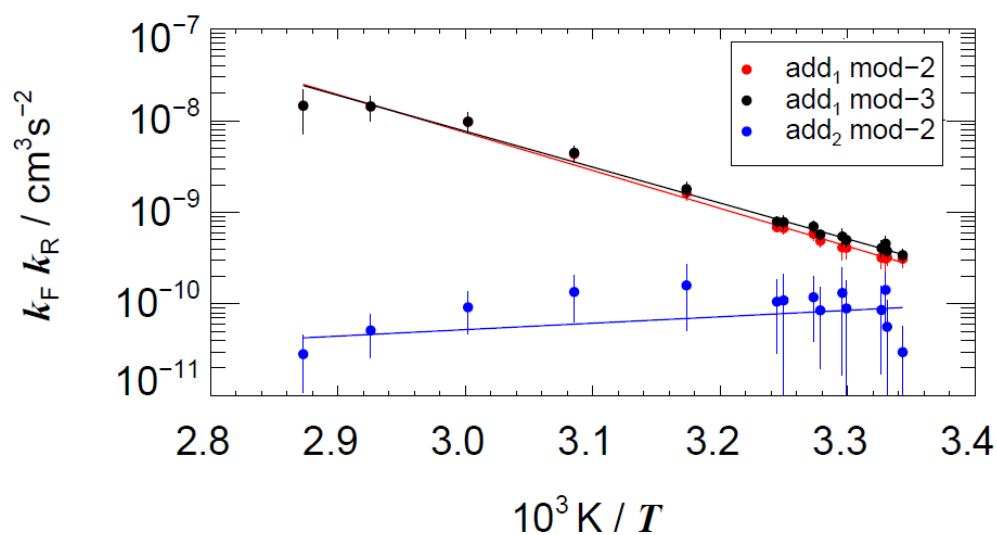


Fig. 9 Arrhenius plots of product of forward and backward rate constants for 135-TMB. Red: $k_{11a} \times k_{-11a}$ (add₁) of model-2; blue: $k_{12a} \times k_{-12a}$ (add₂) of model-2; black: $k_{11a} \times k_{-11a}$ (add₁) of model-3

Equilibrium constants estimated for the p-cymene reaction follow the same pattern shown for the methylated benzenes, with K_c for adduct 2 larger than the respective for adduct

1 in the temperature range studied. Moreover, equilibrium constants calculated from simulated OH decays combining experimental results and theoretical calculations are in reasonable agreement with equilibrium constants experimentally obtained.

Enthalpies and entropies, determined by fitting van't Hoff equations (eqn. 38 and eqn. 39) to the obtained equilibrium constants are shown in table 4. In the case of p-cymene, the entropy of formation for adduct 1 is much smaller than predicted for several aromatics,^{59, 72, 76-78} including our own work.⁵⁵ Moreover, the formation enthalpy is too small, not corresponding to an association reaction, and if anything, reaction enthalpies are expected to be similar for both adducts.⁵⁵ These disagreements indicate the possible contribution of the *ipso* adducts of p-cymene, which cause the reaction mechanism to deviate from a 2-adduct to a very likely 3- and not necessarily impossible 4-adduct system. Nevertheless, based on the unimolecular decays and the equilibrium constants, the adducts formed from the OH + p-cymene reaction were identified as *ortho*-C₃H₇ (adduct 1) and *ortho*-CH₃ (adduct 2).

$$K_c = \frac{k_F}{k_R} = \frac{k_B T}{p^\circ} \times \exp\left(\frac{-\Delta H_{r,m}^\circ}{RT} + \frac{\Delta S_{r,m}^\circ}{R}\right) \quad (38)$$

$$K_i = \frac{k_F}{k_R} = \frac{k_{12}}{k_{21}} = \exp\left(\frac{-\Delta H_{r,m}^\circ}{RT} + \frac{\Delta S_{r,m}^\circ}{R}\right) \quad (39)$$

Tab. 4 Parameters A and B and corresponding molar reaction enthalpies $\Delta H_{r,m}^\circ$ and entropies $\Delta S_{r,m}^\circ$ describing equilibrium constants of reversible OH + aromatics reactions according to the equation: $K_c = A \times T \times \exp(-B/T)$ and of adduct isomerization according to the equation: $K_i = A \times \exp(-B/T)$. Error limits do not include potential systematic effects caused by deficiencies of reaction models.

	$\ln(A / \text{K}^{-1}\text{cm}^3)$	$B / 10^3 \text{ K}$	$\Delta S_{r,m}^\circ / \text{J K}^{-1} \text{ mol}^{-1}$	$\Delta H_{r,m}^\circ / \text{kJ mol}^{-1}$	$\ln(A / \text{K}^{-1}\text{cm}^3), \ln(A)$	$B / 10^3 \text{ K}$	$\Delta S_{r,m}^\circ / \text{J K}^{-1} \text{ mol}^{-1}$	$\Delta H_{r,m}^\circ / \text{kJ mol}^{-1}$
model-2	OH + aromatic \rightarrow add ₁				OH + aromatic \rightarrow add ₂			
p-cymene	-58.0 ± 0.7	-7.1 ± 0.1	-64 ± 6	-59 ± 1	-66.0 ± 3.3	-10.2 ± 1.2	-130 ± 27	-85 ± 10
14-DMB	-60.9 ± 0.6	-8.2 ± 0.2	-88 ± 5	-68 ± 2	-64.6 ± 0.6	-9.6 ± 0.2	-119 ± 5	-80 ± 2
135-TMB	-59.6 ± 1.3	-8.3 ± 0.4	-77 ± 11	-69 ± 4	-73.3 ± 0.7	-12.8 ± 0.2	-191 ± 6	-106 ± 2
1245-TeMB	-68.3 ± 2.2	-10.6 ± 0.7	-149 ± 18	-88 ± 6	-62.1 ± 1.8	-9.4 ± 0.6	-98 ± 15	-78 ± 5
model-3	OH + aromatic \rightarrow add ₁				add ₁ \rightarrow add ₂			
14-DMB	-63.5 ± 0.4	-9.2 ± 0.1	-109 ± 4	-77 ± 1	-0.03 ± 0.65	0.1 ± 0.2	-0.2 ± 5.4	0.5 ± 1.8
135-TMB	-67.1 ± 0.3	-10.8 ± 0.1	-139 ± 3	-90 ± 1	-2.8 ± 0.6	-0.7 ± 0.2	-23 ± 5	-6 ± 2
1245-TeMB	-63.3 ± 1.9	-9.5 ± 0.6	-108 ± 16	-79 ± 5	-1.95 ± 1.3	-0.9 ± 0.4	-16 ± 11	-8 ± 3
model-1	OH + aromatic \rightarrow add							
benzene ^a	-64.5 ± 1.4	-9.0 ± 0.4	-118 ± 11	-75 ± 4	-	-	-	-
HMB	-65.9 ± 1.1	-12.1 ± 0.4	-130 ± 9	-101 ± 3	-	-	-	-

^a Evaluated from k_F and k_R data by Knispel et al.,¹⁷ $K_c = k_F/k_R$.

For the other aromatics, excluding the aforementioned unlikely large enthalpy estimated for 135-TMB, reaction entropies and enthalpies are roughly similar. Equilibrium constants for the isomerization, K_i , show a small temperature dependence (fig. 10) with respective low reaction entropies and enthalpies. As mentioned before, a maximum for the

equilibrium constant for adduct 1 is obtained from mod-3, while a minimum is obtained from mod-2. In the case of adduct 2, a minimum value of K_{c2} for mod-3, as well as a maximum value of K_i for mod-2 can be estimated using a relationship obtained from the analytical solutions for the general mechanism (eq. 40).⁵⁴ Estimated limits for K_{c2} and K_i are shown in fig. 8 and 10.

$$K_i = \frac{K_{c2}}{K_{c1}} = \frac{[k_{12a}k_{-12a}] \times (k_{L1} - k_{12} - k_{31})^2}{[k_{11a}k_{-11a}] \times (k_{L2} - k_{21} - k_{32})^2} \quad (40)$$

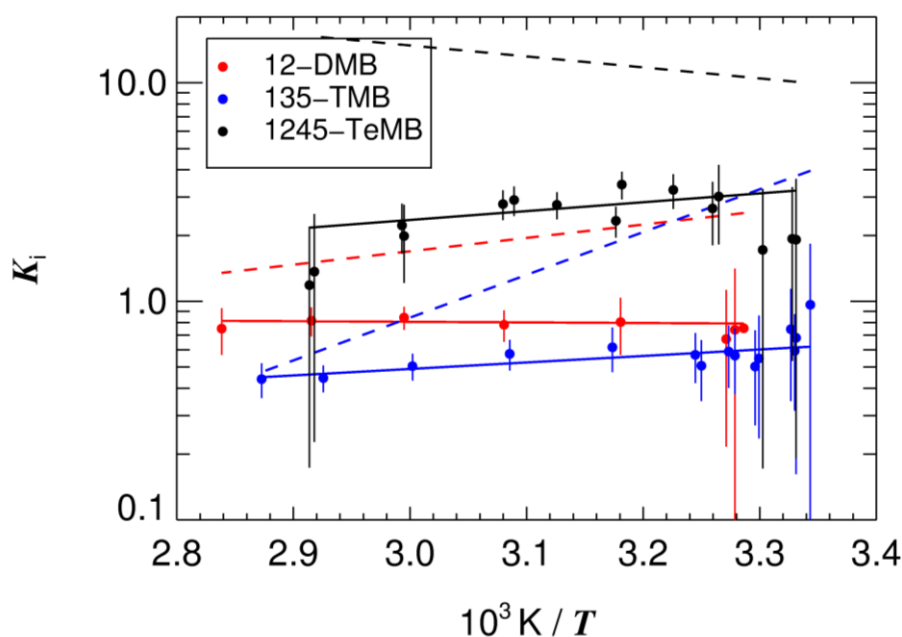


Fig. 10. Van't Hoff plots of equilibrium constants for isomerization $K_i = k_{12}/k_{21}$ of model-3 for 14-DMB (red), 135-TMB (blue), and 1245-TeMB (black). The dashed curves show the calculated, limiting K_i of model-2 according to equation (40).

Experimental results for 14-DMB, 135-TMB and 1245-TeMB were insufficient to determine which model (mod-2 or mod-3) could better explain the reaction mechanism. Only for 135-TMB, one model can be preferred over the other due to discrepancies observed for adduct 2 using mod-2. However, this behaviour was not observed for the other aromatics. Isomerization of one adduct into the other, despite small, is not negligible and therefore one might expect that the real reaction mechanism lies between mod-2 and mod-3.

Theoretical studies of the reaction of OH with toluene predict the predominance of the *ortho*-OH-adduct formation as summarized in tab. 5. From the non-*ipso* adducts the *para* is slightly favoured against the *meta* adduct as one would expect from the *ortho-para* activating

property of the OH-radical addition, and this is further confirmed by the high yield of *o*-cresol experimentally observed. *Ips*o-adduct formation yield has been predicted to range from 3% up to 15% and in one case even 57%; however, this high value might be an overestimation by the level of theory applied.⁵⁹ Similar theoretical studies have been performed for *o*-, *m*- and *p*-xylene^{72, 79-81} and *p*-cymene,⁵⁵ predicting a predominant OH radical addition at *ortho* positions. However, the stability of the *ip*so adduct was predicted to be larger than for the other adducts. These predictions can be used to identify the adducts formed in this work.

Tab. 5. Summary of formation yields predicted by theoretical studies on OH + toluene and cresol formation determined experimentally.

	Predicted formation yield (%)						Cresol formation (%)
	Uc et al. ⁵⁹		Suh et al. ⁷⁶	Wu et al. ⁸²			
	PMP2 ^a	B3LYP ^a	B3LYP ^a	M06-2X ^a	G3MP2 ^a	ROCBS ^a	
<i>ip</i> so	57	4	3	4	7	15	-
<i>ortho</i>	40	85	54	63	52	59	12 – 39 ⁸³⁻⁸⁹
<i>meta</i>	2	5	11	2	3	5	2.6±0.3 ⁸⁸ 2.7±0.7 ⁸⁹
<i>para</i>	1	7	34	24	31	14	3.0±0.3 ⁸⁸ 3.2±0.6 ⁸⁹

^aLevel of theory applied for the theoretical calculations.

Adduct 1 was estimated to be formed at higher or similar yield than adduct 2 at room temperature. On the other hand, decomposition rate constants for adduct 2 are about 10 times smaller than the respective one for adduct 1. Comparing these experimental observations with the theoretical predictions mentioned above, the adducts formed in this study are identified as *ip*so = adduct 2 and *ortho* = adduct 1.

4.6 Dealkylation of OH-aromatic adducts.

Dealkylation pathways have been measured for different alkylated aromatics. Noda et al.,⁹⁰ determined (5.4±1.2)% of phenol-formation yield from the toluene reaction with OH radicals, (11.2±3.8), (4.5±3.1) and (4.3±3.1) % of cresol-formation yield for 13-, 12-, and 14-DMB. Due to the lack of knowledge about the importance of *ip*so adducts, these authors proposed a reaction pathway for the dealkylation *via* OH-radical addition to a free position with subsequent OH migration. As mentioned in the introduction, Berndt and Böge⁴² observed hexamethyl-2,4-cyclohexadienone as a product of the reaction of OH radicals with HMB. For this compound, the only possible reaction pathway is the *ip*so addition. Further investigation, comprising theoretical calculations and fast flow reactor experiments (coupled with a mass spectrometer) was done by Loison et al.³² Theoretical calculations predicted the activation energy for the dealkylation channel to be just 1 kJ mol⁻¹ below the energy of the reactants and the overall reaction energy to be exothermic by 42 kJ mol⁻¹.³² These authors also determined a dealkylation rate constant of $k_{\text{dealk}} = (2.4 \pm 1.4) \times 10^{12} \exp(-10200 \text{ K}/T) \text{ s}^{-1}$

for HMB, which corresponds to $3.3 \times 10^{-3} \text{ s}^{-1}$ and 2.56 s^{-1} at 298 and 370 K, respectively. Aschmann et al.⁵⁶ determined <1% *o*-, *m*-, *p*-cresol-formation yields from the reaction of 13-DMB with OH radicals, and <2% for *p*-cymene in a 7000 L volume Teflon chamber at 297 K. Moreover, as mentioned above, theoretical calculations presented by Alarcon et al.,⁵⁵ also predicted overall reaction energies for the dealkylation pathway of the *ipso*-C₃H₇ adduct to form *p*-cresol and 4-isopropylphenol to be exothermic by 38 and 52 kJ mol⁻¹. Until now, only Noda et al.,⁹⁰ determined high dealkylation yields, however, as later indicated,⁵⁶ the ion peaks observed by these authors could have been due to formation of oxepins and methyloxepins. Thus, dealkylation of *ipso* adducts seems to play a minor role in the global reaction mechanism. Dealkylation in our mechanistic models can be extracted from the temperature-independent parameter C (table 3). As it was mentioned above, parameters C are found typically below 4s⁻¹, except add₁ of *p*-cymene, 1245-TeMB and HMB. For HMB, it can be clearly seen that parameter C does not correspond only to dealkylation processes. The adduct-loss rate found in this work is much higher than the one estimated by Loison et al., at 370 K. In the case of *p*-cymene, this high value for C of add₁ can be attributed to deviations from the triexponential model due to the *ipso* adducts. However, no explanation can be given for the very large value found for parameter C of add₁ for 1245-TeMB, since it would be very unlikely for this compound to dealkylate faster than the fully substituted HMB.

5 CONCLUSIONS

The reaction of OH radicals with alkylated compounds was studied using flash photolysis of water vapour and time-resolved detection of OH by resonance fluorescence and multichannel scaling between room temperature and about 350 K. Rate constants for the overall reaction for 14-DMB, 135-TMB, 1245-TeMB, PMB and *p*-cymene at room temperature are in good agreement with the available literature. Furthermore, rate constants for 1234-TeMB and 1235-TeMB, never measured before, were obtained in this work and were found to be slightly higher than 135-TMB and below PMB. Measurements performed with HMB by von Buttler et al.,³³ were re-evaluated using an improved fit analysis, and the obtained rate constant at room temperature was in agreement with their results but in disagreement with the other only work on HMB from Berndt and Böge.⁴² Nevertheless, for all aromatic studied, negative activation energies of addition were obtained, in agreement with the formation of a pre-reactive complex as predicted theoretically. Reaction mechanisms of aromatic compounds which react with OH radicals to form only two adducts (i.e., *p*-cymene,

14-DMB, 135-TMB and 1245-TeMB) were investigated assuming direct formation of both adducts (mod-2) and direct formation of one adduct and isomerization into the other (mod-3). Triexponential decay curves gave indication of the formation of two adducts and therefore of the formation of the so long neglected *ipso* adducts. Furthermore, it was observed that, independent of the applied model, adduct 1 decomposed much faster than adduct 2, and the latter adduct decomposed at similar rates as the HMB-OH adduct. Formation yields in the studied temperature range estimate the formation of adduct 1 in the same or slightly higher proportion at room temperature, and while with increasing temperatures the formation of one adduct increases, the opposite behaviour for the other adduct is observed. Equilibrium constants, reaction entropies and enthalpies were estimated using both models. Equilibrium constants were located between the estimated equilibrium constants for the reaction with OH+benzene and OH+HMB. Entropies for all adducts are roughly similar and in agreement with theoretical predictions. However, some discrepancies were observed for p-cymene which were attributed to the non-negligible formation of *ipso* adducts at the methyl and at the isopropyl position. Reaction enthalpies were found to be slightly larger for adduct 2 than for adduct 1, except for 1245-TeMB (in which both enthalpies are comparable within experimental uncertainties). However, the reaction enthalpy estimated for adduct 2 of 135-TMB is unrealistically high, which (together with the low activation energy estimated for the unimolecular decay) gave indication of problems with mod-2 for this specific compound. Theoretical calculations, performed for p-cymene by colleagues at Bordeaux, predicted the preferable formation of non-*ipso* adducts and a small production of *ipso*-C₃H₇ adduct (predicted formation yield 18%) which would further dealkylate to form p-cresol. Despite the low formation of the *ipso*-CH₃ adduct and the dealkylation of *ipso*-C₃H₇ adduct, it was observed that these adducts contributed in a lesser extent to the OH decays measured in this work. Nevertheless, based on the experimental results, theoretical predictions and simulated experiments, adduct 1 and 2 were identified as *ortho*-C₃H₇ and *ortho*-CH₃, respectively. In an analogous manner, theoretical predictions available in the literature were compared with experimental results. Based on reaction enthalpies for the adducts and decomposition rates, adduct 1 and 2 were identified as *ortho* and *ipso*. In this work, it was not possible to determine which model (mod-2 or mod-3) better describes the experimental results. Fit quality obtained from both models was exactly the same, and, except for 135-TMB, both models delivered realistic values. It is likely that the real mechanism lies somewhere between mod-2 and mod-3. Nevertheless, this work served to demonstrate the importance of *ipso* adducts and the feasibility of isomerization reactions.

REFERENCES

1. R. Koppmann, *Volatile Organic Compounds in the Atmosphere*, Wiley, United Kindom, 2008.
2. K. H. Kim, H. H. Chun and W. K. Jo, *Environ. Monit. Assess.*, 2015, 187, 12.
3. R. G. Derwent, J. I. R. Dernie, G. J. Dollard, P. Dumitrescu, R. F. Mitchell, T. P. Murrells, S. P. Telling and R. A. Field, *Atmos. Environ.*, 2014, 99, 239-247.
4. A. Guenther, C. Geron, T. Pierce, B. Lamb, P. Harley and R. Fall, *Atmos. Environ.*, 2000, 34, 2205-2230.
5. J. G. Calvert, R. Atkinson, K. H. Becker, R. M. Kamens, J. H. Seinfeld, T. J. Wallington and G. Yarwood, *The Mechanism of Atmospheric Oxidation of Aromatic Hydrocarbons*, Oxford University Press, New York, 2002.
6. D. D. Davis, W. Bollinger and S. Fischer, *J. Phys. Chem.*, 1975, 79, 293-294.
7. T. Ohta and T. Ohshima, *B. Chem. Soc. Jpn*, 1985, 58, 3029-3030.
8. D. A. Hansen, R. Atkinson and J. N. Pitts, *J. Phys. Chem.*, 1975, 79, 1763-1766.
9. R. A. Perry, R. Atkinson and J. N. Pitts, *J. Phys. Chem.*, 1977, 81, 296-304.
10. R. A. Cox, R. G. Derwent and M. R. Williams, *Environ. Sci. Technol.*, 1980, 14, 57-61.
11. F. P. Tully, A. R. Ravishankara, R. L. Thompson, J. M. Nicovich, R. C. Shah, N. M. Kreutter and P. H. Wine, *J. Phys. Chem.*, 1981, 85, 2262-2269.
12. K. Lorenz and R. Zellner, *Ber. Bunsenges. Physikal. Chem*, 1983, 87, 629-636.
13. A. Wahner and C. Zetzsch, *J. Phys. Chem.*, 1983, 87, 4945-4951.
14. M. Rinke and C. Zetzsch, *Ber. Bunsenges. Physikal. Chem*, 1984, 88, 55-62.
15. F. Witte, E. Urbanik and C. Zetzsch, *J. Phys. Chem.*, 1986, 90, 3251-3259.
16. T. J. Wallington, D. M. Neuman and M. J. Kurylo, *Int. J. Chem. Kinet.*, 1987, 19, 725-739.
17. R. Knispel, R. Koch, M. Siese and C. Zetzsch, *Ber. Bunsenges. Phys. Chem*, 1990, 94, 1375-1379.
18. R. Sommerlade, H. Parlar, D. Wrobel and P. Kochs, *Environ. Sci. Technol.*, 1993, 27, 2435-2440.
19. D. Davis and W. Braun, *Appl. Optics*, 1968, 7, 2071-2074.
20. G. J. Doyle, A. C. Lloyd, K. R. Darnall, A. M. Winer and J. N. Pitts, *Environ. Sci. Technol.*, 1975, 9, 237-241.
21. E. O. Edney, T. E. Kleindienst and E. W. Corse, *Int. J. Chem. Kinet.*, 1986, 18, 1355-1371.
22. R. Atkinson and S. M. Aschmann, *Int. J. Chem. Kinet.*, 1989, 21, 355-365.
23. B. J. Finlayson-Pitts, S. K. Hernandez and H. N. Berko, *J. Phys. Chem.*, 1993, 97, 1172-1177.
24. P. N. Anderson and R. A. Hites, *Environ. Sci. Technol.*, 1996, 30, 301-306.
25. F. Kramp and S. E. Paulson, *J. Phys. Chem. A*, 1998, 102, 2685-2690.
26. A. R. Ravishankara, S. Wagner, S. Fischer, G. Smith, R. Schiff, R. T. Watson, G. Tesi and D. D. Davis, *Int. J. Chem. Kinet.*, 1978, 10, 783-804.
27. J. M. Nicovich, R. L. Thompson and A. R. Ravishankara, *J. Phys. Chem.*, 1981, 85, 2913-2916.
28. A. C. Lloyd, K. R. Darnall, A. M. Winer and J. N. Pitts, *J. Phys. Chem.*, 1976, 80, 789-794.

29. D. Mehta, A. Nguyen, A. Montenegro and Z. Li, *J. Phys. Chem. A*, 2009, 113, 12942-12951.
30. B. Bohn and C. Zetzsch, *Phys. Chem. Chem. Phys.*, 2012, 14, 13933-13948.
31. S. M. Aschmann, J. Arey and R. Atkinson, *J. Phys. Chem. A*, 2013, 117, 2556-2568.
32. J.-C. Loison, M.-T. Rayez, J.-C. Rayez, A. Gratien, P. Morajkar, C. Fittschen and E. Villenave, *J. Phys. Chem. A*, 2012, 116, 12189-12197.
33. J. von Buttler, R. Koch, M. Siese and C. Zetzsch, *Geophysical Research Abstracts*, 2008, 10, EGU2008-A-10576.
34. M. E. Jenkin, J. C. Young and A. R. Rickard, *Atmos. Chem. Phys. Discuss.*, 2015, 15, 9709-9766.
35. M. E. Jenkin, K. P. Wyche, C. J. Evans, T. Carr, P. S. Monks, M. R. Alfarra, M. H. Barley, G. B. McFiggans, J. C. Young and A. R. Rickard, *Atmos. Chem. Phys.*, 2012, 12, 5275-5308.
36. C. Bloss, V. Wagner, M. E. Jenkin, R. Volkamer, W. J. Bloss, J. D. Lee, D. E. Heard, K. Wirtz, M. Martin-Reviejo, G. Rea, J. C. Wenger and M. J. Pilling, *Atmos. Chem. Phys.*, 2005, 5, 641-664.
37. M. E. Jenkin, S. M. Saunders, V. Wagner and M. J. Pilling, *Atmos. Chem. Phys.*, 2003, 3, 181-193.
38. S. M. Saunders, M. E. Jenkin, R. G. Derwent and M. J. Pilling, *Atmos. Chem. Phys.*, 2003, 3, 161-180.
39. M. E. Jenkin, S. M. Saunders and M. J. Pilling, *Atmos. Environ.*, 1997, 31, 81-104.
40. R. Atkinson, *J. Phys. Chem. Ref. Data. Monograph 1*, 1989.
41. V. H. Uc, J. R. I. Alvarez-Idaboy, A. Galano and A. Vivier-Bunge, *J. Phys. Chem. A*, 2008, 112, 7608-7615.
42. T. Berndt and O. Böge, *Int. J. Chem. Kinet.*, 2001, 33, 124-129.
43. R. Koch and C. Zetzsch, Bunsentagung Erlangen, 2006.
44. C. Zetzsch, *Final report ATMOCHEM – Novel Approaches in the Understanding of Aromatic Compound Degradation in the Atmosphere: From Theoretical Studies to Simulation Chamber Experiments*, 2015.
45. R. Knispel, PhD Dissertation, Reaktionen von OH-Radikalen mit Aromaten und Folgereaktionen entstandener OH-Addukte von Aromaten, University of Hannover, 1993.
46. R. Koch, R. Knispel, M. Elend, M. Siese and C. Zetzsch, *Atmos. Chem. Phys.*, 2007, 7, 2057-2071.
47. R. Koch, PhD Dissertation, Kinetische Untersuchung der Folgereaktionen der OH-Addukte von Aromaten mit NO, NO₂ und O₂ mit simultaner Auswertung von Kurvenscharen, University of Hannover, 1992.
48. F. Stuhl and H. Niki, *J. Chem. Phys.*, 1972, 57, 3677.
49. P. Alarcon, R. Strekowski and C. Zetzsch, *Phys. Chem. Chem. Phys.*, 2013, 15, 20105-20114.
50. S. Zhang, R. Strekowski, L. Bosland, A. Monod and C. Zetzsch, *Phys. Chem. Chem. Phys.*, 2011, 13, 11671 - 11677.
51. S. Zhang, R. S. Strekowski, L. Bosland, A. Monod and C. Zetzsch, *Int. J. Chem. Kinet.*, 2011, 43, 547-556.
52. S. Zhang, R. S. Strekowski, A. Monod, L. Bosland and C. Zetzsch, *J. Phys. Chem. A*, 2012, 116, 9497-9506.
53. A. C. Davison and D. V. Hinkley, *Bootstrap methods and their application*, Cambridge University Press, Cambridge ; New York, NY, USA, 1997.
54. P. Alarcon, B. Bohn and C. Zetzsch, *Phys. Chem. Chem. Phys.*, 2015, 17, 13053-13065.

55. P. Alarcon, B. Bohn, C. Zetzsch, M. T. Rayez and J. C. Rayez, *Phys. Chem. Chem. Phys.*, 2014, 16, 17315-17326.
56. S. M. Aschmann, J. Arey and R. Atkinson, *Atmos. Environ.*, 2010, 44, 3970-3975.
57. E. S. C. Kwok and R. Atkinson, *Atmos. Environ.*, 1995, 29, 1685-1695.
58. H. Geiger, I. Barnes, K. Becker, B. Bohn, T. Brauers, B. Donner, H.-P. Dorn, M. Elend, C. Freitas Dinis, D. Grossmann, H. Hass, H. Hein, A. Hoffmann, L. Hoppe, F. Hülsemann, D. Kley, B. Klotz, H. Libuda, T. Maurer, D. Mihelcic, G. Moortgat, R. Olariu, P. Neeb, D. Poppe, L. Ruppert, C. Sauer, O. Shestakov, H. Somnitz, W. Stockwell, L. Thüner, A. Wahner, P. Wiesen, F. Zabel, R. Zellner and C. Zetzsch, *J. Atmos. Chem.*, 2002, 42, 323-357.
59. V. H. Uc, I. García-Cruz, A. Hernández-Laguna and A. Vivier-Bunge, *J. Phys. Chem. A*, 2000, 104, 7847-7855.
60. R. M. Stephenson, S. Malanowski and D. Ambrose, *Handbook of the thermodynamics of organic compounds*, Elsevier, 1987.
61. M. Colomina, P. Jiménez, M. V. Roux and C. Turrión, *J. Chem. Thermodyn.*, 1989, 21, 275-281.
62. V. Ruzicka Jr, M. Zabransky, K. Ruzicka and V. Majer, *Thermochim. Acta*, 1994, 245, 121-144.
63. S. M. Aschmann, W. D. Long and R. Atkinson, *J. Phys. Chem. A*, 2006, 110, 7393-7400.
64. J. E. Overberger, W. A. Steele and J. G. Aston, *J. Chem. Thermodyn.*, 1969, 1, 535-542.
65. D. Ambrose, I. J. Lawrenson and C. H. S. Sprake, *J. Chem. Thermodyn.*, 1976, 8, 503-504.
66. S. M. Aschmann, E. C. Tuazon and R. Atkinson, *J. Phys. Chem. A*, 2005, 109, 2282-2291.
67. S. B. Corchnoy and R. Atkinson, *Environ. Sci. Technol.*, 1990, 24, 1497-1502.
68. C. Zetzsch, Predicting the rate of OH-addition to aromatics using σ^+ -electrophilic substituent constants for mono- and polysubstituted benzene, Proc. XVth Informal Conference on Photochemistry, Stanford, CA (USA), 1982, http://www.bayceer.uni-bayreuth.de/atchem/data/aro_ref/aro82.pdf
69. U. S. EPA, 2012, Estimation Programs Interface Suite TM for Microsoft (r) Windows, United States Environmental Protection Agency, Washington, DC, USA,
70. D. L. Singleton and R. J. Cvetanovic, *J. Am. Chem. Soc.*, 1976, 98, 6812-6819.
71. R. A. Kenley, J. E. Davenport and D. G. Hendry, *J. Phys. Chem.*, 1981, 85, 2740-2746.
72. J. Fan and R. Zhang, *J. Phys. Chem. A*, 2006, 110, 7728-7737.
73. M. R. Dash and B. Rajakumar, *Chemical Physics Letters*, 2014, 597, 75-85.
74. F. Witte, A. Wahner and C. Zetzsch, *B. Soc. Chim. Belg.*, 1983, 92, 625-626.
75. G. M. Nazin, *Russian Chemical Reviews*, 1972, 41, 711-725.
76. I. Suh, D. Zhang, R. Zhang, L. T. Molina and M. J. Molina, *Chem. Phys. Lett*, 2002, 364, 454-462.
77. D. Johnson, S. Raoult, R. Lesclaux and L. N. Krasnoperov, *J. Photoch. Photobio. A*, 2005, 176, 98-106.
78. J. M. Andino and A. Vivier-Bunge, in *Adv. Quantum. Chem.*, eds. E. G. Michael and S. J. Matthew, Academic Press, 2008, vol. 55, pp. 297-310.
79. J. Fan and R. Zhang, *J. Phys. Chem. A*, 2008, 112, 4314-4323.
80. M. Huang, W. Zhang, Z. Wang, L. Hao, W. Zhao, X. Liu, B. Long and L. Fang, *Int. J. Quant. Chem.*, 2008, 108, 954-966.
81. M. Q. Huang, Z. Y. Wang, L. Q. Hao and W. J. Zhang, *Comput Theor Chem*, 2011, 965, 285-290.

REFERENCES

82. R. Wu, S. Pan, Y. Li and L. Wang, *J. Phys. Chem. A.*, 2014, 118, 4533-4547.
83. R. Atkinson, W. P. L. Carter, K. R. Darnall, A. M. Winer and J. N. Pitts, *Int. J. Chem. Kinet.*, 1980, 12, 779-836.
84. R. Atkinson, W. P. L. Carter and A. M. Winer, *J. Phys. Chem.*, 1983, 87, 1605-1610.
85. R. Atkinson and S. M. Aschmann, *Int. J. Chem. Kinet.*, 1994, 26, 929-944.
86. M. W. Gery, D. L. Fox, H. E. Jeffries, L. Stockburger and W. S. Weathers, *Int. J. Chem. Kinet.*, 1985, 17, 931-955.
87. R. Seuwen and P. Warneck, *Int. J. Chem. Kinet.*, 1996, 28, 315-332.
88. D. F. Smith, C. D. McIver and T. E. Kleindienst, *J. Atmos. Chem.*, 1998, 30, 209-228.
89. B. Klotz, S. Sørensen, I. Barnes, K. H. Becker, T. Etzkorn, R. Volkamer, U. Platt, K. Wirtz and M. Martín-Reviejo, *J. Phys. Chem. A*, 1998, 102, 10289-10299.
90. J. Noda, R. Volkamer and M. J. Molina, *J. Phys. Chem. A*, 2009, 113, 9658-9666.

APPENDIX A. INDIVIDUAL CONTRIBUTIONS TO THE JOINT PUBLICATIONS

This cumulative thesis consists of publications listed hereafter. Other authors contributed to these papers as well. Therefore my own contribution to the individual manuscripts is specified in this section:

Paper A: Alarcón, P., Strekowski, R., Zetzsch, C., 2013. Reversible addition of the OH radical to p-cymene in the gas phase: Kinetic analysis, assuming formation of a single adduct. Part 1. *Phys. Chem. Chem. Phys.*, 15, 20105.

- Cornelius Zetzsch and Rafal Strekowski (Univ. of Marseille) developed the idea of studying the biogenic aromatic p-cymene.
- Rafal Strekowski performed a first set of experiments as a guest, using a N₂ spark lamp as VUV source. He was supported by the infrastructure ACCENT of the EU and wrote a first draft of the manuscript.
- I carried out all experiments using the Xe flash lamp. I was responsible for the analysis of the obtained data using the old fitting software (written in Turbo Pascal) and the new fitting software (IDL) and for completing the manuscript.
- Cornelius Zetzsch, Birger Bohn and Rafal Strekowski contributed to the manuscript at various stages with advice and fruitful discussions.

Paper B: Alarcón, P., Bohn, B., Zetzsch, C., Rayez, M. T., Rayez, J. C., 2014. Reversible addition of the OH radical to p-cymene in the gas phase: multiple adduct formation. Part 2. *Phys. Chem. Chem. Phys.*, 16, 17315.

- Cornelius Zetzsch developed the idea of improving the analysis of the data of OH + p-cymene, considering the four possible adducts.
- I carried out all experiments using the Xe flash lamp. I was responsible for the analysis of the obtained data using the IDL Software, and for writing the manuscript.
- Marie-Therese Rayez and Jean Claude Rayez (CNRS and Univ. of Bordeaux) were responsible for the prediction of rate constants and adduct yields by theoretical analysis.
- Birger Bohn (Forschungszentrum Jülich) performed numerical simulations joining theoretical predictions and experimental results.
- I was responsible for the coordination of the individual contributions of the co-authors.

- Cornelius Zetsch and Birger Bohn contributed to the manuscript at various stages with advice and fruitful discussions.

Paper C: Alarcón, P., Bohn, B., Zetsch, C., 2015. Kinetic and mechanistic study of the reaction of OH radicals with the methylated benzenes: 1,4- dimethyl-, 1,3,5-trimethyl, 1,2,4,5-, 1,2,3,5-, and 1,2,3,4-tetramethyl-, pentamethyl- and hexamethylbenzene. Phys. Chem. Chem. Phys., 17, 13053-13065

- Cornelius Zetsch developed the idea of investigating the methylated aromatics for a bilateral French-German CNRS/INSU-DFG Project.
- I was responsible for performing the experiments, analysing the results and writing the manuscript.
- Cornelius Zetsch and Birger Bohn contributed to the manuscript at various stages with advice and fruitful discussions.

APPENDIX B. PAPER A: ALARCON ET AL. (2013)

PCCP

RSC Publishing

PAPER

Reversible addition of the OH radical to *p*-cymene in the gas phase: kinetic analysis assuming formation of a single adduct. Part 1

Cite this: *Phys. Chem. Chem. Phys.*, 2013, 15, 20105

Paulo Alarcón,^a Rafal Strekowski^b and Cornelius Zetzsch^{*ac}

A flash photolysis-resonance fluorescence (FP-RF) technique was employed to study the kinetics and mechanism of the reaction of OH radicals with *p*-cymene at temperatures between 297 and 413 K in helium buffer gas. FP-RF experiments involved time-resolved detection of OH radicals by RF following vacuum-UV flash photolysis of H₂O-*p*-cymene-He and H₂O-He mixtures. Biexponential functions were fitted to decays of OH radicals according to reversible addition of OH radicals to *p*-cymene to form a single adduct. A rate constant of $(15.7 \pm 1.1) \times 10^{-12}$ is obtained (in units of cm³ s⁻¹) at room temperature (298 K) for the sum of the addition and abstraction channels ($k_{1a} + k_{1b}$) according to this simplified model. The Arrhenius plot reveals the step function typical of other aromatics and can be described using the expressions: $2 \times 10^{-13} \exp(+1300 \text{ K}/T)$ at temperatures between 297 K and 324 K and $10^{-11} \exp(-250 \text{ K}/T)$ at temperatures between 345 K and 413 K. After consideration of the abstraction channel an equilibrium constant of $k_{1a}/k_{-1a} = 6 \times 10^{-26} \exp(+9700 \text{ K}/T) \text{ cm}^3$ is obtained at temperatures between 297 and 325 K and $2 \times 10^{-36} \exp(+17000 \text{ K}/T) \text{ cm}^3$ at temperatures between 325 and 380 K.

Received 19th July 2013,
Accepted 20th September 2013
DOI: 10.1039/c3cp53040j

www.rsc.org/pccp

1. Introduction

Total regional and global emissions of biogenic compounds have been estimated to be equivalent to or exceed anthropogenic non-methane hydrocarbon emissions.^{1,2} Once emitted into the atmosphere, these biogenic compounds react readily with atmospheric OH radicals to play an important role in tropospheric chemistry including the boundary layer ozone formation in urban and rural settings. However, to date the observed high ozone creation potential of biogenic compounds and even more so of aromatics remains poorly characterized and not fully understood.

The aromatic molecule *p*-cymene (1-methyl-4-isopropyl-benzene) is a compound of biogenic origin emitted into the atmosphere from vegetation. It has been established that direct emissions from vegetation are a major atmospheric source of *p*-cymene.³⁻⁵ Field observations of *p*-cymene emissions from a northern coniferous forest in the United States estimate fluxes of up to $28 \mu\text{g C m}^{-2} \text{ h}^{-1}$, representing about 3% of the total emissions in the northern coniferous forest.⁶

Indirect emissions of *p*-cymene can also occur from the atmospheric transformation of α -pinene.⁷ Laboratory experiments

of *p*-cymene formation in a teflon chamber gave yields of up to 0.12% at 70% relative humidity using acid conditioned walls. Transposing this finding *via* the surface/volume ratio of the chamber to environmental conditions, these authors suggested a contribution to the *p*-cymene emission flux in the northern coniferous forest of up to $0.23 \mu\text{g C m}^{-2} \text{ h}^{-1}$. Furthermore, Aschmann *et al.*⁸ determined the formation of *p*-cymene from the oxidation of the structurally related γ -terpinene by OH radicals with a molar yield of $13.6 \pm 2.5\%$, suggesting a contribution to the *p*-cymene flux up to $0.11 \mu\text{g C m}^{-2} \text{ h}^{-1}$ in the northern coniferous forest, where the direct emissions were estimated to constitute up to $0.8 \mu\text{g C m}^{-2} \text{ h}^{-1}$.⁶

The atmospheric fate of *p*-cymene is governed by OH radical addition to the aromatic ring and H-atom abstraction from the isopropyl and methyl groups. *p*-Cymene is not expected to be significantly degraded by oxygen atoms (O³P), ozone (O₃) or NO₃ because of its plain aromatic structure. The calculated tropospheric lifetimes of *p*-cymene toward the atmospheric attack by ozone during the day and NO₃ at night are >330 days and 1.3 years, respectively.⁹ Its reaction with OH radicals is believed to be the most important atmospheric removal process of *p*-cymene. In addition to the interest in the fundamental properties of the OH + *p*-cymene reaction, an understanding of the relevant *p*-cymene sinks would enhance our knowledge of the atmospheric chemistry of *p*-cymene, that is, ozone and secondary organic aerosol (SOA) formation potentials.

To date, only one laboratory kinetic study reports the room temperature rate constant for the reaction of OH radicals

^a Atmospheric Chemistry Research Laboratory, University of Bayreuth, 95448, Bayreuth, Germany. E-mail: cornelius.zetzsch@uni-bayreuth.de

^b Aix-Marseille Univ. Laboratoire Chimie Environnement, FRE 3416, Marseille, France

^c Fraunhofer-Institute for Toxicology and Experimental Medicine, 30625 Hannover, Germany

with *p*-cymene. Corchnoy and Atkinson⁹ used a relative rate method and report $k = 1.51 \times 10^{-11} \text{ cm}^3 \text{ s}^{-1}$ at 295 K for the OH + *p*-cymene reaction, using cyclohexane as the reference reaction ($k_{\text{cyclohexane}+\text{OH}} = 7.43 \times 10^{-12} \text{ cm}^3 \text{ s}^{-1}$) that results in a tropospheric lifetime of *p*-cymene toward the attack by OH radicals of about 1 day. Recently, the mechanism of the OH + *p*-cymene reaction has been studied at room temperature by Aschmann *et al.*¹⁰ These investigators report that the H-atom abstraction from the isopropyl group accounts for $14.8 \pm 3.2\%$ and that the sum of abstraction from the methyl and isopropyl groups accounts for $20 \pm 4\%$ of the total rate constant for the OH + *p*-cymene reaction at 298 K. In this work, we use a direct, *in situ* and real-time flash photolysis-resonance fluorescence (FP-RF) technique to study the OH + *p*-cymene reaction as a function of temperature over the range 297–413 K in helium buffer gas.

2. Experimental

The experimental methodology, originally developed by Stuhl and Niki¹¹ and since then employed by various other authors,^{12–17} couples radical production by vacuum-UV flash photolysis (FP) with sensitive time-resolved detection of OH using resonance fluorescence (RF). The experimental approach is similar to a number of other studies on OH radical reactions of atmospheric interest.^{18–30} The experiments involved time-resolved detection of OH radicals by resonance fluorescence ($A^2\Sigma^+ \rightarrow X^2\Pi$) at $\lambda = 308 \text{ nm}$ following vacuum-UV flash photolysis of H_2O –*p*-cymene–He and H_2O –He mixtures. The schematic diagram of the FP-RF apparatus is shown in Fig. 1. Details of the experimental approach are given below.

A black anodized aluminium reaction cell was used in all experiments which were carried out under precisely known temperature, pressure and flow conditions. The reaction cell has been described in detail by Witte *et al.*,²¹ and was maintained at a constant temperature ($\pm 1 \text{ K}$) by circulating silicone oil from a temperature controlled bath through the double-walled Wood's horns and the body of the cell. A platinum resistance thermometer, Pt-100, close to the reaction zone, allowed the measurement of the temperature of the experiments. The geometry of the reaction cell and the gas saturation system has been described in detail by Wahner and Zetzsch.¹⁸ The vacuum UV (VUV) beam and the resonance lamp beam enter the cell perpendicular to one another and to the photomultiplier, *i.e.*, the RF detector is orthogonal to the overlapping beams. The direction of the gas flow was perpendicular to the direction of both the photolyzing VUV beam and the photomultiplier tube (PMT) detector.

A few initial experiments were performed using a home-made flash lamp with a spark discharge (at a distance of 25 cm from the observation zone) in N_2 with a flash energy of 600 mJ calculated using 0.01 μF capacitance (Type EC 103 50 M Condenser Products) and 11 kV applied voltage. However, in the majority of the experiments a Perkin Elmer FX 1165 short arc xenon flash lamp with a MgF_2 window served as the photolytic light source to generate the OH radicals from the FP of H_2O . Typical xenon flash lamp energies ranged from 60 to 540 mJ. The lamp spark gap was mounted at a distance of 7.5 cm from the observation zone,

and the VUV beam entered the reaction cell through another MgF_2 window, where the space between the MgF_2 windows (2.5 cm) was constantly flushed by N_2 gas from the liquid nitrogen reservoir of the laboratory. A quartz resonance lamp mounted at right angles to the VUV photolysis beam excited the photolytically produced OH radicals in the reaction cell volume by resonance fluorescence. Optimized optical systems of two plano convex lenses each, (diameter = 38 mm, antireflection-coated for 308 nm), were used for imaging the plasma of the resonance lamp into the center of the fluorescence cell and for collecting the resulting resonance fluorescence onto the photocathode of the photomultiplier. An additional Al coated spherical mirror 5 cm in radius was mounted at the rear of the RF lamp and served to enhance the lamp emission intensity. The microwave power was supplied by a microwave generator (Muegge, Reichelsheim, MW-GPRYJ1511-300-01, 2.45 GHz, 300 W) *via* a water cooled circulator (Philips, Type 2722 163 02071) and operated at $\sim 70 \text{ W}$. A gas mixture of H_2O –He at a total pressure of 130 mbar was allowed to flow through the resonance lamp. The electrodeless microwave discharge dissociated H_2O to produce OH radicals. These radicals were then electronically excited to the $A^2\Sigma^+$ state *via* collisions with either electronically excited He or free electrons. Since the fluorescence is resonant, the $A^2\Sigma^+ \rightarrow X^2\Pi$ radiation leaving the lamp electronically excites OH ($X^2\Pi$) radicals present in the reaction vessel. The resulting resonance fluorescence ($A^2\Sigma^+ \rightarrow X^2\Pi$) at 308 nm was coupled out of the lamp through two quartz lenses (Heraeus, Suprasil, $f_{\text{VIS}} = 50 \text{ mm}$) into the reaction cell. The resonance fluorescence light was collected by another anti-reflection coated quartz lens (Heraeus, Suprasil, $f_{\text{VIS}} = 50 \text{ mm}$) and passed through a 308 nm interference filter (FWHM = 9 nm) which blocked impurity emissions from the resonance lamp radiation on the axis normal to both the photolysis VUV beam and the resonance lamp beam and was imaged by another quartz lens (Heraeus, Suprasil, $f_{\text{VIS}} = 50 \text{ mm}$) onto the photocathode of a photomultiplier tube (Thorn-EMI, 9789QB). The signal was processed and accumulated using photon-counting techniques in conjunction with multichannel scaling (EG&G Ortec, model ACE MCS) and saved in a PC.

All experiments were carried out under “slow flow” conditions with a mean linear flow rate of about 1 cm s^{-1} at 200 mbar and a VUV flash repetition rate of 0.2 Hz, so that the gas mixture within the detection volume was replenished between VUV flashes. The gases used in this work had the following stated minimum purities: He (Riessner) – 99.996%; liquid N_2 (Linde) – 99.999%. The liquid *p*-cymene (Aldrich) had a stated minimum purity of 99%. Deionized water was doubly distilled by a quartz still. Concentrations of H_2O and *p*-cymene in the reaction mixture were calculated from the given vapour pressures, temperature, mass-flow rates and total pressure. The Antoine equation for the vapour pressure of H_2O used in this study was $\log_{10}[P(\text{mbar})] = 5.40221 - [1838.675/(T(\text{K}) - 31.737)]$.³¹ For *p*-cymene the saturator was kept at $T = 293 \text{ K}$. Literature data of the vapour pressure are available for temperatures between 268 and 286 K,³² between 300 and 450 K,³³ between 381 and 452 K,³⁴ and between 314 and 452 K,³⁵ but no direct measurements have been reported near room temperature. Ruzicka Jr. *et al.*³⁶ reviewed vapour pressure

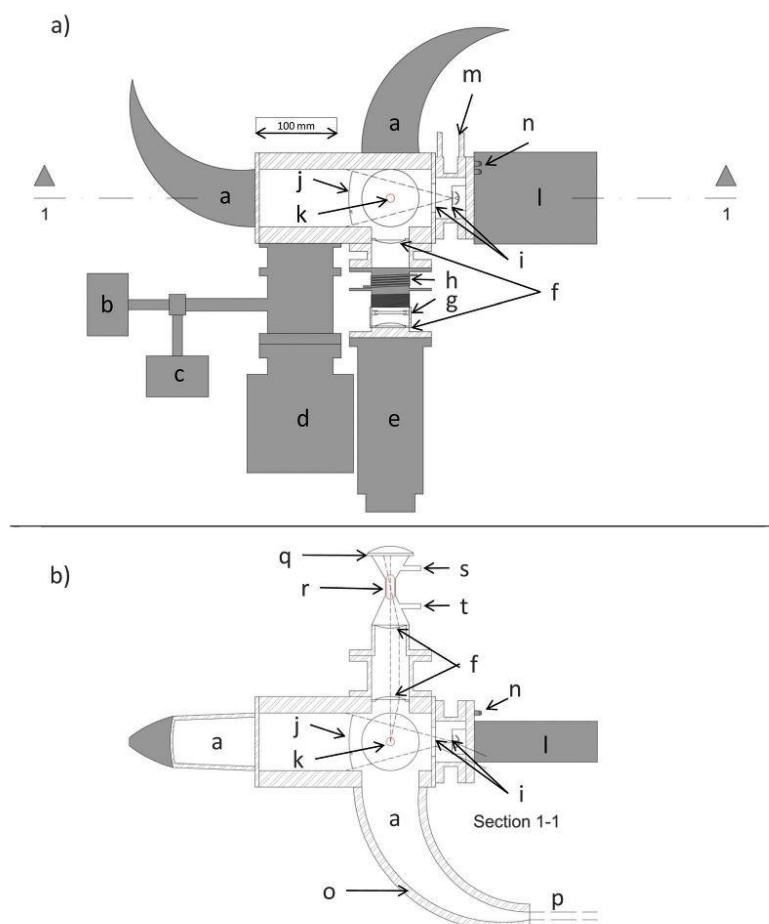


Fig. 1 Top (a) and side (b) views of the flash photolysis resonance fluorescence (FR-RF) system used in this work. (a) Wood's horn; (b) pressure gauge (10 Torr); (c) pressure gauge (1000 Torr); (d) vacuum valve; (e) photomultiplier; (f) focusing lenses; (g) interference filter (308 nm); (h) focusing screw; (i) MgF₂ windows; (j) 60% intensity compared to the central beam; (k) observation zone; (l) lamp power supply; (m) N₂ purge gas inlet; (n) lamp water cooling; (o) mantle with silicon oil circulating from a thermostat; (p) gas mixture inlet; (q) concave mirror; (r) microwave discharge; (s) resonance lamp He–H₂O mixture outlet and (t) inlet.

data for *p*-cymene and a group of other high-boiling alkylbenzenes at temperatures between 223.15 and 323.15 K determined by direct measurements at pressures higher than 1 kPa and related thermodynamic data, where the recommended pressure for *p*-cymene has been calculated using the Cox eqn (1)

$$\ln\left(\frac{P_{\text{sat}}}{P_0}\right) = \left(1 - \frac{T_0}{T}\right) \exp(A_0 + A_1T + A_2T^2) \quad (1)$$

with the following parameters: $A_0 = 2.82209$; $A_1 = -1.438828 \times 10^{-3}$; $A_2 = 1.191725 \times 10^{-6}$; with $T_0 = 450.259$ K and $P_0 = 101.325$ kPa. The calculated *p*-cymene vapour pressure was found to be in good agreement with direct measurements below 268 K³² and

above 300 K³³ within a 10% deviation, leading to a vapour pressure of 1.44 ± 0.14 mbar at 293 K.

The initial OH radical concentration produced by VUV photolysis of H₂O at 1.5×10^{15} cm⁻³ using the N₂ spark discharge lamp was estimated by Koch *et al.*,²⁶ comparing signal intensities corrected for fluorescence quenching by H₂O with measurements of Witte *et al.*,²¹ and leading to a concentration well below 10^{10} cm⁻³ at 2 J flash energy. A FP-RF with similar geometry¹⁸ was used by Zhang *et al.* at the University of Aix-Marseille^{27,28,30} to study other OH radical reactions of atmospheric interest. These investigators determined the initial OH concentration using a Xe flash lamp at

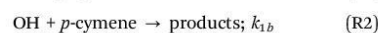
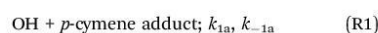
540 mJ flash energy and measured the ozone concentration after the photolysis of a 20% O₂-N₂ mixture to estimate a maximum value for the initial OH concentration of 2×10^{10} cm⁻³ under the experimental conditions employed. These and our OH radical concentrations are two orders of magnitude smaller than the smallest concentration of *p*-cymene used in this work, ensuring pseudo-first-order conditions.

The temperature within the reactor was varied between 297 K and 413 K, and the total pressure was varied between 185 and 596 mbar He.

3. Results and discussion

3.1 Kinetic analysis and data evaluation

The behaviour of OH radicals in the presence of *p*-cymene in our system is described *via* a number of reaction channels, including reversible adduct formation, abstraction and other loss processes of OH and the adduct:



The rate equations that describe the change in the concentrations of OH radicals and the adduct (that regenerates OH) as a function of time are the following:

$$\frac{d}{dt}[\text{OH}] = -a[\text{OH}] + b[\text{add}] \quad (2)$$

$$\frac{d}{dt}[\text{add}] = c[\text{OH}] - d[\text{add}] \quad (3)$$

where the combined first-order rate constants are $a = k_2 + (k_{1a} + k_{1b}) [p\text{-cymene}]$, $b = k_{-1a}$, $c = k_{1a} [p\text{-cymene}]$, and $d = k_{-1a} + k_3$. The analytical solution of the system of differential equations has been published by Wahner and Zetzsch,¹⁸ and the expressions for obtaining a , d and the product bc from the observed biexponential decays rates and intensity ratios²⁹ are given below in eqn (4)–(6).

$$bc = \frac{(\tau_1^{-1} - \tau_2^{-1})^2 \left(\frac{I_1}{I_2}\right)}{\left(1 + \frac{I_1}{I_2}\right)^2} \quad (4)$$

$$a = \frac{\tau_1^{-1} \left(\frac{I_1}{I_2}\right) + \tau_2^{-1}}{1 + \left(\frac{I_1}{I_2}\right)} \quad (5)$$

$$d = \frac{\tau_2^{-1} \left(\frac{I_1}{I_2}\right) + \tau_1^{-1}}{1 + \left(\frac{I_1}{I_2}\right)} \quad (6)$$

Fit parameters obtained for the decay curves of each experiment can be used in eqn (4)–(6) to determine the rate constants a ,

bc and d . Linear fits of a and bc , for a given temperature, against the concentration of *p*-cymene allowed us to determine k_2 and the sum $k_{1a} + k_{1b}$ from a as the intercept a_0 and the slope and the product $k_{1a} k_{-1a}$ from bc . However, the evaluation of individual biexponential decays in the presence of a fixed concentration of *p*-cymene (so-called “*e*-fit”, see Koch *et al.*²⁶) runs into problems if the intensity ratios become too large or too small and if τ_1^{-1} and τ_2^{-1} become similar in certain concentration ranges of *p*-cymene, due to the then large mutual covariances of the exponential parameters.

Koch *et al.*²⁶ improved the evaluation method by fitting sets of biexponential decays at various concentrations but at the same temperature simultaneously to the biexponential model (so-called “*k*-fits”). The fitting program used in this work follows the same concept and was developed using IDL (Interactive Data Language, Research Systems Inc.).²⁹ Similar to the procedure described by Bohn and Zetzsch,²⁹ errors were estimated by varying the combined first-order rate constants until the measured χ^2 was increased by a given factor. This factor was calculated for each set of curves for the degrees of freedom (DOF) given to obtain a probability of 0.68 which corresponds to a 1σ uncertainty. The estimated errors are believed to be rather conservative²⁹ since they are about a factor of three larger than the ones that correspond to 1σ uncertainty.

Table 1 lists the rate constants measured for the reaction of *p*-cymene with OH radicals at the indicated temperatures, pressures and concentration range. Given errors for the temperature and pressure represent the standard deviation of those values for the respective set of experiments. Similar to Koch *et al.*,²⁶ and Bohn and Zetzsch,²⁹ the rate constants observed at constant temperature and pressure were calculated by fitting sets of N biexponential decays simultaneously.

3.2 Background reactivity of OH radicals (k_2)

Reaction (R3) includes the loss of OH radicals by their reactions with impurities that may enter the reactor through tubing connections or outgassing. This reaction also includes the only minor and approximately exponential diffusion loss of the OH radicals from the photolytic production zone, which is defined by the flash lamp, where the Xe lamp contains a spherical mirror (Technical Manual Perkin Elmer FX 1165). The loss rate constant k_2 at room temperature was found to be $(22.2 \pm 5.7) \text{ s}^{-1}$ using the N₂ spark lamp and $(9.8 \pm 4.5) \text{ s}^{-1}$ for the Xe flash lamp, not significantly dependent on total pressure and decreasing slightly with increasing temperature, reaching $(8.1 \pm 3.6) \text{ s}^{-1}$ at 413 K using the Xe lamp. A weighted regression fit for the function $k_2 = x_0 \exp(y/T)$ is represented by the line in Fig. 2, with calculated values of x_0 and y of $(3 \pm 2) \text{ s}^{-1}$ and $(430 \pm 250) \text{ K}$, respectively, and a coefficient of determination, R^2 , of only 10%.

A complete understanding of this parameter is not of great importance, as its small variation does not affect the determination of the other combined constants ($k_{1a} + k_{1b}$, $k_{1a} k_{-1a}$ and $k_{-1a} + k_3$). It was estimated that if k_2 was kept at a fixed value of 10 s^{-1} for the given temperature range, the difference between the new and the old parameters would not exceed about 12% at temperatures below 330 K and above 354 K. Between these

Table 1 Rate constants $a_0 = k_2$, $a = k_{1a} + k_{1b}$, $bc = k_{-1a} k_{1a}$ and $d = k_{-1a} + k_3$ in the reaction system of *p*-cymene with OH radicals at given temperatures

<i>T</i> /K	[<i>p</i> -Cymene]/10 ¹² cm ⁻³	<i>N</i> ^g	<i>k</i> ₂ /s ⁻¹	(<i>k</i> _{1a} + <i>k</i> _{1b})/10 ⁻¹² cm ³ s ⁻¹	(<i>k</i> _{1a} × <i>k</i> _{-1a})/10 ⁻¹² cm ³ s ⁻²	(<i>k</i> _{-1a} + <i>k</i> ₃)/s ⁻¹
297.2 ± 0.4 ^f	4.9–28.9	19	22 ± 6	16.4 ± $\frac{0.8}{1}$	90 ± 9	10.4 ± 0.1
299 ± 0.2	5.3–35.4	24	10 ± 4	14.9 ± $\frac{0.8}{0.7}$	73 ± $\frac{10}{9}$	14.5 ± 0.1
309.9 ± 0.7 ^f	5.3–28.5	19	11 ± 5	15.9 ± $\frac{1}{0.9}$	234 ± 20	24 ± 2
314.6 ± 0.5	5.0–40.4	43	3 ± $\frac{3}{2}$	12.1 ± $\frac{0.9}{0.8}$	204 ± 30	33 ± 3
317 ± 0.2	8.9–43.3	12	17 ± 6	11.7 ± 0.7	221 ± $\frac{30}{20}$	38 ± 3
317 ± 0.2 ^f	5.2–28.4	19	16 ± 4	15.8 ± $\frac{1}{0.9}$	412 ± 4	41 ± 3
322 ± 1 ^f	5.1–28.8	17	12 ± 3	13 ± 1	401 ± $\frac{4}{20}$	49 ± $\frac{5}{4}$
324.2 ± 0.1	12.4–44.7	15	16 ± $\frac{9}{7}$	10.1 ± 1	259 ± 40	50 ± $\frac{5}{4}$
326 ± 2	6.9–16.9	7	10 ± $\frac{6}{4}$	9 ± 2	209 ± $\frac{100}{70}$	41 ± $\frac{10}{8}$
325.9 ± 0.2	9.3–33.2	32	13 ± 5	9.4 ± $\frac{0.9}{0.8}$	228 ± $\frac{40}{30}$	49 ± $\frac{5}{4}$
326.5 ± 0.4 ^f	5.0–28.9	12	17 ± 4	13 ± $\frac{2}{1}$	549 ± 5	66 ± $\frac{8}{7}$
327.3 ± 0.1	7.7–19.9	9	11 ± 5	7.97 ± 1	138 ± $\frac{50}{40}$	39 ± $\frac{7}{6}$
328.5 ± 0.1	7.2–32.6	44	11 ± 5	8.73 ± $\frac{0.7}{0.8}$	233 ± 40	55 ± 5
330 ± 0.2	7.5–43.5	19	10 ± 4	8.01 ± $\frac{1}{0.9}$	191 ± $\frac{60}{50}$	50 ± $\frac{8}{7}$
332 ± 0.2	7.1–33.3	52	12 ± 3	6.42 ± $\frac{0.7}{0.3}$	109 ± $\frac{30}{20}$	40 ± 5
334.1 ± 0.4	4.9–40.8	15	3 ± $\frac{2}{1}$	7.3 ± $\frac{2}{0.9}$	207 ± $\frac{100}{90}$	60 ± 20
334.3 ± 0.3	7.4–33.1	11	16 ± 3	6.05 ± 0.06	136 ± $\frac{50}{30}$	50 ± 7
335.4 ± 0.1	9.2–27.6	15	13 ± 4	5.27 ± $\frac{0.1}{0.05}$	80 ± $\frac{30}{20}$	38 ± $\frac{7}{6}$
335.6 ± 0.3	6.8–40.2	15	13 ± 3	4.92 ± 0.05	82 ± $\frac{40}{20}$	35 ± $\frac{7}{6}$
336.2 ± 0.1	7.3–33.6	59	12 ± 2	5.28 ± 0.05	76 ± 20	38 ± 5
338.0 ± 0.2 ^f	4.9–28.6	17	15 ± 2	6.13 ± $\frac{1}{0.2}$	165 ± $\frac{80}{50}$	50 ± 10
340 ± 1	8.0–42.7	28	9 ± 2	5.0 ± 0.1	97 ± $\frac{40}{30}$	48 ± $\frac{9}{7}$
343.5 ± 0.2	7.1–43.0	12	6 ± 2	4.96 ± $\frac{0.2}{0.1}$	98 ± $\frac{50}{30}$	50 ± 10
344.3 ± 0.4 ^f	4.8–34.3	34	16 ± 2	5.54 ± $\frac{0.1}{0.4}$	164 ± $\frac{70}{50}$	70 ± 10
345.2 ± 0.1	7.5–38.0	17	7 ± 2	4.97 ± $\frac{0.3}{0.1}$	92 ± $\frac{30}{40}$	50 ± $\frac{10}{9}$
348 ± 0.5	7.6–43.0	14	9 ± 2	4.44 ± 0.04	70 ± $\frac{30}{20}$	50 ± 10
348.9 ± 0.1	6.8–40.5	37	3 ± $\frac{3}{2}$	5.05 ± 0.05	82 ± $\frac{70}{40}$	60 ± 20
353.5 ± 0.1	7.4–37.7	14	7 ± 2	4.6 ± 0.1	86 ± $\frac{60}{30}$	70 ± 20
353.8 ± 0.1	7.0–27.4	31	11 ± 1	4.18 ± 0.04	30 ± $\frac{7}{5}$	36 ± $\frac{5}{4}$
368.9 ± 0.1	7.7–33.1	20	7 ± 2	4.26 ± $\frac{0.09}{0.04}$	6 ± $\frac{3}{2}$	20 ± $\frac{7}{1}$
382.8 ± 0.1	9.0–44.2	12	9 ± 2	4.05 ± 0.04	4 ± $\frac{2}{1}$	17.8 ± 0.2
382.8 ± 0.1	7.0–27.7	13	5.2 ± $\frac{1}{0.9}$	4.22 ± 0.04	2.1 ± $\frac{1}{0.6}$	11.3 ± $\frac{0.1}{0.2}$
384.4 ± 0.1	7.3–43.6	27	6 ± 2	4.48 ± 0.04	2.3 ± $\frac{2}{0.7}$	9.51 ± 0.1

Paper

PCCP

Table 1 (continued)

T/K	$[p\text{-Cymene}]/10^{12} \text{ cm}^{-3}$	N^g	k_2/s^{-1}	$(k_{1a} + k_{1b})/10^{-12} \text{ cm}^3 \text{ s}^{-1}$	$(k_{1a} \times k_{-1a})/10^{-12} \text{ cm}^3 \text{ s}^{-2}$	$(k_{-1a} + k_3)/s^{-1}$
386.9 ± 0.1	7.2–43.1	12	6 ± 1	$4.56 \pm \begin{smallmatrix} 0.09 \\ 0.05 \end{smallmatrix}$	$2.2 \pm \begin{smallmatrix} 1 \\ 0.9 \end{smallmatrix}$	12.4 ± 0.1
403.9 ± 0.1	7.1–47.2	12	10 ± 2	$4.8 \pm \begin{smallmatrix} 0.1 \\ 0.05 \end{smallmatrix}$	$2.5 \pm \begin{smallmatrix} 1 \\ 0.9 \end{smallmatrix}$	9.93 ± 0.1
406 ± 1^a	7.6–44.2	9	9 ± 2	$4.95 \pm \begin{smallmatrix} 0.2 \\ 0.2 \end{smallmatrix}$	$3 \pm \begin{smallmatrix} 2 \\ 1 \end{smallmatrix}$	9.36 ± 0.09
408 ± 2^e	9.6–40.3	12	11 ± 3	$4.96 \pm \begin{smallmatrix} 0.1 \\ 0.05 \end{smallmatrix}$	$7 \pm \begin{smallmatrix} 5 \\ 3 \end{smallmatrix}$	18.8 ± 0.2
407.6 ± 0.7^d	11.1–42.0	9	$9 \pm \begin{smallmatrix} 5 \\ 4 \end{smallmatrix}$	5.12 ± 0.05	$8 \pm \begin{smallmatrix} 6 \\ 4 \end{smallmatrix}$	$20 \pm \begin{smallmatrix} 20 \\ 1 \end{smallmatrix}$
408.3 ± 0.9^b	8.8–40.7	12	12 ± 3	$4.85 \pm \begin{smallmatrix} 0.1 \\ 0.05 \end{smallmatrix}$	$4 \pm \begin{smallmatrix} 3 \\ 2 \end{smallmatrix}$	14.7 ± 0.1
413 ± 1^c	10.3–45.0	9	8 ± 4	$5.34 \pm \begin{smallmatrix} 0.05 \\ 0.2 \end{smallmatrix}$	$5 \pm \begin{smallmatrix} 4 \\ 2 \end{smallmatrix}$	15.4 ± 0.2

^a 296 ± 5 mbar. ^b 384 ± 16 mbar. ^c 463 ± 15 mbar. ^d 491 ± 56 mbar. ^e 588 ± 7 mbar. ^f 259.4 ± 0.2 mbar. ^g Number of measurements.

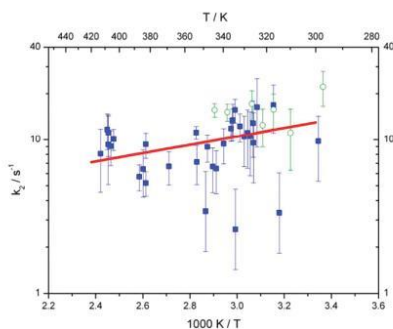


Fig. 2 The Arrhenius plot for the background loss of OH, k_2 , with the regression line. Solid blue squares were obtained using the Xe flash lamp as the photolytic source while the open green circles were obtained by using the N_2 spark discharge lamp.

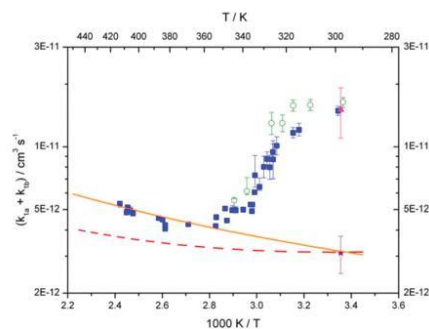


Fig. 3 The Arrhenius plot of the total rate constant (addition plus abstraction) for the reaction between OH and *p*-cymene. Data obtained using the Xe flash lamp as photolytic source are marked as solid squares (in several cases statistical errors are smaller than the symbols), those obtained by using the N_2 spark discharge lamp as open circles. The asterisk represents the abstraction for *p*-cymene measured by Aschmann *et al.*,¹⁰ at 298 K; the triangle represents the total rate constant from a chamber experiment at 298 K by Corchnoy and Atkinson,⁹ the dashed line is the estimated abstraction using Structure Activity Relationships (SARs),³⁷ the solid line represents an extrapolation of high temperature data down to room temperature (see Section 3.3).

temperatures the model becomes very unstable as will be shown below.

3.3 Abstraction and addition channels ($k_{1a} + k_{1b}$)

The solution of the differential equation system (eqn (4)–(6)) does not allow us to separate the addition (k_{1a}) and abstraction (k_{1b}) rate constants, but only to determine the sum of both. The total rate constants determined in this investigation at 297 K using the N_2 spark lamp, $(16.4 \pm 1.1) \times 10^{-12} \text{ cm}^3 \text{ s}^{-1}$, and at 299 K using the Xe flash lamp, $(14.9 \pm 0.8) \times 10^{-12} \text{ cm}^3 \text{ s}^{-1}$, agree within the calculated errors and they agree well with the value obtained by Corchnoy and Atkinson⁹ in a chamber study at 298 K $(15.1 \pm 4.1) \times 10^{-12} \text{ cm}^3 \text{ s}^{-1}$ (triangle in Fig. 3). On the other hand, the higher value obtained by the N_2 spark lamps is somewhat suspect because of the significantly higher a_0 value, indicating an influence of minor impurities in this first series of runs.

The total rate constants observed in our study decrease slowly at temperatures lower than 320 K and then their decrease becomes steepest at $T \sim 330$ K and flattens again until around

$T \sim 360$ K. At temperatures higher than 360 K, the total rate constants increase slowly again, mainly due to abstraction. At room temperature, the total rate constant for OH and *p*-cymene is quite similar to the ones measured for *m*-xylene and *p*-xylene. Doyle *et al.*,³⁸ Hansen *et al.*,³⁹ Lloyd *et al.*,⁴⁰ Perry *et al.*,¹³ Ravishankara *et al.*,⁴¹ Cox *et al.*,⁴² Nicovich *et al.*,⁴³ Ohta and Ohya,⁴⁴ Edney *et al.*,⁴⁵ and Atkinson and Aschmann⁴⁶ reported rate constants to range from 18.8 to $25.4 \times 10^{-12} \text{ cm}^3 \text{ s}^{-1}$ for *m*-xylene, and between 10.7 and $15.3 \times 10^{-12} \text{ cm}^3 \text{ s}^{-1}$ for *p*-xylene. The rate constant obtained in this work is twice as large as the one found for a substituted benzene with only one isopropyl group, isopropyl benzene, with reported values at room temperature of $(7.79 \pm 0.50) \times 10^{-12} \text{ cm}^3 \text{ s}^{-1}$ by Ravishankara *et al.*,⁴¹ and $(6.1 \pm 0.33) \times 10^{-12} \text{ cm}^3 \text{ s}^{-1}$ by Ohta and Ohya,⁴⁴ resulting in an arithmetic mean of $6.95 \times 10^{-12} \text{ cm}^3 \text{ s}^{-1}$.

This kinetic result is consistent with the activating property of the additional methyl group in the *para* position according to the Hammett equation.⁵⁰

As suggested by Zetzsch⁵⁰ and adopted by Kwok and Atkinson,³⁷ the Hammett constants for electrophilic addition in aqueous solution obtained by Brown and Okamoto⁵¹ can be used to estimate the rate constant for the addition of OH to *p*-cymene in the gas phase.

Results of the calculation using the EPI (Estimation Program Interface)⁴⁷ Suite do not show good agreement with our already published results on *p*-xylene.⁴⁸ The measured overall rate constant for these two compounds was found to be twice as high as the ones expected using Hammett constants (see Table 2). Only for the OH + isopropylbenzene reaction the calculation and the measurement are in agreement. It is clear that the structure activity relationship (SAR) only gives a rough estimate and that such SARs are convenient but need to be improved.

This prediction does not yet consider any inductive/mesomeric influence of the isopropyl group on the abstraction channel from the methyl group, but this would be negligible, as follows from the average for abstraction from benzylic methyl groups suggested in the review by Atkinson and Aschmann.⁴⁶

Kwok and Atkinson³⁷ reported a way of estimating the contribution of the abstraction to the total rate constant, based on the SARs by comparing related compounds. The molecule *p*-cymene has ten aliphatic hydrogen atoms that could be abstracted by an OH radical (see Fig. 4). Hydrogen atoms directly attached to the aromatic ring (a and b in Fig. 4) are not important for the estimation of the abstraction at room temperature, as observed previously for the reaction of OH radicals with benzene where the abstraction rate constant is about $0.5 \times 10^{-13} \text{ cm}^3 \text{ s}^{-1}$ for the six equivalent H atoms.¹³

Table 2 Estimated rate constants using Hammett constants for electrophilic addition and measured overall rate constants at $T = 298 \text{ K}$

Compound	Estimated rate constant ($\times 10^{-12} \text{ cm}^3 \text{ s}^{-1}$) ⁴⁷	Measured rate constant ($\times 10^{-12} \text{ cm}^3 \text{ s}^{-1}$)
<i>p</i> -Xylene	6.51	14.3 ^{48,49}
<i>p</i> -Cymene	8.54	15.7 (this work)
Isopropylbenzene	6.90	6.3 ⁴⁹

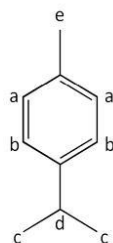


Fig. 4 The *p*-cymene molecule with indicated non-equivalent C-H bonds.

Rate constants for H-atom abstraction from other groups (atoms c, d and e in Fig. 4) can be estimated as follows:

$$k(\text{CH}_3\text{-X}) = k_{\text{prim}}F(\text{X}) \quad (7)$$

$$k(\text{X-CH(Y)-Z}) = k_{\text{tert}}F(\text{X})F(\text{Y})F(\text{Z}) \quad (8)$$

$$k_{\text{abs}} = 3k(\text{CH}_3\text{-X}) + k(\text{X-CH(Y)-Z}) \quad (9)$$

$$k_{\text{prim}} = 4.49 \times 10^{-18} (T/\text{K})^2 \exp(-320 \text{ K}/T) \quad (10)$$

$$k_{\text{tert}} = 2.12 \times 10^{-18} (T/\text{K})^2 \exp(+696/T) \quad (11)$$

where $F(\text{X})$, $F(\text{Y})$ and $F(\text{Z})$ are the substituent factors for the groups X, Y, and Z and k_{prim} and k_{tert} are the group rate constants for abstraction from $-\text{CH}_3$ and $-\text{CH}$ for a standard aliphatic non-aromatic substituent.³⁷

In the case of *p*-cymene, there is no information on the substituent factors available other than for $F(-\text{CH}_3) = 1$. As a rough simplification it was assumed that the substituent factors for the groups c, d and e presented in Fig. 4 have the same value.

$$F(\text{X})_c = F(\text{X})_d = F(\text{X})_e = F \quad (12)$$

$$k_{\text{abs}} = 3k_{\text{prim}}F + k_{\text{tert}}F \quad (13)$$

Aschmann *et al.*¹⁰ measured the formation yields of 4-methylacetophenone (the major product formed after the H-atom abstraction from the isopropyl group) from the reaction between OH and *p*-cymene in a teflon chamber at $297 \pm 2 \text{ K}$ and 1 atm pressure of dry pure air. They found that the H-atom abstractions from the methyl and isopropyl group account for $20 \pm 4\%$ of the total rate constant, which would mean that in this work the rate constant for the abstraction channel at room temperature should be $(3.1 \pm 0.7) \times 10^{-12} \text{ cm}^3 \text{ s}^{-1}$ (asterisk in Fig. 3). With this value, and calculating k_{prim} and k_{tert} at 298 K using eqn (10) and (11), the value for F can be easily found ($F = 1.33 \pm 0.27$). This value is dependent on the temperature in the following way:

$$F = \exp(E_x/T) \quad (14)$$

E_x was found to be 85 K. Using eqn (10), (11) and (13) with an E_x of 85 K, an estimate of the abstraction can be made for *p*-cymene. This estimation is shown as a red dashed line in Fig. 3, and it can be seen how the increase of the measured data for temperatures higher than 380 K is consistent with the estimated abstraction at these temperatures within the applied approximations.

At high temperatures the reversible addition becomes negligible compared to the irreversible abstraction, and thus high temperature data can be used to estimate the H-atom abstraction. In this work, the obtained total rate constants for temperatures greater than 380 K and the abstraction value at room temperature reported by Aschmann *et al.*¹⁰ were used. A function of the form: $k = A (T/\text{K})^2 \exp(-E/RT)$ was fitted to the observations at those temperatures, obtaining values for A of $2 \times 10^{-17} \text{ cm}^3 \text{ s}^{-1}$ and for $-E/RT$ of 170 K. This function is shown as a solid line in Fig. 3.

3.4 Forward and backward reactions (k_{1a} k_{-1a})

The analytical solution to the differential equation system is only able to determine the contributions of the forward and backward reactions as a product of both rate constants. From the Arrhenius plot of this product (Fig. 5) only the combined activation energy can be calculated. Between room temperature and 324 K the product of both rate constants increases with an activation energy of 45 kJ mol⁻¹, then it starts to decrease very quickly with an activation energy of -78 kJ mol⁻¹ until around 387 K where it starts to increase again with an activation energy of +32 kJ mol⁻¹.

The change in the slope, that is, the change in the sign of the activation energy, may indicate that the system does not fully follow the mechanism proposed in this paper. The second change in the slope could be due to the increasing importance of the abstraction channel at given higher temperatures. On the other hand, the product $k_{1a} k_{-1a}$ should be unaffected by k_{1b} if the proposed model is correct.

3.5 Unimolecular decay and background loss of the adduct ($k_{-1a} + k_3$)

The last parameter that can be directly calculated from the OH radical decay curves includes the sum of the unimolecular decay of the adduct and the rate constant for background loss. As in the case of the OH radicals, k_3 is the rate constant that represents background reactions of the adduct with any impurities that might be present in the cell. The Arrhenius plot for these combined reactions of the adduct is shown in Fig. 6. It is very interesting to note that a similar behaviour is observed as before for the product of forward and backward reaction rate constants, and also at the same temperatures. Weighted fits of the Arrhenius plot between room temperature and 324, 324 and 387 and above 387 K allow us to calculate the activation energy of these three temperature ranges to be 48, -27 and 75 kJ mol⁻¹. Again, this change in the slope of the curve at 324 and 387 K indicates that the proposed mechanism could be incomplete and that other reactions are taking place at mid temperatures.

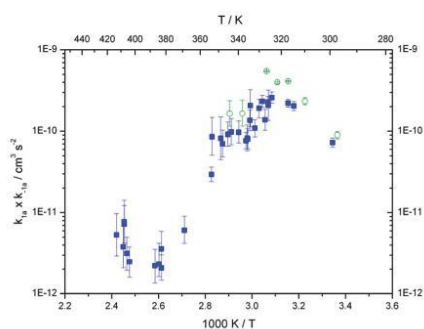


Fig. 5 The Arrhenius plot of the product of the forward and backward reaction rate constants for *p*-cymene. Data depicted as blue squares were obtained using the Xe flash lamp as the photolytic source while data depicted as green open circles were obtained using the N₂ spark discharge lamp.

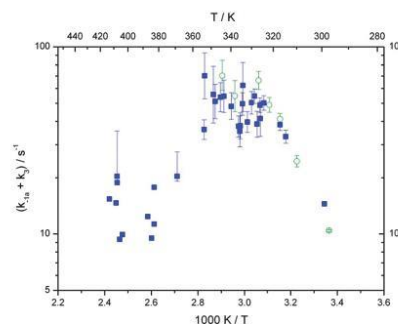


Fig. 6 Arrhenius plot of the unimolecular decay plus background loss rate constants of the adduct. The blue squares mark data obtained using the Xe flash lamp as the photolytic source while the green open circles mark those obtained using the N₂ spark discharge lamp.

3.6 Equilibrium constant (K_{eq})

The equilibrium rate constant for the reaction between *p*-cymene and the OH radical was determined using the measured rate constants for the individual processes. This can be done by using eqn (15) and calculating the H-atom abstraction as explained above (Section 3.3) to be described by the expression: $k_{abs} = 2 \times 10^{-17} (T/K)^2 \exp(+170 K/T) \text{ cm}^3 \text{ s}^{-1}$. The equilibrium constant follows the same behaviour as presented before with two clearly defined temperature ranges. At temperatures higher than 384 K no constants can be calculated due to the approximation used to estimate the abstraction (reversible addition at temperature higher than 384 K is negligible against the abstraction). Plots of the van't Hoff equation are presented in Fig. 7 and lead to $K_{eq} = 6 \times 10^{-26} \exp(9700 K/T) \text{ cm}^3$ at temperatures below 325 K and $K_{eq} = 2 \times 10^{-36} \exp(17000 K/T) \text{ cm}^3$ at temperatures above 320 K. The equilibrium constant can be related to the standard reaction enthalpy and entropy using eqn (16),

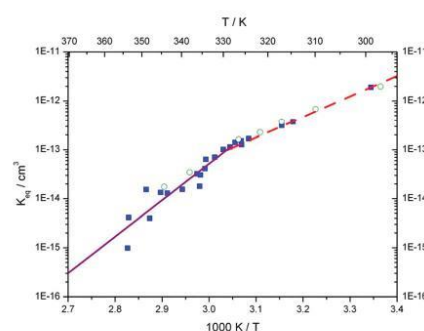


Fig. 7 Van't Hoff plot of the equilibrium constant. Solid square data were obtained using the Xe flash lamp as the photolytic source while the open green circles data were obtained using the N₂ spark discharge lamp. The red dashed line is expressed by: $K_{eq} = 2 \times 10^{-26} \exp(9700 K/T) \text{ cm}^3$. The blue solid line is expressed by $K_{eq} = 2 \times 10^{-36} \exp(17000 K/T) \text{ cm}^3$.

and a standard enthalpy change of -74 kJ mol^{-1} and an entropy of $-100 \text{ J K}^{-1} \text{ mol}^{-1}$ were found at temperatures below 324 K and a standard enthalpy change of -324 kJ mol^{-1} and an entropy change of $-147 \text{ J K}^{-1} \text{ mol}^{-1}$ at temperatures above 324 K.

$$K_{\text{eq}} = \frac{k_{1a}}{k_{-1a}} = \frac{((k_{1a} + k_{1b}) - k_{\text{obs}})^2}{k_{1a}k_{-1a}} \quad (15)$$

$$K_{\text{eq}} = \frac{k_b T}{P^{\theta}} \exp\left(\frac{-\Delta H}{RT} + \frac{\Delta S}{R}\right) \quad (16)$$

3.7 Goodness of the biexponential fit

Reduced χ^2 values, *i.e.*, χ^2 divided by the degrees of freedom, DOF, were calculated for each measurement and are presented in Fig. 8. It can be observed that between $T = 317$ and 344 K the values for the reduced χ^2 are very high, indicating that the model used does not explain our observations. These results indicate that the current model cannot explain processes occurring at temperatures where the addition reaction channel appears to be more important than the abstraction channel. It is also evident that the addition path changes somehow with increasing temperature, indicating a possible OH-*p*-cymene adduct formation with a different energy or an isomerization into more stable adducts.

A deeper examination of each decay curve of experiments performed between $T = 317$ and 344 K revealed the presence of a third exponential component that may be indicative of another reversible process taking place. Each curve was fitted to a triexponential model of the form:

$$[\text{OH}](t) = I_1 \exp\left(-\frac{t}{\tau_1}\right) + I_2 \exp\left(-\frac{t}{\tau_2}\right) + I_3 \exp\left(-\frac{t}{\tau_3}\right) \quad (17)$$

The slow component, τ_3^{-1} , was found to depend on the temperature and the concentration of *p*-cymene, indicating that this new parameter is not a mathematical artefact but has a chemical origin. The dependence on the temperature is shown in Fig. 9, and it can be seen how τ_3^{-1} increases with increasing temperature up to about 355 K, where it starts decreasing again.

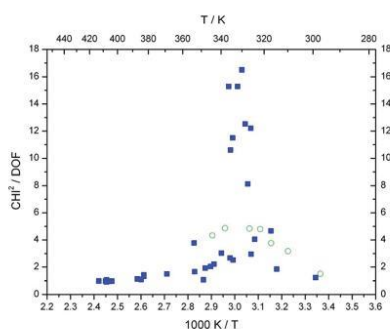


Fig. 8 Reduced χ^2 for all the measurements of Table 1. The filled blue squares data were obtained using the Xe flash lamp as the photolytic source and the open green circles data were obtained using the N_2 spark discharge lamp.

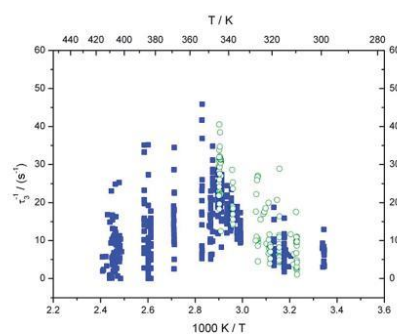


Fig. 9 The slow component, τ_3^{-1} , of the triexponential fit of all measurements. Solid squares were obtained using the Xe flash lamp as the photolytic source while open circles were obtained using the N_2 spark discharge lamp.

A similar behaviour was observed for the χ^2/DOF (Fig. 8), indicating that the deviations of the proposed biexponential model from our measurements are due to another process between OH and *p*-cymene over the temperature range studied.

The aromatic molecule *p*-cymene differs from the other already studied substituted aromatics (toluene, xylene, mesitylene, hexamethylbenzene) in its symmetry. While these aromatics contain methyl groups as substituents, *p*-cymene contains a methyl and an isopropyl group. The formation of two ipso adducts with different energies can be expected, at two equivalent positions *ortho* to the methyl group, and two other equivalent ones *ortho* to the isopropyl group, making a total of 4 distinguishable adducts. The triexponential behaviour of the OH decay curves implies that an improved evaluation of the observed decays is feasible²⁹ in order to obtain information about the formation of other adducts. This will be demonstrated in part 2 of this study.

4. Conclusions

A simplified model that includes the formation of either one or several undistinguishable adducts was fitted to the observed OH decay curves in the presence of *p*-cymene. The fit procedure was done by simultaneously fitting the model to a set of decay curves at the same temperature and pressure but different *p*-cymene concentrations. Rate constants and Arrhenius expressions were determined and compared with available kinetic data of similar aromatic compounds. The observed slope changes for the determined rate constants around 324 K and again around 387 K indicated that the chosen model does not perfectly fit our data over the given temperature range, as confirmed by the χ^2/DOF values. Between these temperatures, the OH decay curves were found to be no longer biexponential but triexponential, indicating the formation of more than one single adduct.

Acknowledgements

This work was supported by the Deutsche Forschungsgemeinschaft (DFG ZE792/6-1) within the French-German CNRS-INSU/DFG

bilateral program ATMOCHEM. We thank Birger Bohn, Forschungszentrum Jülich, for providing IDL routines, and Roger Atkinson, University of California at Riverside, for providing information about the abstraction channels.

References

- Guenther, C. N. Hewitt, D. Erickson, R. Fall, C. Geron, T. Graedel, P. Harley, L. Klinger, M. Lerdau, W. A. McKay, T. Pierce, B. Scholes, R. Steinbrecher, R. Tallamraju, J. Taylor and P. Zimmerman, *J. Geophys. Res.*, 1995, **100**, 8873–8892.
- Lamb, D. Gay, H. Westberg and T. Pierce, *Atmos. Environ., Part A*, 1993, **27**, 1673–1690.
- D. C. Degenerhardt and D. E. Lincoln, *J. Chem. Ecol.*, 2006, **32**, 725–743.
- S. D. Maleknia, T. M. Vail, R. B. Cody, D. O. Sparkman, T. L. Bell and M. A. Adams, *Rapid Commun. Mass Spectrom.*, 2009, **23**, 2241–2246.
- M. Staudt and L. Lhoutellier, *Tree Physiol.*, 2007, **27**, 1433–1440.
- C. Geron, R. Rasmussen, R. R. Arnts and A. Guenther, *Atmos. Environ.*, 2000, **34**, 1761–1781.
- A. Gratién, S. N. Johnson, M. J. Ezell, M. L. Dawson, R. Bennett and B. J. Finlayson-Pitts, *Environ. Sci. Technol.*, 2011, **45**, 2755–2760.
- S. M. Aschmann, J. Arey and R. Atkinson, *Atmos. Environ.*, 2011, **45**, 4408–4411.
- S. B. Corchnoy and R. Atkinson, *Environ. Sci. Technol.*, 1990, **24**, 1497–1502.
- S. M. Aschmann, J. Arey and R. Atkinson, *Atmos. Environ.*, 2010, **44**, 3970–3975.
- F. Stuhl and H. Niki, *J. Chem. Phys.*, 1972, **57**, 3677.
- D. D. Davis, W. Bollinger and S. Fischer, *J. Phys. Chem.*, 1975, **79**, 293–294.
- R. A. Perry, R. Atkinson and J. N. Pitts, *J. Phys. Chem.*, 1977, **81**, 296–304.
- F. P. Tully, A. R. Ravishankara, R. L. Thompson, J. M. Nicovich, R. C. Shah, N. M. Kreutter and P. H. Wine, *J. Phys. Chem.*, 1981, **85**, 2262–2269.
- K. Lorenz and R. Zellner, *Ber. Bunsenges. Phys. Chem.*, 1983, **87**, 629–636.
- S. Madronich and W. Felder, *J. Phys. Chem.*, 1985, **89**, 3556–3561.
- T. J. Wallington and M. J. Kurylo, *J. Phys. Chem.*, 1987, **91**, 5050–5054.
- A. Wahner and C. Zetzsch, *J. Phys. Chem.*, 1983, **87**, 4945–4951.
- F. Witte, A. Wahner and C. Zetzsch, *Bull. Soc. Chim. Belg.*, 1983, **92**, 625–626.
- M. Rinke and C. Zetzsch, *Ber. Bunsenges. Phys. Chem.*, 1984, **88**, 55–62.
- F. Witte, E. Urbanik and C. Zetzsch, *J. Phys. Chem.*, 1986, **90**, 3251–3259.
- R. Knispel, R. Koch, M. Siese and C. Zetzsch, *Ber. Bunsenges. Phys. Chem. Chem. Phys.*, 1990, **94**, 1375–1379.
- M. Siese and C. Zetzsch, *Z. Phys. Chemie-Int. J. Res. Phys. Chem. Chem. Phys.*, 1995, **188**, 75–89.
- R. Koch, H. U. Krüger, M. Elend, W. U. Palm and C. Zetzsch, *Int. J. Chem. Kinet.*, 1996, **28**, 807–815.
- R. Koch, W. U. Palm and C. Zetzsch, *Int. J. Chem. Kinet.*, 1997, **29**, 81–87.
- R. Koch, R. Knispel, M. Elend, M. Siese and C. Zetzsch, *Atmos. Chem. Phys.*, 2007, **7**, 2057–2071.
- S. Zhang, R. Strekowski, L. Bosland, A. Monod and C. Zetzsch, *Phys. Chem. Chem. Phys.*, 2011, **13**, 11671–11677.
- S. Zhang, R. S. Strekowski, L. Bosland, A. Monod and C. Zetzsch, *Int. J. Chem. Kinet.*, 2011, **43**, 547–556.
- B. Bohn and C. Zetzsch, *Phys. Chem. Chem. Phys.*, 2012, **14**, 13933–13948.
- S. Zhang, R. S. Strekowski, A. Monod, L. Bosland and C. Zetzsch, *J. Phys. Chem. A*, 2012, **116**, 9497–9506.
- O. C. Bridgeman and E. W. Aldrich, *J. Heat Transfer*, 1964, **86**, 279–286.
- E. G. Linder, *J. Phys. Chem.*, 1931, **35**, 531–535.
- K. A. Kobe, T. S. Okabe, M. T. Ramstad and P. M. Huemmer, *J. Am. Chem. Soc.*, 1941, **63**, 3251–3252.
- R. A. McDonald, S. A. Shrader and D. R. Stull, *J. Chem. Eng. Data*, 1959, **4**, 311–313.
- W. Strubell, *J. Prakt. Chem.*, 1964, **26**, 319–323.
- V. Ruzicka Jr, M. Zabransky, K. Ruzicka and V. Majer, *Thermochim. Acta*, 1994, **245**, 121–144.
- E. S. C. Kwok and R. Atkinson, *Atmos. Environ.*, 1995, **29**, 1685–1695.
- G. J. Doyle, A. C. Lloyd, K. R. Darnall, A. M. Winer and J. N. Pitts, *Environ. Sci. Technol.*, 1975, **9**, 237–241.
- D. A. Hansen, R. Atkinson and J. N. Pitts, *J. Phys. Chem.*, 1975, **79**, 1763–1766.
- A. C. Lloyd, K. R. Darnall, A. M. Winer and J. N. Pitts, *J. Phys. Chem.*, 1976, **80**, 789–794.
- A. R. Ravishankara, S. Wagner, S. Fischer, G. Smith, R. Schiff, R. T. Watson, G. Tesi and D. D. Davis, *Int. J. Chem. Kinet.*, 1978, **10**, 783–804.
- R. A. Cox, R. G. Derwent and M. R. Williams, *Environ. Sci. Technol.*, 1980, **14**, 57–61.
- J. M. Nicovich, R. L. Thompson and A. R. Ravishankara, *J. Phys. Chem.*, 1981, **85**, 2913–2916.
- T. Ohta and T. Ohyama, *Bull. Chem. Soc. Jpn.*, 1985, **58**, 3029–3030.
- E. O. Edney, T. E. Kleindienst and E. W. Corse, *Int. J. Chem. Kinet.*, 1986, **18**, 1355–1371.
- R. Atkinson and S. M. Aschmann, *Int. J. Chem. Kinet.*, 1989, **21**, 355–365.
- U. S. EPA, *Estimation Programs Interface Suite™ for Microsoft(r) Windows*, United States Environmental Protection Agency, Washington, DC, USA, 2012.
- R. Atkinson, *J. Phys. Chem. Ref. Data Monogr.*, 1989, 228.
- J. G. Calvert, R. Atkinson, K. H. Becker, R. M. Kamens, J. H. Seinfeld, T. J. Wallington and G. Yarwood, *The Mechanisms of Atmospheric Oxidation of Aromatic Hydrocarbons*, Oxford University Press, Oxford, New York, 2002.
- C. Zetzsch, *Predicting the rate constant of OH addition to aromatics using σ^+ -electrophilic substituent constants for mono- and polysubstituted benzenes*, Abstract A11, XVth Informal Conf. on Photochemistry, Stanford, CA, USA, 1982.
- H. C. Brown and Y. Okamoto, *J. Am. Chem. Soc.*, 1958, **80**, 4979–4987.

APPENDIX C. PAPER B: ALARCON ET AL. (2014)



PCCP

PAPER

Reversible addition of the OH radical to *p*-cymene in the gas phase: multiple adduct formation. Part 2

Cite this: *Phys. Chem. Chem. Phys.*, 2014, 16, 17315

Paulo Alarcón,^a Birger Bohn,^b Cornelius Zetzsch,^{*ac} Marie-Thérèse Rayez^{*d} and Jean-Claude Rayez^{*d}

A flash photolysis-resonance fluorescence (FP-RF) system was used to study the *p*-cymene (PC) + OH reaction at temperatures between 299 and 349 K in helium. Triexponential functions were fitted to groups of observed OH decay curves according to a model considering a reversible addition to form two adducts as thermolabile reservoirs of OH. Compared to Part 1 of this paper, consideration of a second adduct strongly improved the fits to our measurements, and the rate constants for the major pathways were optimized between 299 and 349 K. The Arrhenius expression for the rate constant of the sum of OH addition and H-atom abstraction pathways was found to be $k_{\text{OH}} = 1.9 \times 10^{-12} \exp[(610 \pm 210) \text{ K}/T] \text{ cm}^3 \text{ s}^{-1}$. Rate constants of unimolecular decomposition reactions of the adducts were similar to other aromatic compounds with the following Arrhenius expressions: $1 \times 10^{12} \exp[(-7600 \pm 800) \text{ K}/T] \text{ s}^{-1}$ for adduct 1 and $4 \times 10^{11} \exp[(-8000 \pm 300) \text{ K}/T] \text{ s}^{-1}$ for adduct 2. Adduct yields increased and decreased with temperature for adduct 1 and 2, respectively, but were similar (~0.4) around room temperature. Equilibrium constants yielded values for reaction enthalpies and entropies of adduct formations. While for one adduct reasonable agreement was obtained with theoretical predictions, there were significant deviations for the other adduct. This indicates the presence of more than two adduct isomers that were not accounted for in the reaction model. Quantum chemical calculations (DFT M06-2X/6-31G(d,p)) and RRKM kinetics were employed with the aim of clarifying the mechanism of the OH addition to PC. These calculations show that formation of adducts with OH in *ortho* positions to the isopropyl and methyl substituents is predominant (55% and 24%) to those with OH in *ipso* positions (21% and 3%). A large fraction (>90%) of the *ipso*-C₃H₇ adduct is predicted to react by dealkylation forming *p*-cresol (in the absence of oxygen) and isopropyl radicals. These theoretical results agree well with the interpretation of the experimental results showing that the two *ortho* adducts (which appeared as OH reservoirs in the experiment) have been observed.

Received 13th May 2014,
Accepted 30th June 2014

DOI: 10.1039/c4cp02073a

www.rsc.org/pccp

1. Introduction

Non methane volatile organic compounds (NMVOCs) are emitted into the atmosphere by anthropogenic and biogenic sources. It has been estimated that globally biogenic emissions significantly exceed anthropogenic emissions.^{1,2} NMVOCs play a major role in the photochemical formation of ozone and secondary organic

aerosols, and both processes are initiated by OH radicals, NO₃ radicals and O₃ oxidation.^{3,4}

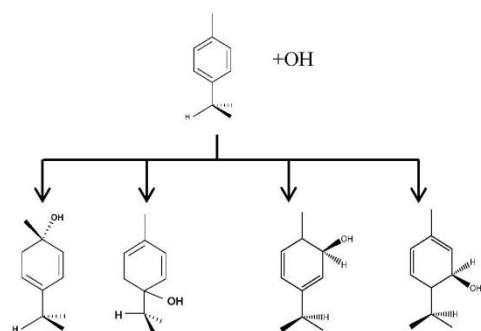
The biogenic aromatic compound *p*-cymene (1-methyl-4-isopropylbenzene or 4-isopropyltoluene) has four distinguishable positions where the OH radicals may add to the aromatic ring, as illustrated in Scheme 1: two equivalent ones *ortho* to the isopropyl group (PC_{*ortho*}-C₃H₇), two equivalent ones *ortho* to the methyl group (PC_{*ortho*}-CH₃), and two non-equivalent *ipso* positions at the site of the methyl and the isopropyl group (PC_{*ipso*}-CH₃ and PC_{*ipso*}-C₃H₇). Addition to an already occupied position (*ipso*-addition) is in general considered to be less important, but triexponential decays of OH have been observed by VUV flash photolysis/resonance fluorescence (FP-RF) in the presence of 1,3,5-trimethylbenzene, indicating that two different thermolabile adducts can regenerate OH.⁵ The observation of hexamethyl-2,4-cyclohexadienone by GC-MS as the

^a Atmospheric Chemistry Research Laboratory, University of Bayreuth, 95448, Germany

^b Institut für Energie - und Klimaforschung IEK-8: Troposphäre, Forschungszentrum Jülich, 52425 Jülich, Germany

^c Fraunhofer Institute for Toxicology and Experimental Medicine, 30625 Hannover, Germany. E-mail: cornelius.zetzsch@uni-bayreuth.de

^d Institut des Sciences Moléculaires, Université de Bordeaux, ISM UMR 5255, 33405 Talence, France. E-mail: mt.rayez@ism.u-bordeaux1.fr, jc.rayez@ism.u-bordeaux1.fr



Scheme 1 *p*-Cymene + OH addition reactions, leading to the four adducts. From left to right: $PC_{ipso}-C_3H_7$, $PC_{ipso}-C_3H_7$, $PC_{ortho}-C_3H_3$ and $PC_{ortho}-C_3H_2$.

only product from the reaction of OH with hexamethylbenzene in the presence of NO_2 implies that an addition of OH is a major first step of this reaction.⁶ Biexponential FP-RF-decays of OH in the presence of hexamethylbenzene as a prototype molecule, where *ipso* positions alone are available for addition, demonstrated a reversible reaction,⁷ and the molecular ion of the adduct has been observed by single-photon VUV photoionization as an intermediate in a flow reactor very recently.⁸ *Ips*o-type adducts may react by dealkylation and corresponding products from the reaction of toluene, *o*-, *m*-, and *p*-xylene with OH radicals have been observed by chemical ionization mass spectrometry in a flowtube study (5.4% phenol from toluene and similar yields of the cresols expected from dealkylation of the xylenes).⁹ However, these results are not in agreement with an earlier smog chamber result of a phenol yield <0.1% from OH + toluene¹⁰ and are not confirmed in a more recent smog chamber study with GC-FID analysis¹¹ that stated an upper limit of <1% formation of each cresol from OH + *m*-xylene and <2% for each cresol isomer from OH + *p*-cymene.

A total OH rate constant of $(15.1 \pm 4.1) \times 10^{-12} \text{ cm}^3 \text{ s}^{-1}$ was derived in a previous study on *p*-cymene¹² in a smog chamber at room temperature and 1 atm pressure of air. In another work,¹¹ the rate constant of H-atom abstraction was determined measuring the 4-methylacetophenone yield (the major product formed subsequent to the H-atom abstraction from the isopropyl substituent) and assuming a H-atom abstraction rate constant from the methyl substituent similar to the one determined for toluene. This led to an estimated $20 \pm 4\%$ contribution of abstraction to the overall OH rate constant. In our previous work,¹³ the *p*-cymene + OH reaction was studied over a wide temperature range assuming a single adduct formation (biexponential model). This simplification was found to be satisfactory for temperatures below 320 K and higher than about 350 K, but between these temperatures our applied model could not describe the data. A preliminary study of the OH decay curves in the intermediate temperature range revealed that triexponential functions led to better fits to groups of observed curves than biexponential ones, indicating that more than one adduct was being formed. A similar behaviour has been observed

for 1,3,5-trimethylbenzene, for which a kinetic model was proposed and the system of differential equations was solved.⁵ In the present work we apply that new model of formation of two adducts (triexponential model) to the kinetic data previously¹³ obtained on *p*-cymene by the flash photolysis-resonance fluorescence (FP-RF) technique over the temperature range between 297 and 350 K in helium buffer gas and perform theoretical calculations in order to identify the adducts, their energies and transition states.

2. Experimental

The experimental setup used in this work has been described elsewhere.^{5,13–15} Briefly, OH radicals were generated by flash photolysis of water vapour using a Perkin Elmer FX 1165 short arc xenon flash lamp as photolytic light source at an energy of 540 mJ per flash. A quartz resonance lamp was mounted at right angles to the VUV photolysis beam and to the photomultiplier. A gas mixture of H_2O -He was allowed to flow through the resonance lamp. The electrodeless microwave discharge dissociated H_2O to produce electronically excited OH ($A^2\Pi$). The radiation leaving the lamp was focused into the observation zone exciting the photochemically produced OH radicals in the reaction cell.

The fluorescence from the reaction cell passed through a 308 nm interference filter and was focused onto the photocathode of a photomultiplier tube (Thorn-EMI, 9789QB). The signal was processed and accumulated using the photon-counting technique with a discriminator and a multichannel scaler board (EG&G Ortec, model ACE MCS) at a dwell time of 0.98 ms, corresponding to a total of 4 s observation time after the flash. The concentration of water vapour in the reaction cell was kept constant at $1.5 \times 10^{15} \text{ cm}^{-3}$, leading to an estimated initial OH radical concentration of $2 \times 10^{10} \text{ cm}^{-3}$.^{16,17} The *p*-cymene concentration was varied between $5 \times 10^{12} \text{ cm}^{-3}$ and $43 \times 10^{12} \text{ cm}^{-3}$, which is high enough to assure pseudo first order conditions for OH. In contrast

Table 1 Experimental conditions. Total pressure 203 ± 2 mbar of helium

Set #	<i>T</i> and $\Delta T/K$	N^a	[<i>p</i> -Cymene] (min., max.)/ 10^{12} cm^{-3}		
1	299.0	0.2	28	5.1	38.8
2	314.6	0.5	43	4.9	39.2
3	316.8	0.5	15	7.0	42.1
4	324.1	0.3	22	7.6	43.4
5	325.9	0.2	36	7.0	42.2
6	326.0	1.8	9	6.7	16.4
7	327.3	0.0	12	7.5	19.8
8	328.5	0.0	57	7.1	42.9
9	329.9	0.2	22	7.3	42.4
10	332.0	0.2	58	6.9	42.6
11	334.2	0.3	21	4.8	39.6
12	334.3	0.2	20	7.2	32.3
13	335.3	0.2	20	6.7	42.1
14	335.7	0.2	26	6.6	39.8
15	336.2	0.0	66	7.1	42.7
16	339.9	1.0	38	5.8	41.6
17	343.5	0.2	18	6.9	41.7
18	345.2	0.1	23	7.3	42.3
19	348.0	0.4	19	7.4	41.7
20	348.9	0.1	45	4.8	39.3

^a Number of measurements.

to our previous work,¹³ only experiments performed with the xenon flash lamp were used as the set made with the N₂ spark discharge lamp seemed to be affected by impurities increasing the reactivity towards OH. The experimental conditions are summarized in Table 1. Differences between this table and Table 1 of the preceding part arise because some curves were removed from the biexponential fits. These curves were assumed to be deficient when the intensity ratio and lifetime of the first decay did not increase with increasing *p*-cymene concentration. The results presented in this work were obtained from all measurements as fits to individual decays were found to be difficult to perform at some combinations of temperature and *p*-cymene concentrations.

The gases used in this work had the following stated minimum purities: He (Rießner) – 99.996%; N₂ (Linde) – 99.999%. Liquid *p*-cymene (Aldrich) had a stated minimum purity of 99%. Deionized water was doubly distilled by a quartz still.

3. Theoretical approach

The reaction of OH with *p*-cymene (PC) is complex due to the presence of two alkyl chains, isopropyl and methyl, which differentiates each site of the molecule with respect to OH attack. The aim of the theoretical calculations is to shed some light into this complex mechanism and help to interpret the experimental results by presenting a comprehensive theoretical investigation of the OH attack on *p*-cymene. No theoretical investigation of this type has been reported so far on this system.

3.1 Computational details

All calculations were performed using the GAUSSIAN 09 package.¹⁸ The geometries and energies were optimized using density functional theory (DFT) with the hybrid meta exchange–correlation functional M06-2X,¹⁹ coupled to the split valence basis set 6-31G(d,p). This highly nonlocal M06-2X functional developed by Zhao and Truhlar¹⁹ is well suited for structures and energetics, specifically for the determination of energy barriers. The unrestricted Hartree–Fock (UHF) formulation has been used since it is a convenient way to describe open-shell and bond-breaking processes. Its use is justified in our study because we did not observe any significant spin contamination for all the stationary points explored, the quantum average value $\langle S^2 \rangle$ of the square of the total spin operator remaining close to 0.75, *i.e.*, the characteristic value for a doublet state. Full geometry optimization has been performed throughout. We have checked carefully that all the saddle points found are correctly connected to two minima and are characterized by the existence of only one negative eigenvalue of the Hessian matrix corresponding to an imaginary frequency in the normal-mode analysis.

Since one of our goals is the determination of branching ratios of all the reactive channels, Transition State Theory (TST) is a convenient tool to determine rate constants. In terms of activation free energy ΔG^\ddagger , TST formula reads:

$$k_T \propto g \left(\frac{k_B T}{h} \right) \exp \left[\frac{-\Delta G^\ddagger}{RT} \right] \quad (1)$$

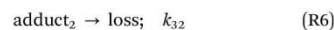
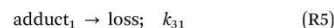
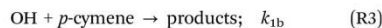
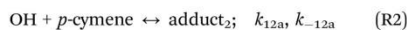
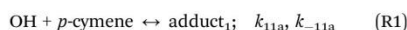
where k_B and h are respectively the Boltzmann and Planck constants and g is the number of equivalent carbon atom sites. Our aim in these calculations is not to obtain absolute values for the rate constants, but rather to look at the relative reactivity of each carbon atom site with respect to OH.

4. Experimental results and discussion

4.1 Kinetic analysis and data evaluation

As outlined above the reversible addition of OH radicals to the aromatic ring in *p*-cymene can occur at four different positions, leading to the formation of adducts with potentially different properties. The decay curves of OH can deliver first hints about the quantity of distinguishable adducts formed. The initial fast decay corresponds to the consumption of OH radicals by H-atom abstraction and OH addition, while the subsequent slower OH decays are caused by regeneration of OH by a unimolecular decomposition of unstable adducts. A biexponential OH decay indicates the formation of only one adduct or the formation of several adducts with similar kinetic properties, whereas a triexponential OH decay indicates the formation of at least two distinguishable adducts.

Decays curves of OH in the presence of *p*-cymene were found to be mostly biexponential at temperatures below around 320 K and at temperatures above about 350 K (Fig. 1).¹³ In the intermediate range deviations from biexponential behaviour were observed, and the following mechanism for the formation of two adduct species that results in triexponential decay curves was applied to fit the decay curves:⁵



The rate equations that describe the change in the concentrations of OH radicals and of the adducts are shown below.

$$\frac{d}{dt}[\text{OH}] = -a[\text{OH}] + b[\text{adduct}_1] + e[\text{adduct}_2] \quad (2)$$

$$\frac{d}{dt}[\text{adduct}_1] = c[\text{OH}] - d[\text{adduct}_1] \quad (3)$$

$$\frac{d}{dt}[\text{adduct}_2] = f[\text{OH}] - g[\text{adduct}_2] \quad (4)$$

The combined first-order rate constants are given by:

$$a = k_2 + (k_{11a} + k_{12a} + k_{1b})[p\text{-cymene}] \quad (5)$$

$$b = k_{-11a} \quad (6)$$

$$c = k_{11a}[p\text{-cymene}] \quad (7)$$

$$d = k_{-11a} + k_{31} \quad (8)$$

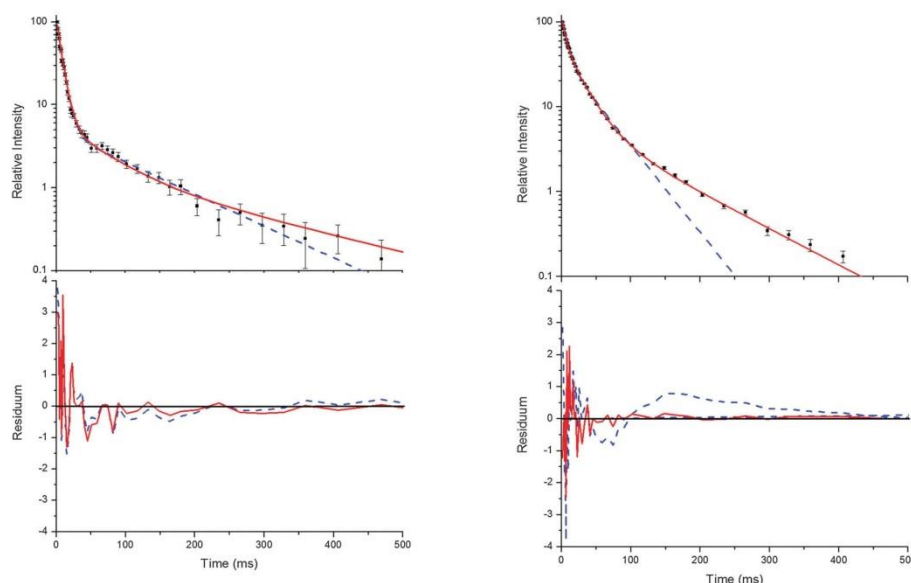


Fig. 1 Typical decay curves of OH (background subtracted), biexponential (blue dashed line) and triexponential (red solid line) model curves and fit residuals for measurements at 299 K (left side) and 330 K (right side) at a *p*-cymene concentration of $9 \times 10^{12} \text{ cm}^{-3}$ from simultaneous fits to a number (28 and 20 for the left and right side, respectively) of such curves at various concentrations. Obviously, the biexponential model curve satisfactorily describes the data at 299 K but not at 330 K while the triexponential model curves are applicable at both temperatures in agreement with the reaction model considering two adduct species ((R1)–(R6)).

$$e = k_{-12a} \quad (9)$$

$$f = k_{12a}[p\text{-cymene}] \quad (10)$$

$$g = k_{-12a} + k_{32} \quad (11)$$

Bohn and Zetzsch⁵ proposed the mechanism shown above ((R1)–(R6)) for the reaction of the trimethylbenzenes with OH radicals and obtained the analytical solution of the corresponding system of differential equations. This solution allows us to determine the parameters *a*, *bc*, *d*, *ef*, and *g* for a set of measurements at a given temperature and total pressure. Details on the analytical solution and its limitations in terms of separable parameters are given elsewhere.⁵ Although up to four different adducts can be formed in the OH reaction studied here, we confined our reaction model to two adduct species for two reasons. Firstly, because analytical solutions are not available for a greater number of adducts. Secondly, because the precision of the OH decay curves is too poor to permit a proper distinction of three or even four exponentials (Fig. 1).

Independent of the model applied, the approach has further limitations. If the decay time of the first exponential decay approaches the time resolution of our experiment (0.98 ms) fit results become distorted. Another limit is reached when the intensity ratio of the first and the second or third decay becomes too small. Then a small and quickly vanishing contribution of the first exponential remains, turning the decays

into apparently bi- or monoexponentials. In this work, these limits were reached at temperatures larger than about 350 K and therefore higher temperatures were not considered.

Technical details on the fitting procedure and on the estimation of parameter uncertainties can be found elsewhere.^{5,13} Error estimates for the exponential term in the Arrhenius and van't Hoff expressions were obtained by fitting the maximum and minimum parameter values, respectively. Due to the small temperature range, errors in the pre-exponential factors were large and therefore will not be presented here. Table 2 summarizes the combined rate constants for each isothermal set of measurements.

4.2 Background losses of OH radicals (k_2)

OH radicals may also react with minor impurities that can enter the cell from the dosing system (previous or present sample), the carrier gas or from wall desorption and leaks. Diffusion of OH radicals from the observation zone due to concentration gradient between the irradiated volume and the cell walls as well as transport due to the constant gas flow may contribute to the OH radical losses described by the rate constant k_2 . This rate constant comprised several processes, and therefore its complete understanding is complicated and related to the experimental conditions applied. In this work, the average loss rate constant was found to be 4 s^{-1} in good agreement with the experimental lifetime of OH radicals in our system without any

Table 2 Rate constants fitted for the *p*-cymene + OH reaction system (reactions (R1)–(R6))

Set #	k_2/s^{-1}	$k_{11a} + k_{12a} + k_{11b}/10^{-12} \text{ cm}^3 \text{ s}^{-1}$	$k_{11a} k_{-11a}/10^{-12} \text{ cm}^3 \text{ s}^{-2}$	$k_{-11a} + k_{31}/s^{-1}$	$k_{12a} k_{-12a}/10^{-12} \text{ cm}^3 \text{ s}^{-2}$	$k_{-12a} + k_{32}/s^{-1}$
1	-9.9 ± 4.5	14.9 ± 0.9	81 ± 18	24 ± 18	13 ± 25	6 ± 0.2
2	2.3 ± 2.1	13.1 ± 0.8	303 ± 45	52 ± 8	11 ± 6	7.1 ± 2.3
3	12.9 ± 1.9	12.7 ± 0.5	310 ± 26	61 ± 5	18 ± 5	10.3 ± 1.5
4	5.7 ± 2.1	12 ± 0.7	443 ± 56	85 ± 7	15 ± 3	10.4 ± 1.3
5	8.3 ± 1.8	11.9 ± 0.5	496 ± 52	92 ± 7	15 ± 3	11 ± 1.4
6	5.4 ± 4.4	14.7 ± 2.9	919 ± 56	107 ± 26	17 ± 10	10.2 ± 3.2
7	6.5 ± 2.1	11.5 ± 0.7	513 ± 88	99 ± 10	15 ± 3	11.4 ± 1.4
8	7 ± 1.4	11.8 ± 0.5	598 ± 62	109 ± 7	17 ± 3	12.2 ± 1
9	6.2 ± 0.1	11.7 ± 0.7	684 ± 102	123 ± 10	18 ± 3	13.1 ± 1.4
10	6.3 ± 1.2	11.7 ± 0.7	791 ± 100	141 ± 12	18 ± 2	13.9 ± 1.3
11	0.1 ± 1.6	12.4 ± 2.1	1255 ± 25	189 ± 32	19 ± 7	16.1 ± 3.1
12	12.1 ± 1.8	10 ± 1	713 ± 74	152 ± 23	26 ± 7	20.3 ± 2.6
13	2.1 ± 1.3	13 ± 1.3	1387 ± 28	209 ± 22	28 ± 4	18.8 ± 1.6
14	6.8 ± 2.4	13.1 ± 0.5	1541 ± 31	203 ± 45	29 ± 11	19.2 ± 3.7
15	4.1 ± 1.1	11.7 ± 2.2	1089 ± 22	186 ± 15	21 ± 3	16.8 ± 1.4
16	4.9 ± 1.7	11.1 ± 1.6	1450 ± 29	241 ± 36	27 ± 8	22.5 ± 3.4
17	0.8 ± 2.1	11.3 ± 1.5	1854 ± 37	309 ± 32	35 ± 6	29.8 ± 3.0
18	0.1 ± 0.8	12.6 ± 2.5	2520 ± 50	354 ± 75	35 ± 11	30.6 ± 5.8
19	-1.3 ± 4.8	16.2 ± 3.4	4860 ± 2500	486 ± 86	46 ± 14	36.7 ± 6.0
20	-1.6 ± 1.3	10.6 ± 4.9	1847 ± 970	360 ± 127	35 ± 18	34.3 ± 8.9
	-1.6 ± 1.6	10.6 ± 4.4	1847 ± 40	360 ± 480	35 ± 59	34.3 ± 19.4

reactant of about 3 s^{-1} . In contrast to the previous paper, applying the triexponential model to our measurements, some k_2 values were negative. This irregularity was found to have no effect on the determination of other combined rate constants, corroborated by the good agreement with other constants determined at similar temperatures.

4.3 OH + *p*-cymene ($k_{\text{OH}} = k_{11a} + k_{12a} + k_{1b}$)

Analogous to the biexponential model, the fitting procedure allows us to determine the total rate constant for the reaction between OH radicals and *p*-cymene, but not each rate constant individually. In the case of the triexponential model, the total rate constant consists of three rate constants: OH addition for the formation of adducts 1 (k_{11a}) and 2 (k_{12a}), and H-atom abstraction (k_{1b}). The total rate constant was found to be $(14.9 \pm 0.9) \times 10^{-12} \text{ cm}^3 \text{ s}^{-1}$ at 299 K. This value is in good agreement with the value published by Corchnoy and Atkinson $(15.1 \pm 4.1) \times 10^{-12} \text{ cm}^3 \text{ s}^{-1}$.¹² At temperatures up to around 320 K, biexponential¹³ and triexponential models show

good agreement, but deviating results at higher temperatures where the fit quality for the biexponential model was also poor (Fig. 2). This behaviour was also observed for 1,3,5-trimethylbenzene,⁵ an aromatic compound which can react with OH radicals to form two different adducts alone.

The Arrhenius expression for the total rate constant was determined as $k_{\text{OH}} = 1.9 \times 10^{-12} \exp(610 \pm 210) \text{ K}/T \text{ cm}^3 \text{ s}^{-1}$, comparable with the previously obtained for temperatures below 320 K.¹³

4.4 Forward and backward reactions ($k_{11a}k_{-11a}$; $k_{12a}k_{-12a}$)

The analytical solution of the differential equation system for the triexponential model does not allow us to separate the rate constants for the forward (k_{11a} and k_{12a}) and backward reactions (k_{-11a} and k_{-12a}), but allows us to determine their products ($k_{11a}k_{-11a}$ and $k_{12a}k_{-12a}$).⁵ A semi-logarithmic plot of these products *versus* the inverse temperature (Fig. 3) was used to determine the sum of the activation energies for OH addition and unimolecular decay for each of the adducts.

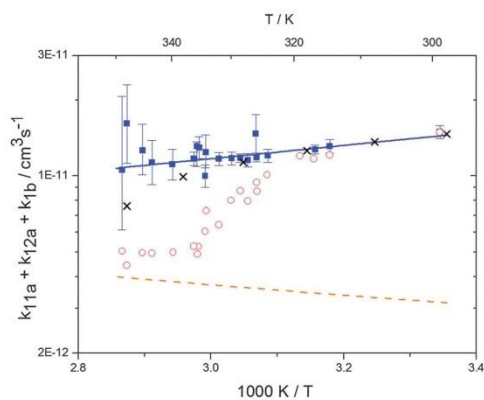


Fig. 2 Arrhenius plot of the total rate constant ($k_{11a} + k_{12a} + k_{1b}$) for the reaction OH + *p*-cymene. The blue solid line shows the Arrhenius curve for the total rate constants from the triexponential model (blue squares). Red open circles show the results of the biexponential model.¹³ The orange dashed line shows the estimated H-atom abstraction for *p*-cymene.¹³ Exes show simulated results from a combined theoretical/experimental approach (Section 6).

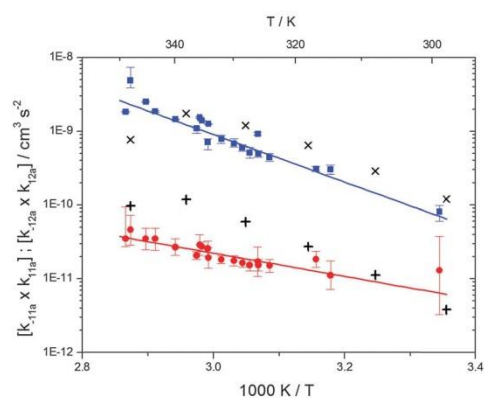


Fig. 3 Arrhenius plot for the product of the forward and backward reaction rate constants for the formation of adduct 1 (blue squares) and adduct 2 (red circles). Solid blue and red lines represent the Arrhenius curves for adduct 1 and 2, respectively. Exes and crosses show simulated results from a combined theoretical/experimental approach (Section 6) for adduct 1 and 2, respectively.

The product of the rate constants for the forward and backward reaction for both adducts increases with increasing temperature. Simple Arrhenius expressions of the form $k = A \exp(-B/T)$ were fitted to the data at temperatures between 299 and 349 K resulting in $k_{11a}k_{-11a} = 4 \exp[(-7400 \pm 550) \text{ K}/T] \text{ cm}^3 \text{ s}^{-2}$ for adduct 1 and $k_{12a}k_{-12a} = 1.2 \times 10^{-6} \exp[(-3620 \pm 1200) \text{ K}/T] \text{ cm}^3 \text{ s}^{-2}$ for adduct 2. The sums of activation energies of forward and backward reactions were calculated from the B parameters to be $(62 \pm 5) \text{ kJ mol}^{-1}$ and $(30 \pm 10) \text{ kJ mol}^{-1}$ for adduct 1 and 2 respectively.

4.5 Unimolecular decay and background loss of the adducts ($k_{-11a} + k_{31}$; $k_{-12a} + k_{32}$) and adduct formation yields

Another combined rate constant that can be directly determined is the sum of the rate constants of unimolecular decay of the adducts back to the reactants and other products and of background losses by reactions with impurities. Possible perturbations by radical-radical reactions and diffusion processes have been already investigated.⁵ While the unimolecular decay of the adducts strongly depends on the temperature, background reactions are assumed to be constant in the studied temperature range. Adduct loss rate constants for each adduct were fitted between 299 and 350 K to a function of the form $k = A \exp(-B/T) + C$. However, in a first step optimized parameters C (Fig. 4) were determined using expressions for the adduct yields and OH budget considerations.

Adduct formation yields were determined using eqn (12)–(15). The rate constants k_{1b} of H atom abstraction were taken from our previous work:¹³ $k_{1b} = 2 \times 10^{-17} (T/\text{K})^2 \exp(170 \text{ K}/T) \text{ cm}^3 \text{ s}^{-1}$. At low temperatures, the denominators $(d - k_{31})$ and $(g - k_{32})$ are getting very small, making the obtained yields strongly dependent on k_{31} and k_{32} . Optimized values (7.5 ± 3.2) and $(4.1 \pm 0.3) \text{ s}^{-1}$ were determined for k_{31} and k_{32} , respectively, that correspond to an average total yield of unity.

$$\Phi_1 = \frac{k_{11a}}{k_{\text{OH}}} = \frac{k_{11a}k_{-11a}}{k_{\text{OH}}k_{-11a}} = \frac{bc}{k_{\text{OH}}(d - k_{31})} \quad (12)$$

$$\Phi_2 = \frac{k_{12a}}{k_{\text{OH}}} = \frac{k_{12a}k_{-12a}}{k_{\text{OH}}k_{-12a}} = \frac{ef}{k_{\text{OH}}(g - k_{32})} \quad (13)$$

$$\Phi_{\text{abst}} = \frac{k_{1b}}{k_{\text{OH}}} \quad (14)$$

$$\sum \Phi_i = 1 \quad (15)$$

The various yields are shown in Fig. 5. The yields of adduct 1 and adduct 2 are similar at room temperature but then increase and decrease with temperature, respectively. Expectedly, the total adduct yield decreases with temperature because of an increasing yield of H-atom abstraction. Background loss rate constants were found to be in good agreement with those found in the literature for benzene,^{20,21} toluene,^{20,21} *p*-xylene,²² 1,3,5-TMB⁵ and hexamethylbenzene,¹⁶ ranging from 2 to 8 s^{-1} . Using the optimized values of k_{31} and k_{32} , Arrhenius expressions for the rate constants of unimolecular decompositions of the adducts were obtained: $k_{-11a} = 1 \times 10^{12} \exp[(-7600 \pm 800) \text{ K}/T] \text{ s}^{-1}$ and $k_{-12a} = 3 \times 10^{11} \exp[(-8000 \pm 300) \text{ K}/T] \text{ s}^{-1}$.

Activation energies for both adducts are very similar with values of 60 ± 7 and $67 \pm 2 \text{ kJ mol}^{-1}$ for adduct 1 and 2, respectively. These are rather similar to adducts formed from the OH radical addition to a non-occupied position as in the case of benzene (72 kJ mol^{-1}).²⁰ Fig. 4 shows the adduct loss rate constants for both *p*-cymene adducts in comparison with hexamethylbenzene⁷ and both mesitylene⁵ adducts. The dissociation rate constants found for the *p*-cymene adducts are very similar to the ones corresponding to the mesitylene

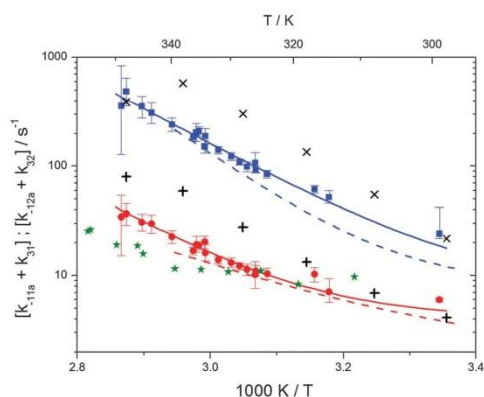


Fig. 4 Arrhenius plot for the sum of unimolecular and background loss rate constants for adduct 1 (blue squares) and adduct 2 (red circles), the hexamethylbenzene adduct (green asterisks).⁷ The blue and red dashed lines show the rate constants of the *ortho* and *ipso* adduct of 1,3,5-trimethylbenzene.⁵ Solid lines represent the modified Arrhenius curves for the adduct 1 and 2, respectively. Exes and crosses show simulated results from a combined theoretical/experimental approach (Section 6) for adduct 1 and 2, respectively.

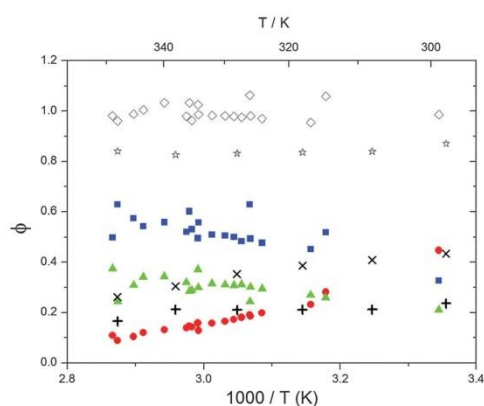


Fig. 5 Formation yields for adduct 1 (blue squares), adduct 2 (red circles) and H-atom abstraction (green triangles) after optimization of k_{31} and k_{32} . Rhombi show the sum of the calculated yields. Exes, crosses and asterisks show simulated results of a combined theoretical/experimental approach (Section 6) for adduct 1 and 2, and their sum, respectively.

adducts where only two isomers, *ipso* and *ortho*, can be formed. Furthermore, adducts 2 of *p*-cymene and mesitylene have low dissociation rate constants that are comparable to those obtained for hexamethylbenzene¹⁶ where only *ipso* adducts are possible. The similarity of the activation energies of the adducts with the one of benzene, as well as the similarity of the dissociation rate constants of adduct 2 with the ones published for hexamethylbenzene make it very difficult to identify which

adduct or group of adducts is responsible for the triexponential OH decays observed.

4.6 Equilibrium constants ($K_{\text{eq}1}$, $K_{\text{eq}2}$) and thermochemical data

A measure of the stability of the adducts is given by their equilibrium constants, $K_{\text{eq}1}$, $K_{\text{eq}2}$ (Fig. 6). These constants were estimated using eqn (16) and (17) with background losses (k_{31} and k_{32}) determined in the previous section.

$$K_{\text{eq}1} = \frac{bc}{[d - k_{31}]^2} \quad (16)$$

$$K_{\text{eq}2} = \frac{ef}{[g - k_{32}]^2} \quad (17)$$

Equilibrium constants for both adducts are shown in Fig. 6 and can be expressed between 299 and 345 K by following equations:

$$K_{\text{eq}1} = 6.2 \times 10^{-26} (T/K) \exp[(7150 \pm 170) K/T] \text{ cm}^3 \quad (18)$$

$$K_{\text{eq}2} = 2.3 \times 10^{-29} (T/K) \exp[(10200 \pm 1200) K/T] \text{ cm}^3 \quad (19)$$

Standard reaction enthalpies and entropies were determined for each adduct using a van't Hoff expression (20). The values obtained were: $\Delta H_1 = (-59 \pm 1) \text{ kJ mol}^{-1}$, $\Delta S_1 = (-64 \pm 6) \text{ J mol}^{-1} \text{ K}^{-1}$ for the first and $\Delta H_2 = (-85 \pm 10) \text{ kJ mol}^{-1}$, $\Delta S_2 = (-130 \pm 27) \text{ J mol}^{-1} \text{ K}^{-1}$ for the second adduct.

$$K_{\text{eq}} = \frac{k_{\text{B}}T}{p^{\nu}} \exp\left(-\frac{\Delta H}{RT} + \frac{\Delta S}{R}\right) \quad (20)$$

The reaction enthalpy of adduct 2 is in reasonable agreement with results for other OH aromatics adducts from the literature.²³ However, the reaction enthalpy of adduct 1 is significantly smaller

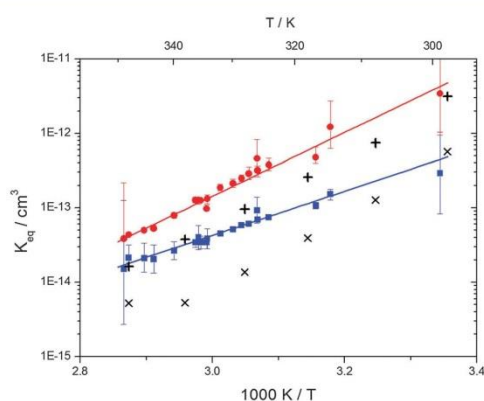


Fig. 6 Equilibrium constants for adduct 1 (blue squares) and adduct 2 (red circles). Solid lines represent the regression curves between 299 and 345 K (eqn (18) and (19)). Exes and crosses show the simulated results from a combined theoretical/experimental approach (Section 6) for adduct 1 and 2, respectively.

which is also in contradiction with theoretical predictions for different adduct isomers from other aromatics.^{24–28} Moreover, the reaction entropy of adduct 1 is clearly too small for an association reaction and should in any case be very similar for both adducts. These inconsistencies point towards a perturbation possibly caused by the presence of more than two adduct species.

In our previous work,¹³ the reduced χ^2 was applied to reject the simpler model for the formation of one single adduct. The mechanism proposed in the present work strongly improves the fit quality. However, despite the huge improvements reached by the triexponential model, there are still some high χ^2 values at temperatures between 330 and 340 K. These values might indicate the influence of further adduct species producing a departure from triexponential decays. To evaluate these deviations, OH decay curves with much higher precision would be needed as well as numerical tools to fit these curves but this is beyond our current capabilities.

5. Theoretical results

5.1 OH addition to *p*-cymene

As shown in Scheme 1, OH radical addition to the aromatic ring of *p*-cymene may form four isomers of *p*-cymene-OH adducts,

two *ipso* isomers ($PC_{ipso}\text{-CH}_3$ and $PC_{ipso}\text{-C}_3\text{H}_7$) and two *ortho* isomers ($PC_{ortho}\text{-CH}_3$ or $PC_{ortho}\text{-C}_3\text{H}_7$). The correlation diagram between the relevant stationary states is illustrated in Fig. 7, and the corresponding zero-point corrected energies are gathered in Table 3. The pathways are initiated by the formation of the pre-reactive complex (PRC in Fig. 7) typical of electrophilic addition to aromatics²⁹ which corresponds to a long range interaction between *p*-cymene and the OH radical and is common to each addition channel. In this structure, the radical OH is situated above the aromatic ring. This PRC lies 26 kJ mol^{-1} below the energy of the separated reactants. On the way from the PRC to TS_{add} , the C–O distance diminishes from 2.5 \AA to $\sim 2.0\text{ \AA}$. It can be seen that the reactions are all exothermic by -85 kJ mol^{-1} in a narrow range of 5 kJ mol^{-1} . The ΔE_0^\ddagger barriers, called TS_{add} in a generic way, are also very close together in a range between -2.4 and $+2.5\text{ kJ mol}^{-1}$. Such small values could suggest that the yields of *ipso* and *ortho* adducts are similar. In fact, the entropy change from the reactants to the TS is no more negligible and its value can be different from one pathway to the other. It is therefore essential to take into account the change of entropy in each pathway by calculating the Gibbs free energy barriers $\Delta G_T^\ddagger = \Delta H_T^\ddagger - T\Delta S_T^\ddagger$ at temperature T . On the basis of the calculated ΔG_{298}^\ddagger values, bimolecular OH-addition rate constants

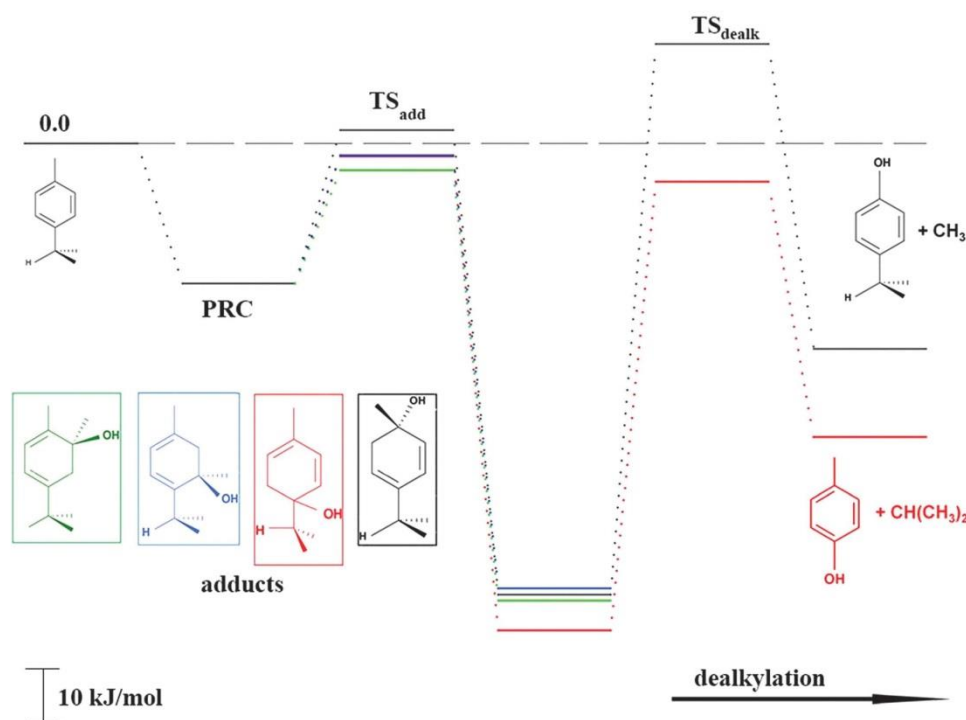


Fig. 7 Energy diagram for the addition reaction *p*-cymene + OH and successive dealkylation of the *ipso* adducts.

Table 3 M06-2X/6-31G(d,p) zero-point corrected energy barriers (ZPE), ΔE_0^\ddagger , activation enthalpies ΔH_{298}^\ddagger , activation entropies ΔS_{298}^\ddagger , free energy barriers, ΔG_{298}^\ddagger , and reaction energies, relative to the reactants *p*-cymene + OH,^a and branching ratios, ρ_{add} (i.e. the percentage of each addition site). The ZPE barrier for dealkylation ΔE_0^\ddagger (TS_{dealk}) and energy for cresol formation, ΔE_0 (cresol formation). The energy of the pre-reactive complex, ΔE_0 (PRC), is $-25.9 \text{ kJ mol}^{-1}$.^{a,b}

	ΔE_0^\ddagger	ΔH_{298}^\ddagger	ΔS_{298}^\ddagger	ΔG_{298}^\ddagger	ΔE_0	ρ_{add}	ΔE_0^\ddagger	ΔE_0	cresol formation
PC _{<i>ipso</i>} -CH ₃	2.5	-1.9	-149.8	42.7	-83.6	3	18.4	-38.1	
PC _{<i>ipso</i>} -C ₃ H ₇	-2.4	-6.6	-151.3	38.5	-90.3	18	-7.1	-52.3	
PC _{<i>ortho</i>} -CH ₃	-0.8	-5.1	-149.5	39.5	-84.7	24			
PC _{<i>ortho</i>} -C ₃ H ₇	-2.2	-6.2	-146.3	37.4	-82.4	55			

^a Energies are given in kJ mol^{-1} . ^b Entropies in $\text{J mol}^{-1} \text{K}^{-1}$.

were calculated from eqn (1). The branching ratios ρ_{add} are easily determined from the ratio of each rate constant channel over the total rate constant. All these data are collected in Table 3.

As a result of our calculations, it can be predicted that, among the four different addition possibilities: (i) the formation of the *ipso*-CH₃ adduct can be neglected from the reaction mechanism (3% of the total addition); (ii) the formation of *ortho* adducts is predominant (79%); (iii) the *ipso*-C₃H₇ adduct is formed (by 18% of total addition) but can further dissociate, *via* dealkylation, to give new products. This is the subject of the following section.

5.2 Formation of cresol by dealkylation of *ipso* adducts

PC_{*ipso*}-C₃H₇ and PC_{*ipso*}-CH₃ may dealkylate to form the phenol type compounds *p*-cresol + isopropyl radical (C₃H₇) and 4-isopropyl phenol + methyl radical (CH₃). The calculated transition state and reaction energies for both of these decompositions are sketched in the right part of Fig. 7. The overall reaction energies OH + *p*-cymene, leading to the formation of 4-isopropyl phenol + CH₃ or *p*-cresol + C₃H₇, are exothermic by -38 kJ mol^{-1} and -52 kJ mol^{-1} .

The corresponding free energies of activation, ΔG_{298}^\ddagger for 298 K, suggest that only the isopropyl departure from the *ipso*-C₃H₇ adduct can occur at room temperature, since the energy barrier is lower by -7 kJ mol^{-1} than the energy of the reactants *p*-cymene + OH. In order to test this assumption, we have performed some preliminary kinetic calculations on this dealkylation channel by using a statistical approach based on a Rice-Ramsperger-Kassel-Marcus-like (RRKM)³⁰ methodology. Based on the potential energy profile obtained from DFT calculations, data presented in Table 3 was used for the kinetic analysis. For each of these stationary points, harmonic vibrational wavenumbers and the rotational constants calculated by the GAUSSIAN09 quantum chemistry program¹⁸ were used. Table 4 summarizes these results at two temperatures and two pressures.

While there is no significant direct formation of cresol from OH + cymene, cresol is the main product of the unimolecular decomposition of the stabilized PC_{*ipso*}-C₃H₇ as indicated by the factor β . This finding is not in contradiction with product studies that showed no significant (<2%) cresol formation¹¹ because in the presence of O₂ cresol formation competes with the PC_{*ipso*}-C₃H₇ + O₂ reaction that is expected to be much faster

Table 4 Kinetic calculations on the dealkylation channel from the *ipso*-C₃H₇ adduct^a

T/K	P/mbar	$k_{\text{loss}}/10^{-13} \text{ cm}^3 \text{ s}^{-1}$	$k_{\text{prod}}/10^{-15} \text{ cm}^3 \text{ s}^{-1}$	$k_{\text{adduct}}/10^{-13} \text{ cm}^3 \text{ s}^{-1}$	β
298	760	0.166	6.18	0.166	0.05
400	760	0.194	116	0.193	0.1
298	380	0.166	12.3	0.166	0.05

^a k_{loss} : disappearance of the reactants for this addition channel; k_{prod} : immediate formation of products *p*-cresol + C₃H₇; k_{adduct} : stabilization of the *ipso* adduct; β : rate of regeneration of the reactants OH and *p*-cymene from the adduct divided by the formation of products *p*-cresol + C₃H₇ from the adduct.

under atmospheric conditions. However, in the absence of O₂, confirmation of cresol formation would be a strong indicator for the presence of the *ipso* adduct.

5.3 Results for reaction entropies, enthalpies and equilibrium constants

Reaction entropies ΔS_{298} , reaction enthalpies ΔH_{298} and equilibrium constants K_{eq} have been calculated for the addition reactions at 298 K and are collected in Table 5, together with the corresponding experimental results obtained in this work. Calculated enthalpies are in good agreement with literature data for different OH adduct isomers from other aromatics.^{23–28} As the *ipso*-CH₃ contribution is minor, and the *ipso*-C₃H₇ is expected to mainly dealkylate to cresol, the two adducts that are theoretically expected to determine OH regeneration are the remaining *ortho*-CH₃ and *ortho*-C₃H₇ adducts. Experimental entropy and enthalpy changes for adduct 1 are much smaller than those obtained from DFT calculations. This disagreement might arise from a wrongful application of the triexponential model to a system with three or four adducts, as mentioned in Section 4.6. Even though the obtained experimental enthalpy and entropy for adduct 2 are more comparable with the theoretical values, the experimental uncertainty does not allow to clearly identify this adduct. Nevertheless, the lower yields and greater equilibrium constants are closer to the predictions for the *ortho*-CH₃ adduct. In order to make the theoretical and experimental results more comparable, numerical simulations were performed and will be presented in the following section.

Table 5 Calculated M06-2X/6-31G(d,p) reaction entropies^a ΔS_{298} , reaction enthalpies, ΔH_{298} , reaction free energies, ΔG_{298} at 298 K (relative to the reactants *p*-cymene + OH^b) and calculated equilibrium constants, $K_{\text{eq}}(T) = k_{\text{f}}/k_{\text{r}} \text{ exp}[-\Delta G_{\text{f}}/RT]$ for the four theoretically possible adducts and experimental results for comparison

	ΔS_{298}^a	ΔH_{298}^b	ΔG_{298}^b	K_{eq}^c (298 K)/10 ⁻¹³
PC _{<i>ipso</i>} -CH ₃	-161.1	-89.2	-41.2	7.0
PC _{<i>ipso</i>} -C ₃ H ₇	-155.2	-95.3	-49.0	160
PC _{<i>ortho</i>} -CH ₃	-154.0	-89.6	-43.7	19
PC _{<i>ortho</i>} -C ₃ H ₇	-163.2	-87.9	-39.3	3.2
Adduct 1 ^d	-64 ± 6	-59 ± 1	-40 ± 1	4.9
Adduct 2 ^d	-130 ± 27	-85 ± 10	-46 ± 2	50

^a Entropies in $\text{J mol}^{-1} \text{K}^{-1}$. ^b Energies in kJ mol^{-1} . ^c K_{eq} in cm^3 . ^d This work (experimental).

6. Comparison of experimental and theoretical results using simulated OH decays

The theoretical results presented in the previous section predict the formation of all four possible adduct isomers. However, the relative yields and kinetic properties regarding back-decomposition and dealkylation are different for the different isomers. The question arises what results would be obtained from corresponding OH decay curves using the same data analysis that was applied for the experimental data of this work. To answer this question, OH decay curves were simulated by numerical calculations at a similar range of temperatures and reactant concentrations for direct comparison. For this purpose, a complete set of rate constants as a function of temperature is necessary.

We used the TST predicted adduct yields and the measured total rate constants of adduct formation (k_{add}) to make simulations and measurements more comparable. Values of k_{add} were obtained by subtracting the rate constants of abstraction k_{1b} from the k_{OH} obtained in this work:

$$k_{\text{add}} = k_{\text{OH}} - k_{1b} \quad (21)$$

using the Arrhenius expressions of k_{OH} and k_{1b} given in Sections 4.3 and 4.5. The total rate constant k_{OH} is considered to be a robust quantity that can be extracted from the experimental data without knowing the actual number of isomers formed. Using eqn (1) and the $\Delta H_{298}^{\ddagger}$ and $\Delta S_{298}^{\ddagger}$ data (Table 3), adduct yields ρ_T were calculated for six temperatures in a range 298–348 K and scaled with the corresponding k_{add} :

$$k_{\text{add}}(i) = k_{\text{add}} \times \rho(i) \quad (22)$$

Here i stands for the different isomers and the resulting individual rate constants $k_{\text{add}}(i)$ are listed in Table 6. It should be noted that the temperature dependencies of enthalpies and

entropies are negligible ($<1\%$) in the narrow range considered here. In a second step, the first-order rate constants of adduct dissociation back to OH + *p*-cymene, $k_{\text{cym}}(i)$ were determined from the equilibrium constants K_{eq} obtained from the theoretically calculated ΔH_{298} and ΔS_{298} of the adduct formation reactions (Table 5).

$$k_{\text{cym}}(i) = k_{\text{add}}(i)/K_{\text{eq}}(i) \quad (23)$$

For the PC_{ipso}-C₃H₇ isomer also the rate constants of cresol formation were calculated from the estimated ratios β of rate constants of back-dissociation and cresol formation for this isomer (Table 4).

$$k_{\text{cresol}}(\text{PC}_{\text{ipso}}\text{-C}_3\text{H}_7) = k_{\text{cym}}(\text{PC}_{\text{ipso}}\text{-C}_3\text{H}_7)/\beta \quad (24)$$

In Table 7 the obtained first-order rate constants $k_{\text{cresol}}(\text{PC}_{\text{ipso}}\text{-C}_3\text{H}_7)$ and the $k_{\text{cym}}(i)$ for all isomers are listed. The rate constants in Tables 6 and 7 reveal that theoretically only a slight variation of adduct yields with temperature is expected. Moreover, the yield of PC_{ipso}-CH₃ remains below 5% at all temperatures and the predicted main fate of PC_{ipso}-C₃H₇ is decomposition to cresol + C₃H₇.

Based on the rate constants in Tables 6 and 7, OH decay curves were simulated numerically using FACSIMILE (MCPA Software Ltd., Oxfordshire, UK) assuming a realistic OH starting concentration of $1 \times 10^{10} \text{ cm}^{-3}$. Additional background loss rate constants of 3 s^{-1} for all adduct isomers and 10 s^{-1} for OH were also implemented to improve the comparability with experimental conditions. Decay curves were produced for five *p*-cymene concentrations in the range $0.8\text{--}4 \times 10^{13} \text{ cm}^{-3}$ as in the real experiments for the six temperatures under consideration. The obtained concentration profiles were then converted to count rates including background and finally to count numbers binned exactly as in the real experiments. Poisson random noise was added dependent on the count numbers and 150 single OH decay curves were accumulated to simulate the typical repetition of single shot experiments.

Table 6 k_{OH} , k_{1b} and individual rate constants of adduct formation $k_{\text{add}}(i)$ of four adduct isomers at different temperatures. The $k_{\text{add}}(i)$ were calculated from theoretically predicted isomer yields and the experimental total rate constant of adduct formation $k_{\text{add}} = k_{\text{OH}} - k_{1b}$

T/K	$k_{\text{OH}}/10^{-11} \text{ cm}^3 \text{ s}^{-1}$	$k_{1b}/10^{-12} \text{ cm}^3 \text{ s}^{-1}$	$k_{\text{add}}(\text{PC}_{\text{ipso}}\text{-CH}_3)/10^{-13} \text{ cm}^3 \text{ s}^{-1}$	$k_{\text{add}}(\text{PC}_{\text{ipso}}\text{-C}_3\text{H}_7)/10^{-12} \text{ cm}^3 \text{ s}^{-1}$	$k_{\text{add}}(\text{PC}_{\text{ortho}}\text{-CH}_3)/10^{-12} \text{ cm}^3 \text{ s}^{-1}$	$k_{\text{add}}(\text{PC}_{\text{ortho}}\text{-C}_3\text{H}_7)/10^{-12} \text{ cm}^3 \text{ s}^{-1}$
298.0	1.47	3.14	0.380 (3%)	2.06 (18%)	2.78 (24%)	6.35 (55%)
308.0	1.38	3.29	0.362	1.84	2.54	5.73
318.0	1.29	3.45	0.344	1.65	2.32	5.16
328.0	1.22	3.61	0.326	1.48	2.12	4.66
338.0	1.15	3.78	0.307	1.33	1.93	4.20
348.0	1.10	3.95	0.289 (4%)	1.19 (17%)	1.76 (25%)	3.78 (54%)

Table 7 First-order rate constants of cresol + C₃H₇ formation from the PC_{ipso}-C₃H₇ isomer and individual rate constants of OH + *p*-cymene formation $k_{\text{cym}}(i)$ from all four OH adduct isomers at different temperatures. The $k_{\text{cym}}(i)$ were calculated from theoretically predicted equilibrium constants and the $k_{\text{add}}(i)$ of Table 5. The ratios $k_{\text{cym}}/k_{\text{cresol}}$ correspond to the theoretically predicted β (see Section 5.2)

T/K	$k_{\text{cresol}}(\text{PC}_{\text{ipso}}\text{-C}_3\text{H}_7)/\text{s}^{-1}$	$k_{\text{cym}}(\text{PC}_{\text{ipso}}\text{-CH}_3)/\text{s}^{-1}$	$k_{\text{cym}}(\text{PC}_{\text{ipso}}\text{-C}_3\text{H}_7)/\text{s}^{-1}$	$k_{\text{cym}}(\text{PC}_{\text{ortho}}\text{-CH}_3)/\text{s}^{-1}$	$k_{\text{cym}}(\text{PC}_{\text{ortho}}\text{-C}_3\text{H}_7)/\text{s}^{-1}$
298.0	2.56	0.545	0.128	1.48	19.8
308.0	7.06	1.62	0.387	4.24	54.6
318.0	18.1	4.46	1.08	11.3	141
328.0	43.8	11.5	2.83	28.0	339
338.0	99.5	27.6	6.93	65.6	769
348.0	214	62.7	16.0	145	1650

Table 8 Mean fit results and fit qualities with standard deviations from the analysis of numerically calculated OH decay curves and simulated experiments with random noise. Parameters correspond to those in Table 2 but standard deviations were obtained from 100 simulated experiments for each set of OH decay curves

<i>T</i> /K	k_2/s^{-1}	$k_{11a} + k_{12a} + k_{1b}/10^{-11} \text{ cm}^3 \text{ s}^{-1} (=k_{\text{OH}})$	$k_{11a}k_{-11a}/10^{-10} \text{ cm}^3 \text{ s}^{-2}$	$k_{12a}k_{-12a}/10^{-11} \text{ cm}^3 \text{ s}^{-2}$	$k_{-11a} + k_{31}/s^{-1}$	$k_{-12a} + k_{32}/s^{-1}$	χ^2/DOF
298.0	9.3 ± 1.1	1.464 ± 0.013	1.20 ± 0.02	0.38 ± 0.10	21.9 ± 0.6	4.1 ± 0.6	1.17 ± 0.10
308.0	8.9 ± 0.8	1.365 ± 0.014	2.91 ± 0.06	1.13 ± 0.07	55.1 ± 0.9	6.9 ± 0.3	1.12 ± 0.09
318.0	9.4 ± 0.7	1.258 ± 0.022	6.44 ± 0.28	2.73 ± 0.11	135.6 ± 3.3	13.3 ± 0.3	1.09 ± 0.09
328.0	10.1 ± 0.6	1.134 ± 0.034	12.0 ± 1.2	5.92 ± 0.21	303 ± 15	27.8 ± 0.6	1.07 ± 0.09
338.0	10.4 ± 0.8	0.996 ± 0.091	17.5 ± 7.1	11.8 ± 0.8	580 ± 110	59.0 ± 1.6	1.05 ± 0.08
348.0	11.2 ± 1.0	0.76 ± 0.11	7.7 ± 8.5	9.7 ± 8.5	390 ± 310	80 ± 38	1.04 ± 0.10

For each temperature simultaneous fits to the five decay curves at different *p*-cymene concentrations were then performed with the software tools developed for the experimental data. Fit results varied slightly when the procedure described in the last paragraph was repeated caused by the applied random noise. Experiment simulations and fits were therefore repeated 100 times to obtain mean values and standard deviations of fit parameters and fit qualities. The results are listed in Table 8 and shown as black symbols for direct comparison in Fig. 2–6.

Previous applications of the method showed that simulations based on the pure two-adduct model ((R1)–(R6)) exactly returned the rate constants used for the numerical calculations. Moreover, in these cases the mean fit quality parameter χ^2/DOF was unity.⁵ This is the expected ideal result when experimental uncertainties are known as for the simulations. A significant deviation from unity therefore indicates a departure of the mechanism from the two-adduct model. In the case discussed here there is merely a slight deviation which is hardly significant. Thus within the simulated uncertainties OH decay curves are effectively triexponential in agreement with the two-adduct model. The explanation of course is that two of the four adduct isomers that are formed play a minor role because either their yield is low (PC_{ipso}-CH₃) or they mainly decompose to products other than OH (PC_{ipso}-C₃H₇).

While the OH background loss rate constant k_2 is reproduced in all cases, with increasing temperature the fitted k_{OH} tend to deviate from those applied in the simulations (Table 6). Note that this deviation is not accompanied by a decrease of fit quality, so there are compensating effects, and fit quality therefore is a necessary but not sufficient condition that a reaction model is correct. Moreover, in the presence of a fast decomposing adduct the range of useful temperatures for such an analysis is clearly limited as explained in Section 4.1. In the simulated measurements this limit is already reached around 340 K as is evident from the levelling off of adduct 1 rate constants at greater temperatures.

Expectedly, the parameters $k_{11a}k_{-11a}$ and $k_{12a}k_{-12a}$ roughly correspond to the products $k_{\text{add}}(\text{PC}_{\text{ortho}}-\text{C}_3\text{H}_7) \times k_{\text{cym}}(\text{PC}_{\text{ortho}}-\text{C}_3\text{H}_7)$ and $k_{\text{add}}(\text{PC}_{\text{ortho}}-\text{CH}_3) \times k_{\text{cym}}(\text{PC}_{\text{ortho}}-\text{CH}_3)$, respectively. And the parameters $k_{-11a} + k_{31}$ and $k_{-12a} + k_{32}$ more or less resemble $k_{\text{cym}}(\text{PC}_{\text{ortho}}-\text{C}_3\text{H}_7) + 3 \text{ s}^{-1}$ and $k_{\text{cym}}(\text{PC}_{\text{ortho}}-\text{CH}_3) + 3 \text{ s}^{-1}$, respectively, but the agreement is not perfect showing that the influence of the two *ipso*-isomers is not completely negligible even at the lowest temperature. Nevertheless, the further analysis reveals that the two adduct approach is also sufficient to extract

reasonable values of adduct yields (Fig. 5) and equilibrium constants (Fig. 6) of the two adducts.

Moreover, the decomposition of the PC_{ipso}-C₃H₇ to cresol can be recognized by the fact that only about 90% of k_{OH} can be accounted for by $k_{11a} + k_{12a} + k_{1b}$. However, no such missing yield was recognized in the experiments that show no evidence for any unaccounted loss of OH.

Regarding the thermodynamic data, reaction enthalpies of -90 kJ mol^{-1} (adduct 1) and -89 kJ mol^{-1} (adduct 2) were obtained considering a temperature range $<340 \text{ K}$ that compare very well with the data applied to calculate the rate constants: -88 kJ mol^{-1} (PC_{ortho}-C₃H₇) and -90 kJ mol^{-1} (PC_{ortho}-CH₃). Reaction entropies are also in good agreement: $-166 \text{ J mol}^{-1} \text{ K}^{-1}$ (adduct 1) and $-146 \text{ J mol}^{-1} \text{ K}^{-1}$ (adduct 2) compared to $-163 \text{ J mol}^{-1} \text{ K}^{-1}$ (PC_{ortho}-C₃H₇) and $-154 \text{ J mol}^{-1} \text{ K}^{-1}$ (PC_{ortho}-CH₃) listed in Table 5. For all fit parameters in Fig. 2–6 a qualitative agreement is obtained but differences are clearly outside experimental uncertainties. Because the accuracies of the experimental and the theoretical approach are hard to quantify we conclude that the experimental results are not inconsistent with the theoretical prediction that the two experimentally distinguished adducts are PC_{ortho}-C₃H₇ (adduct 1) and PC_{ortho}-CH₃ (adduct 2).

7. Conclusions

The reaction *p*-cymene + OH was reinvestigated using a reaction model assuming formation of two adduct species. This model results in triexponential OH decay curves in the presence of *p*-cymene that can be evaluated to extract the rate constants of the underlying reaction model. Despite the fact that the reaction between *p*-cymene and OH radicals can form four different adducts (two *ipso*-type and two *ortho*-type adducts) observed OH decays fit to that model within experimental error. Good agreement with literature data was found for the rate constant of OH reaction at room temperature. In a temperature range between 299 and 349 K Arrhenius expressions for rate constants of the reaction model were obtained, as well as the yields of the supposed two adducts. Thermodynamic data were derived from temperature dependent equilibrium constants. For one adduct reasonable results were obtained but for the second adduct the reaction enthalpy and reaction entropy are not within expectations and probably influenced by the presence of further adduct species. DFT calculations were made that indeed predict the formation of all four possible adducts with different

yields. A full set of thermodynamic data for all relevant reactions was obtained. The formation of the two *ortho*-adducts was found to be predominant while the *ipso*-adducts are either almost negligible (*ipso*-CH₃) or react mostly by dealkylation rather than back-dissociation to OH and *p*-cymene (*ipso*-C₃H₇). This led to the conclusion that mainly the two *ortho* adducts were in equilibrium with OH and therefore detected in the experiments, resulting in triexponential OH decays. Finally, numerical simulations of OH decay curves were made using a combination of the theoretical results and measured OH rate constants. These decay curves were evaluated to quantify any departure from triexponential behavior and to reproduce the consequences of using the simplified reaction model. Results from these simulations show a qualitative agreement with experiments but differences are outside experimental uncertainties. The results from these simulations show a reasonable agreement with experimental results confirming the theoretical prediction that two distinguished adducts are PC_{ortho}-C₃H₇ (adduct 1) and PC_{ortho}-CH₃ (adduct 2).

Acknowledgements

This work was supported by the Deutsche Forschungsgemeinschaft under grant ZE 792/6-1 and BO 1580/3-1, and by CNRS/INSU within the French-German CNRS-INSU/DFG bilateral program ATMOCHEM. We thank Rafal Strekowski (University of Provence) for the first, exploratory experiments with *p*-cymene and OH and the group of Roger Atkinson (University of California, Riverside) for the determination of the abstraction and dealkylation channels.

References

- 1 S. D. Piccot, J. J. Watson and J. W. Jones, *J. Geophys. Res.: Atmos.*, 1992, **97**, 9897–9912.
- 2 A. Guenther, C. N. Hewitt, D. Erickson, R. Fall, C. Geron, T. Graedel, P. Harley, L. Klinger, M. Lerdau, W. A. McKay, T. Pierce, B. Scholes, R. Steinbrecher, R. Tallamraju, J. Taylor and P. Zimmerman, *J. Geophys. Res.*, 1995, **100**, 8873–8892.
- 3 R. Atkinson and J. Arey, *Atmos. Environ.*, 2003, **37**, 197–219.
- 4 J. G. Calvert, R. Atkinson, K.-H. Becker, R. M. Kamens, J. H. Seinfeld, T. J. Wallington and G. Yarwood, *The Mechanisms of Atmospheric Oxidation of Aromatic Hydrocarbons*, Oxford University Press, 2002.
- 5 B. Bohn and C. Zetzsch, *Phys. Chem. Chem. Phys.*, 2012, **14**, 13933–13948.
- 6 T. Berndt and O. Böge, *Int. J. Chem. Kinet.*, 2001, **33**, 124–129.
- 7 J. von Buttler, R. Koch, M. Siese and C. Zetzsch, *Geophys. Res. Abstr.*, 2008, **10**, EGU2008-A-10576.
- 8 J.-C. Loison, M.-T. Rayez, J.-C. Rayez, A. Gratien, P. Morajkar, C. Fittschen and E. Villenave, *J. Phys. Chem. A*, 2012, **116**, 12189–12197.
- 9 J. Noda, R. Volkamer and M. J. Molina, *J. Phys. Chem. A*, 2009, **113**, 9658–9666.
- 10 D. F. Smith, C. D. McIver and T. E. Kleindienst, *J. Atmos. Chem.*, 1998, **30**, 209–228.
- 11 S. M. Aschmann, J. Arey and R. Atkinson, *Atmos. Environ.*, 2010, **44**, 3970–3975.
- 12 S. B. Corchnoy and R. Atkinson, *Environ. Sci. Technol.*, 1990, **24**, 1497–1502.
- 13 P. Alarcon, R. Strekowski and C. Zetzsch, *Phys. Chem. Chem. Phys.*, 2013, **15**, 20105–20114.
- 14 A. Wahner and C. Zetzsch, *J. Phys. Chem.*, 1983, **87**, 4945–4951.
- 15 R. Koch, R. Knispel, M. Elend, M. Siese and C. Zetzsch, *Atmos. Chem. Phys.*, 2007, **7**, 2057–2071.
- 16 S. Zhang, R. Strekowski, L. Bosland, A. Monod and C. Zetzsch, *Phys. Chem. Chem. Phys.*, 2011, **13**, 11671–11677.
- 17 S. Zhang, R. S. Strekowski, L. Bosland, A. Monod and C. Zetzsch, *Int. J. Chem. Kinet.*, 2011, **43**, 547–556.
- 18 M. J. Frisch, G. W. Trucks, H. B. Schlegel, G. E. Scuseria, M. A. Robb, J. R. Cheeseman, G. Scalmani, V. Barone, B. Mennucci, G. A. Petersson, H. Nakatsuji, M. Caricato, X. Li, H. P. Hratchian, A. F. Izmaylov, J. Bloino, G. Zheng, J. L. Sonnenberg, M. Hada, M. Ehara, K. Toyota, R. Fukuda, J. Hasegawa, M. Ishida, T. Nakajima, Y. Honda, O. Kitao, H. Nakai, T. Vreven, J. A. Montgomery Jr., J. E. Peralta, F. Ogliaro, M. Bearpark, J. J. Heyd, E. Brothers, K. N. Kudin, V. N. Staroverov, R. Kobayashi, J. Normand, K. Raghavachari, A. Rendell, J. C. Burant, S. S. Iyengar, J. Tomasi, M. Cossi, N. Rega, J. M. Millam, M. Klene, J. E. Knox, J. B. Cross, V. Bakken, C. Adamo, J. Jaramillo, R. Gomperts, R. E. Stratmann, O. Yazyev, A. J. Austin, R. Cammi, C. Pomelli, J. W. Ochterski, R. L. Martin, K. Morokuma, V. G. Zakrzewski, G. A. Voth, P. Salvador, J. J. Dannenberg, S. Dapprich, A. D. Daniels, Ö. Farkas, J. B. Foresman, J. V. Ortiz, J. Cioslowski and D. J. Fox, *Gaussian 09, Revision A.1*, Gaussian Inc., Wallingford, CT, 2009.
- 19 Y. Zhao and D. Truhlar, *Theor. Chem. Acc.*, 2008, **120**, 215–241.
- 20 R. Knispel, R. Koch, M. Siese and C. Zetzsch, *Ber. Bunsenges. Phys. Chem.*, 1990, **94**, 1375–1379.
- 21 R. Koch, *Kinetische Untersuchung der Folgereaktionen der OH-Addukte von Aromaten mit NO, NO₂ und O₂ mit simultaner Auswertung von Kurvenscharen*, PhD dissertation, University of Hannover, 1992.
- 22 R. Knispel, *Reaktionen von OH-Radikalen mit Aromaten und Folgereaktionen entstandener OH-Addukte von Aromaten*, PhD dissertation, University of Hannover, 1993.
- 23 R. A. Perry, R. Atkinson and J. N. Pitts, *J. Phys. Chem.*, 1977, **81**, 296–304.
- 24 V. H. Uc, I. García-Cruz, A. Hernández-Laguna and A. Vivier-Bunge, *J. Phys. Chem. A*, 2000, **104**, 7847–7855.
- 25 I. Suh, D. Zhang, R. Zhang, L. T. Molina and M. J. Molina, *Chem. Phys. Lett.*, 2002, **364**, 454–462.
- 26 D. Johnson, S. Raouf, R. Lesclaux and L. N. Krasnoperov, *J. Photochem. Photobiol., A*, 2005, **176**, 98–106.
- 27 J. Fan and R. Zhang, *J. Phys. Chem. A*, 2006, **110**, 7728–7737.
- 28 J. M. Andino and A. Vivier-Bunge, in *Adv. Quantum Chem.*, ed. E. G. Michael and S. J. Matthew, Academic Press, 2008, vol. 55, pp. 297–310.
- 29 I. V. Tokmakov and M. C. Lin, *J. Phys. Chem. A*, 2002, **106**, 11309–11326.
- 30 M. R. Berman and M. C. Lin, *J. Phys. Chem.*, 1983, **87**, 3933–3942.

APPENDIX D. PAPER C: ALARCON ET AL. (2015)



PCCP

PAPER

View Article Online
View Journal | View IssueCite this: *Phys. Chem. Chem. Phys.*,
2015, 17, 13053

Kinetic and mechanistic study of the reaction of OH radicals with methylated benzenes: 1,4-dimethyl-, 1,3,5-trimethyl-, 1,2,4,5-, 1,2,3,5- and 1,2,3,4-tetramethyl-, pentamethyl-, and hexamethylbenzene†

P. Alarcón,^a B. Bohn*^b and C. Zetzsch^{ac}

The reaction of OH radicals with a series of methylated benzenes was studied in a temperature range 300–350 K using a flash-photolysis resonance fluorescence technique. Reversible OH additions led to complex OH decays dependent on the number of distinguishable adducts. Except for hexamethylbenzene, triexponential OH decay curves were obtained, consistent with formation of at least two adduct species. For three compounds that can strictly form two adduct isomers for symmetry reasons (1,4-dimethyl-, 1,3,5-trimethyl-, and 1,2,4,5-tetramethylbenzene) with OH bound *ortho* or *ipso* with respect to the methyl groups, OH decay curves were analysed in terms of a reaction mechanism in which the two adducts can be formed directly by OH addition or indirectly by isomerization. In all cases one adduct (add₁) is dominating the decomposition back to OH. The other (add₂) is more elusive and only detectable at elevated temperatures, similar to the single OH adduct of hexamethylbenzene. Two limiting cases of the general reaction mechanism could be examined quantitatively: reversible formation of add₂ exclusively in the OH reaction or by isomerization of add₁. Total OH rate constants, adduct loss rate constants and products of forward and reverse rate constants of reversible reactions were determined. From these quantities, adduct yields, equilibrium constants, as well as reaction enthalpies and entropies were derived for the three aromatics. Adduct yields strongly depend on the selected reaction model but generally formation of add₁ predominates. For both models equilibrium constants of OH reactions lie between those of OH + benzene from the literature and those obtained for OH + hexamethylbenzene. The corresponding reaction enthalpies of add₁ and add₂ formations are in a range -87 ± 20 kJ mol⁻¹, less exothermic than for hexamethylbenzene (-101 kJ mol⁻¹). Reaction enthalpies of possible add₁ → add₂ isomerizations are comparatively small. Because results for 1,3,5-trimethylbenzene are partly inconsistent with a direct formation of add₂, we promote the existence of isomerization reactions. Moreover, based on available theoretical work in the literature, add₁ and add₂ are tentatively identified as *ortho* and *ipso* adducts, respectively. Total OH rate constants were obtained for all title compounds. They can be described by Arrhenius equations: $k_{\text{OH}} = A \times \exp(-B/T)$. The parameters $\ln(A/(\text{cm}^3 \text{s}^{-1})) = -25.6 \pm 0.3, -25.3 \pm 0.6, -27.3 \pm 0.3, -24.6 \pm 0.3, -26.2 \pm 0.4, -26.2 \pm 0.4$ and -24.5 ± 0.2 , and $B/K = -160 \pm 90, -550 \pm 180, -1120 \pm 90, -330 \pm 100, -820 \pm 100, -980 \pm 130$, and -570 ± 40 were determined for 1,4-dimethyl-, 1,3,5-trimethyl-, 1,2,4,5-, 1,2,3,5- and 1,2,3,4-tetramethyl-, pentamethyl-, and hexamethylbenzene.

Received 15th January 2015,
Accepted 17th April 2015

DOI: 10.1039/c5cp00253b

www.rsc.org/pccp

Introduction

Atmospheric degradation of aromatic compounds is initiated to a large extent by OH radicals.^{1–3} At room temperature and below, OH addition is the prevailing reaction channel for benzene and its methylated and poly-methylated derivatives. At higher temperatures, the addition becomes more and more reversible, and the competing abstraction of an H atom from the methyl groups (leading to an irreversible loss of OH) gains importance.

^a Atmospheric Chemistry Research Laboratory, University of Bayreuth, 95440 Bayreuth, Germany

^b Institut für Energie-und Klimaforschung IEK-8: Troposphäre, Forschungszentrum Jülich, 52425 Jülich, Germany. E-mail: b.bohn@fz-juelich.de

^c Fraunhofer Institute for Toxicology and Experimental Medicine, 30625 Hannover, Germany

† Electronic supplementary information (ESI) available. See DOI: 10.1039/c5cp00253b

However at tropospheric temperatures, H abstraction is generally of minor importance² and back-decomposition is negligible at atmospheric O₂ concentrations because of competing adduct + O₂ reactions.^{4,5} Nevertheless, the reversibility of adduct formation was utilized in the laboratory to study the reactive properties of OH-aromatics adducts and to obtain rate constants of atmospheric relevance.^{4,5} Here we use the reversibility to investigate the formation and yields of possible adduct isomers that, together with the OH rate constants, are also important to understand the OH-initiated atmospheric degradation, as well as combustion processes at elevated temperatures.

In a system with pulsed production of OH in the presence of an excess of the aromatic, OH has been observed to disappear in a biexponential fashion.^{4–6} The initial, fast OH decay is governed by the addition plus abstraction reaction while the final decay is determined by adduct decomposition back to OH and irreversible losses of OH and the adduct. Biexponential behaviour of decays has also been observed for OH in the presence of hexamethylbenzene (HMB, mellitene)⁷ where all positions of the aromatic ring are occupied by methyl substituents. This indicates formation of an *ipso* adduct where OH is bound to an already occupied position. Berndt and Böge⁸ found that the rate constant of the OH reaction with HMB was about 30 times greater than the expected rate constant for H-atom abstraction from a total of six methyl groups,² demonstrating the importance of the *ipso* addition in the case of HMB. Further measurements by von Buttler *et al.*,⁹ and recently by Loison *et al.*,¹⁰ confirmed the reversibility of the OH + HMB reaction, where formation of an *ipso* adduct is the only plausible reaction channel in the temperature range of these investigations.

Another interesting case is the addition of OH to 1,3,5-trimethylbenzene, where two addition channels are feasible: formation of an *ipso* adduct and an *ortho* adduct (at three equivalent positions each). Bohn and Zetzsch¹¹ investigated the reversible OH addition to this aromatic compound and observed triexponential OH decay curves, consistent with the formation of two distinguishable adduct species. However, the interpretation of the experimental data turned out to be difficult because two possible mechanisms for the formation of the second adduct – *via* OH reaction and isomerization – were found to lead to the same triexponential OH decays. Based on thermochemical reasons, a slow formation of the more stable adduct *via* isomerization was tentatively favoured and assigned to the *ipso* adduct of 1,3,5-trimethylbenzene in analogy to the very stable *ipso* adduct of HMB.⁹ Another result of this previous study¹¹ was that the use of the simpler single-adduct reaction model led to presumably wrong, smaller OH rate constants above room temperature. This finding is generally applicable to all aromatic compounds that can form more than one adduct species, as demonstrated for 1,2,3-trimethylbenzene and 1,2,4-trimethylbenzene¹¹ and more recently also for 1-methyl-4-isopropylbenzene (*p*-cymene).¹²

In this work, using the VUV flash-photolysis/resonance-fluorescence (FP-RF) technique, we investigated and reinvestigated the temperature dependent OH-decay kinetics for three aromatic compounds where the two-adduct reaction model should hold strictly for symmetry reasons: 1,4-dimethylbenzene (1,4-DMB,

p-xylene), 1,3,5-trimethylbenzene (135-TMB, mesitylene) and 1,2,4,5-tetramethylbenzene (1245-TeMB, durene) in an attempt to further elucidate the underlying mechanism. Moreover, based on the simpler, single-adduct model, previously obtained experimental data with HMB⁹ were re-evaluated, and former results from our laboratory on benzene⁴ were consulted for direct comparison. In addition, though not strictly applicable because of a greater number of possible adducts, the two-adduct approach was applied to derive best estimates of temperature dependent OH rate constants for the aromatic compounds 1,2,3,4-tetramethylbenzene (1234-TeMB, prehnitene), 1,2,3,5-tetramethylbenzene (1235-TeMB, isodurene) and pentamethylbenzene (PMB).

Experimental

The experimental setup used in this work has been described elsewhere.^{5,6} OH radicals were generated by flash photolysis of water vapour, recently optimized using a Perkin Elmer FX 1165 short arc xenon flash lamp (flash energy 540 mJ) as VUV photolytic light source^{12,13} with a MgF₂ window and improved trigger stability. A gas mixture of H₂O–He was allowed to flow through a resonance lamp, mounted at right angles to the VUV photolysis beam. A microwave discharge dissociated H₂O to produce electronically excited OH radicals. The radiation leaving the lamp was focused into the observation zone exciting the photolytically produced OH radicals in the reaction cell. The resonance fluorescence from the reaction cell passed through a 308 nm interference filter and was focused onto the photocathode of a photomultiplier tube (Thorn-EMI, 9789QB). The experiments were carried out under slow flow conditions in He. The procedure was fully automated by a PC with a software⁵ that ran defined series of experiments at the desired temperature and total pressure unattended, triggering the flash lamp, collecting the fluorescence signals and saving the data from the multichannel scaler board (EG&G Ortec, model ACE MCS), as well as monitoring flow controllers, pressure gauges and platinum resistance thermometers to obtain a full set of the experimental data. Gas-phase concentrations of water and reactant were controlled by feeding known flows of He through saturators with water and the aromatic, adopting available Antoine constants from the literature and keeping the saturator for the aromatic compound precisely at the temperatures shown in Table S8 of the ESI.†

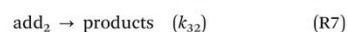
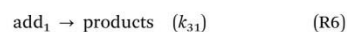
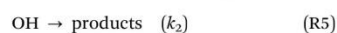
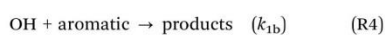
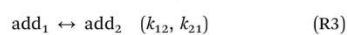
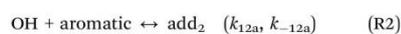
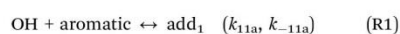
The initial OH radical concentration was estimated to be below $2 \times 10^{10} \text{ cm}^{-3}$ for a water concentration of $1.5 \times 10^{15} \text{ cm}^{-3}$.¹⁴ Based on a measured spectrum of the Xe flash lamp,¹⁵ the initial concentration of OH, and VUV spectra from the literature,^{16–18} the fractions of the aromatics that were photolysed were estimated to be below 6×10^{-4} . Because of the high OH reactivities of the aromatics this is not expected to influence the investigated OH decay kinetics, *e.g.* by radical + radical reactions. Corresponding sensitivity tests using numerical simulations were made previously.¹¹

Aromatics concentrations, temperatures and total pressures are presented in Tables S1 and S2 (ESI†). The gases used in this work had the following stated minimum purities: He (Riessner) – 99.996%;

N₂ (Linde) – 99.999%. Deionised water was doubly distilled in a quartz still. Minimum purity for the aromatics was: liquid 14-DMB (Aldrich) 99%; liquid 135-TMB (Janssen Chimica) 99%; solid 1245-TeMB (Aldrich) 98%, liquid 1234-TeMB (Chemos GmbH) 99.2%; liquid 1235-TeMB (prepared from the Grignard reaction of bromomesitylene¹⁹) 99% and solid PMB (Aldrich) 98%. 1245-TeMB and PMB were further purified by sublimation under vacuum at 70 °C and 45 °C, respectively.

Reaction model and data evaluation

The general reaction model that leads to triexponential OH decay curves in the presence of aromatics forming two adduct species was introduced recently.¹¹ It can be summarised by the following list of reactions with the corresponding rate constants given in parentheses:



Reversible reactions (R1)–(R3) represent redistributions between radical species that together with the loss processes determine the exact shape of the OH decays. Irreversible reactions (R4)–(R7) are responsible for radical losses from the system, eventually leading to a decay of OH after its pulsed formation. The system of differential equations corresponding to (R1)–(R7) was solved analytically for various starting conditions. These solutions were used to fit experimental OH decays and to determine the reaction rate constants indicated. Mathematical and technical details of the analytical solutions and the fitting procedures are given elsewhere.¹¹ A number of important aspects are repeated here to explain our approach:

(i) Sets of OH decay curves obtained at the same temperature but different aromatics concentrations were fitted simultaneously to improve the quality of fitted parameters. More details on concentration ranges and the number of decay curves used are given in the ESI.†

(ii) The number of fit parameters is smaller than the number of rate constants involved in the mechanism and only certain sums and products of individual rate constants can be determined even by fitting sets of decay curves. The parameters are: k_2 , $[k_{11a} + k_{12a} + k_{1b}]$, $[k_{11a} k_{-11a}]$, $[k_{12a} k_{-12a}]$, $[k_{12} k_{21}]$, $[k_{-11a} + k_{12} + k_{31}]$, and $[k_{-12a} + k_{21} + k_{32}]$. Where necessary, we put the combined quantities into square brackets to indicate that the rate constants within these brackets cannot be separated from each other.

(iii) A further complication arises because there is one more fit parameter than there are curve parameters describing a

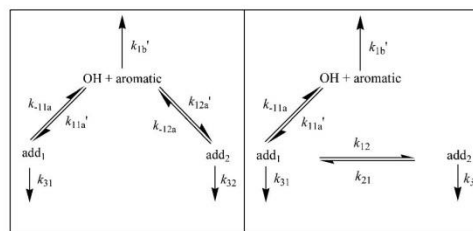


Fig. 1 Schematic diagrams of model-2 (left) and model-3 (right) for the OH radical addition to aromatic compounds. The k_i' = $k_i \times [\text{aromatic}]$ denote pseudo first-order rate constants of bimolecular reactions.

given set of triexponential decay curves. Consequently, different reaction mechanisms can lead to the same OH decay curves. We handle this problem by defining two limiting model cases where specific rate constants are set to zero. Two parameters, namely k_2 and $[k_{11a} + k_{12a} + k_{1b}]$, *i.e.*, the total OH + aromatics rate constant, are not affected by this.

(iv) Uncertainties of fit parameters were estimated by rating the decrease of fit qualities upon a stepwise change of the parameters from the optimised values while allowing all other fit parameters to adjust. These uncertainty estimates also reflect the mutual dependencies of fit parameters, but they are not absolute and do not account for model deficiencies. Nevertheless, they are reasonable on a relative scale and are therefore suitable to weight data points in subsequent analyses, *e.g.* in Arrhenius fits.

In the following, three reaction models will be considered and fitted to experimental OH decay curves. Reaction model-2 and model-3 are shown schematically in Fig. 1.

Model-1: one adduct (biexponential OH decays). This can also be taken as a limiting case of the more general reaction model outlined above by setting $k_{12a} = [k_{12a} k_{-12a}] = 0$ and $k_{12} = [k_{12} k_{21}] = 0$. Model-1 will only be used to re-evaluate previously obtained data with HMB and to assess the improvements obtained in the fit qualities by applying the triexponential model for all investigated compounds.

Model-2: two adducts (triexponential OH decays). No isomerization is permitted by setting $[k_{12} k_{21}] = 0$. Both adducts are exclusively formed in the OH reaction, so we also assume $k_{12} = k_{21} = 0$. By definition, add₁ is specified as the kinetically less stable adduct with the greater total loss rate constant, *i.e.* $k_{-11a} > k_{-12a}$. Both adducts decompose back to OH.

Model-3: two adducts (triexponential OH decays). The kinetically more stable add₂ is assumed to be formed only by isomerization by setting $[k_{12a} k_{-12a}] = 0$. Moreover, no dissociation of add₂ to OH is permitted, *i.e.* $k_{12a} = k_{-12a} = 0$ is a further assumption. Here add₂ also serves as a reservoir for OH, but only indirectly.

In addition, the following relationships (that generally apply for model-2, model-3 and any intermediate case) have been established previously:¹¹

$$[k_{11a} + k_{12a} + k_{1b}] = k_{\text{OH}} = \text{const} \quad (1)$$

$$[k_{11a} k_{-11a}] + [k_{12a} k_{-12a}] = \text{const} \quad (2)$$

$$[k_{-11a} + k_{12} + k_{31}] \times [k_{-12a} + k_{21} + k_{32}] - [k_{12}k_{21}] = \text{const} \quad (3)$$

$$[k_{-11a} + k_{12} + k_{31}] + [k_{-12a} + k_{21} + k_{32}] = \text{const} \quad (4)$$

$$\begin{aligned} & [k_{11a}k_{-11a}] \times [k_{-12a} + k_{21} + k_{32}] \\ & + [k_{12a}k_{-12a}] \times [k_{-11a} + k_{12} + k_{31}] \\ & + 2\sqrt{[k_{11a}k_{-11a}] \times [k_{12a}k_{-12a}] \times [k_{12}k_{21}]} = \text{const} \end{aligned} \quad (5)$$

Results and discussion

Fit qualities and useful temperature range

A common feature, observed for benzene and all alkylated aromatics studied so far, is that OH regeneration is dominated by the presence of at least one quickly decomposing adduct species, whose decomposition rate constant increases from around 10 s^{-1} at 300 K to $200\text{--}400 \text{ s}^{-1}$ at 350 K.^{4-6,11,12,20} The only exception is HMB, where OH regeneration is negligible ($<0.1 \text{ s}^{-1}$) at 300 K and only about 10 s^{-1} at 350 K.⁹ As a consequence, OH decay curves for all other compounds investigated in this work are close to biexponential, and the presence of further, more stable adduct species is merely leading to small, but detectable deviations from a biexponential decay.

In order to check if the single-adduct model is sufficient to describe the OH decay curves or if the influence of a second adduct is noticeable, we determined the sum of squared residuals divided by the degrees of freedom (χ^2/DOF) for bi- and triexponential fits.¹¹ DOF is the total number of data points minus the number of fitted parameters. Fig. 2 shows the obtained χ^2/DOF . Though negligible around room temperature, a clear decline of fit qualities towards greater temperatures was obtained for all compounds using biexponential fits. This indicates that in all cases there is evidence for the presence of more than one adduct species. Examples of bi- and triexponential fit curves obtained in the presence of 14-DMB are shown in Fig. S1 (ESI†) under conditions with the greatest differences in fit qualities (334 K).

In contrast, the same χ^2/DOF were achieved in bi- and triexponential fits for HMB, independent of temperature in a reanalysis of experimental data by von Buttlar *et al.*⁹ As expected, the same applies to data from an earlier work on benzene²¹ that will not be discussed here any further.

A similar temperature dependence of fit qualities as shown in Fig. 2 has already been observed in previous work on TMB isomers¹¹ and *p*-cymene.^{12,13} The common biexponential behaviour around room temperature and below is attributed to high stabilities of adduct species whose presence becomes noticeable only at elevated temperatures, as in the case of HMB. However, with increasing temperature also the decomposition rate constants of the kinetically less stable adducts increase exponentially, which makes it difficult to quantify the initial decay of OH overlapping with a high level of regenerated OH (eventually resulting in effective biexponential OH decays). This limits the range of useful temperatures, dependent on aromatics concentrations, experimental time resolution and decomposition rate constants. Under the conditions of this work, these limits were reached between 340 and 360 K. Data analysis will

therefore be confined to temperatures below these maxima. To make the OH decay curves triexponential at higher temperatures, much higher concentrations of aromatics would have to be used. Consequently, the initial OH decay would become extremely fast and the level of regenerated OH would go down. To monitor such OH decays requires an instrument with much higher time resolution and sensitivity than the one that was available in this work.

As mentioned in the introduction, 14-DMB, 135-TMB and 1245-TeMB can, because of their symmetry, add OH only at two positions: *ipso* and *ortho* with respect to the methyl groups. In these cases, the two-adduct model is expected to apply strictly, and a detailed data analysis is conducted in the following sections. The other three compounds, 1234-TeMB, 1235-TeMB, and PMB, can form three or four different adducts. For these compounds, despite similar fit qualities, triexponential OH decays are considered to be approximations, and therefore the data analysis was confined to the determination of OH rate constants. Because of the improved fit qualities, we expect these rate constants to be more reliable than those based on simpler models at least above room temperature. The same reasoning prompted a recent revision¹¹ of OH rate constants of 123-TMB and 124-TMB with regard to previously published parameterisations.²²

OH + aromatics rate constants

The total OH + aromatics rate constants k_{OH} are direct parameters obtained by fitting arrays of OH decay curves. As outlined in the previous section, we used triexponential fits to determine the $k_{\text{OH}} = [k_{11a} + k_{12a} + k_{1b}]$, except for the reanalysis of HMB data⁹ where the model-1 approach was applied. All temperature dependent k_{OH} are listed in Tables S3, S5 and S7 (ESI†). Simple Arrhenius expressions were suitable to describe the temperature dependencies: $k_{\text{OH}} = A \times \exp(-B/T)$. In these fits, the k_{OH} were weighted by their estimated uncertainties as explained in the data evaluation section. Uncertainty estimates of the Arrhenius parameters A and B were derived using a bootstrap method where the k_{OH} data sets were repeatedly (500 times) resampled using N randomly selected data points from the original set, also containing N data points. The standard deviations of the returned parameters A and B then define their estimated uncertainty.²³ For the parameters A , it turned out that the bootstrap results were close to normal distributed on a logarithmic scale. Instead of the A themselves, we therefore report natural logarithms of A and their uncertainties. The bootstrap method is suitable when absolute uncertainties of single data points are poorly known, as is the case here. However, we consider these uncertainty estimates of A and B lower limits because the true T -dependence of k_{OH} could deviate from Arrhenius behaviour. Moreover, the k_{OH} also rely on the use of correct vapour pressures of the reactants that are documented in the ESI.†

Table 1 presents room temperature k_{OH} and Arrhenius parameters compared with available literature data. In Fig. 3, all data are plotted as a function of temperature. Slightly negative activation energies were consistently obtained for the

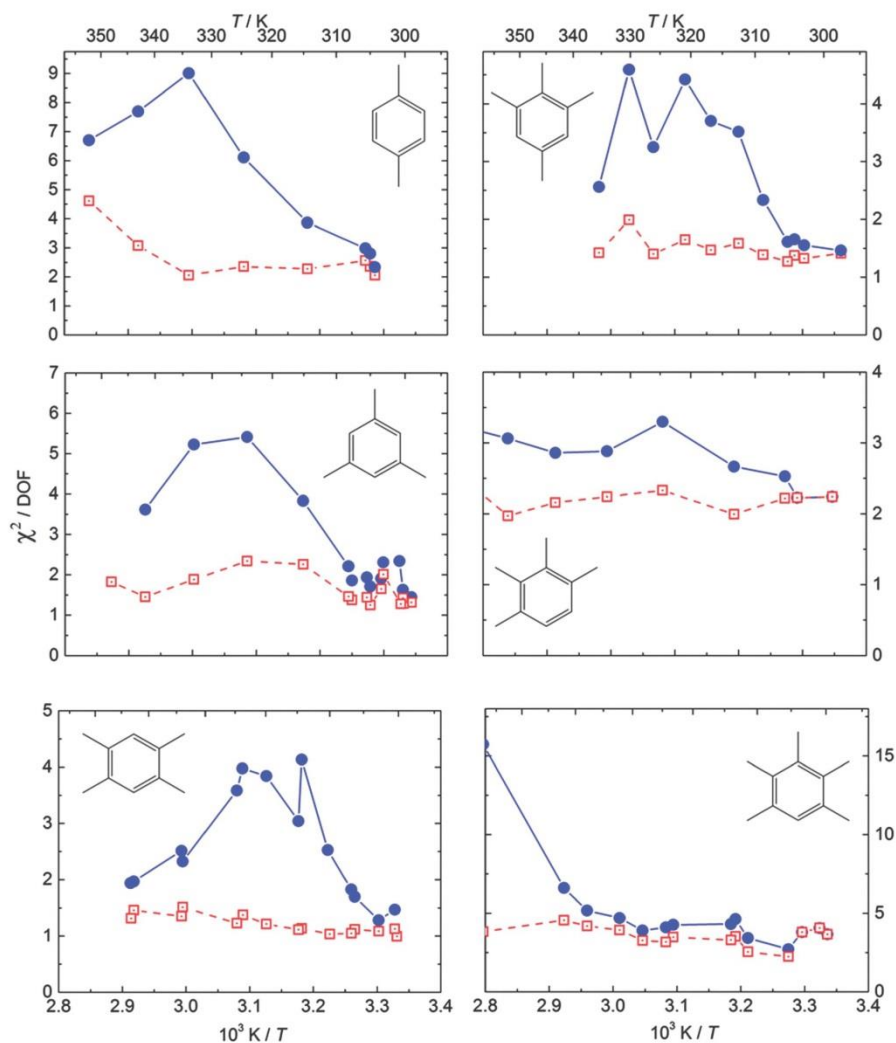


Fig. 2 Normalised residuals of biexponential fits (model-1, blue) and triexponential fits (model-2 or model-3, red) to arrays of OH decay curves in the presence of different aromatic compounds. Compounds on the left: two adducts possible. Compounds on the right: three and four adducts possible.

k_{OH} of all compounds indicating common formation of a pre-reactive complex, as predicted from DFT calculations for many aromatics,^{12,24–29} including HMB.¹⁰

The k_{OH} generally increase with increasing methylation. For 14-DMB, the room temperature k_{OH} was found to be in good agreement with previous determinations that used absolute and relative methods (Table 1).

Arrhenius parameters derived from k_{OH} of a recent relative rate study with mass spectrometric detection of 14-DMB by Mehta *et al.*³⁰ also show good agreement with our results. The k_{OH} of

135-TMB led to a slightly weaker temperature dependence than in previous work of Aschmann *et al.*,³¹ but in agreement with the work of Bohn and Zetzsch.¹¹ However, the k_{OH} of this work are greater by about 25%. Room temperature k_{OH} for 1245-TeMB and PMB are in good agreement with recent relative rate measurements by Aschmann *et al.*³² at 298 K while for 1234-TeMB and 1235-TeMB no literature data are available. For HMB re-evaluated k_{OH} are very similar to those originally obtained by von Buttler *et al.*,⁹ as expected. The k_{OH} for HMB were the greatest of the compounds studied. The room temperature

Table 1 Total rate constants k_{OH} of the reaction OH + aromatic at room temperature and Arrhenius parameters A and B according to the equation: $k_{\text{OH}} = A \times \exp(-B/T)$ from the literature and this work. FP-RF: flash photolysis-resonance fluorescence technique. RR: relative rate technique. Error limits of this work do not include potential systematic effects caused by deficiencies of reaction models or uncertainties of reactant concentrations (10–20%, see ESI)

	$\ln(A/\text{cm}^3 \text{ s}^{-1})$	B/K	$k_{\text{OH}}(298 \text{ K})/10^{-12} \text{ cm}^3 \text{ s}^{-1}$	Exper. technique		
14-DMB (<i>p</i> -xylene)	-25.8 ± 1.6	-300 ± 500	12.2 ± 1.2^{33}	FP-RF		
			10.7 ± 2.4^{34}	RR		
			15.3 ± 1.7^{20}	FP-RF		
			10.5 ± 1.0^{35}	FP-RF		
			13.5 ± 1.4^{36}	FP-RF		
			13.6 ± 0.6^{37}	RR		
			13.6^{38}	RR		
			13.0 ± 2.0^{39}	RR		
			14.7 ± 3.0^{40}	RR		
			11.9 ± 0.7^{30}	RR		
-25.7^a	-150^a	13.1 ± 0.3	FP-RF (this work)			
-25.6 ± 0.3^b	-160 ± 90^b					
135-TMB (mesitylene)	-26.2 ± 3.2	-860 ± 1010	47.2 ± 4.8^{33}	FP-RF		
			44.4 ± 5.3^{34}	RR		
			62.4 ± 7.5^{20}	FP-RF		
			40.9 ± 5.6^{37}	RR		
			57.5 ± 9.2^{39}	RR		
			57.3 ± 5.3^{41}	RR		
			59.1 ± 1.1^{42}	RR		
			-26.1	-740 ± 180	51.7 ± 1.1^{31}	RR
			-25.1	-450 ± 50	59.5 ± 2.0^{11}	FP-RF
			-25.3 ± 0.6^c	-550 ± 180^c	68.4 ± 0.9	FP-RF (this work)
1245-TeMB (durene)	-27.3 ± 0.3^d	-1120 ± 90^d	55.5 ± 3.4^{32}	RR		
			57.8 ± 0.6	FP-RF (this work)		
1235-TeMB (isodurene)	-24.6 ± 0.3^e	-330 ± 100^e	62.4 ± 0.8	FP-RF (this work)		
1234-TeMB (prehnitene)	-26.2 ± 0.4^f	-820 ± 100^f	66.4 ± 1.8	FP-RF		
PMB	-26.2 ± 0.4^g	-980 ± 130^g	103 ± 8.0^{32}	RR		
			110 ± 4	FP-RF (this work)		
HMB (mellitene)	-24.3	-498	113 ± 11^h	RR ⁱ		
			149^9	FP-RF		
			153 ± 2^9	FP-RF (this work)		
	-24.5 ± 0.2^h	-570 ± 40^h				

^a Arrhenius parameter calculated from k_{OH} of indicated reference (240–340 K). Arrhenius parameter for the following temperature ranges (K). ^b 304–352 K. ^c 299–348 K. ^d 300–343 K. ^e 297–335 K. ^f 298–362 K. ^g 299–362 K. ^h 311–370 K. ⁱ 295 K.

value is almost 40% greater than that determined by Berndt and Böge.⁸ The reason for this discrepancy is unknown, but we note that HMB is difficult to handle because of an extremely low vapour pressure (see ESI† for more details).

Model-dependent fit parameters

In contrast to the k_{OH} , all other fit parameters for 14-DMB, 135-TMB and 1245-TeMB depend on the reaction model. Regarding the parameters representing rate constant products, it turned out that the $[k_{12a}k_{-12a}]$ of model-2 were comparatively small while the $[k_{11a}k_{-11a}]$ were much greater. This demonstrates the dominance of add₁ for the regeneration of OH for all compounds. However, the presence of add₂ is not negligible as the $[k_{12a}k_{-12a}]$ of model-2 and the $[k_{12}k_{21}]$ of model-3 are all significantly greater than zero (Fig. 4). Fitted rate constant products can be found in Tables S3 and S4 (ESI†). Note that eqn (2) implies that the sum $[k_{11a}k_{-11a}] + [k_{12a}k_{-12a}]$ of model-2 is identical to $[k_{11a}k_{-11a}]$ of model-3. Simple Arrhenius-type functions turned out to be suitable to describe the temperature dependencies of the rate constant products of forward (F) and

reverse (R) reactions: $k_{\text{F}} \times k_{\text{R}} = A \times \exp(-B/T)$. The corresponding parameters A and B can be found in Table 2 including reevaluated model-1 results for HMB.⁹ For model-2, positive temperature coefficients B were obtained for all $[k_{11a}k_{-11a}]$ and $[k_{12a}k_{-12a}]$ except for 135-TMB where for $[k_{12a}k_{-12a}]$ it was slightly negative in accordance with a previous investigation.¹¹ The parameters B for the rate constant products multiplied by the gas constant R represent the sum of activation energies of OH addition and reverse decomposition. This indicates that for add₂ of 135-TMB the activation energy for the endothermic decomposition has to be over-compensated by a negative activation energy for OH addition, as will be confirmed in the next section. Given the generally weak, negative T -dependence of OH additions to aromatics, this possibility seems unrealistic. At least for 135-TMB model-2 is therefore equivocal. On the other hand, for model-3 positive temperature coefficients were obtained for the products $[k_{12}k_{21}]$, which is in qualitative agreement with expectations, *i.e.* positive sums of activation energies for potential isomerization reactions for all compounds (Fig. 5).

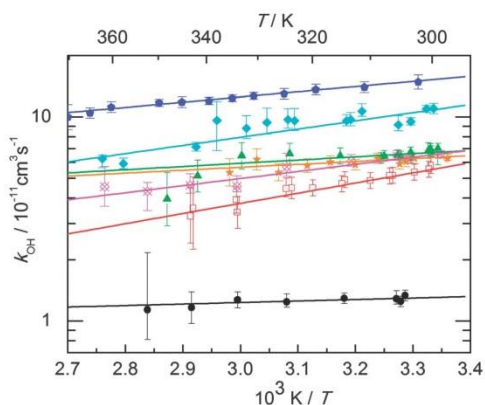


Fig. 3 Arrhenius plots of k_{OH} of methylated benzenes and respective regression lines (Table 1). 14-DMB (filled circles), 1245-TeMB (open squares), 135-TMB (filled triangles), 1235-TeMB (filled asterisks), PMB (filled diamonds), 1234-TeMB (crossed diamonds), and HMB (filled pentagons).

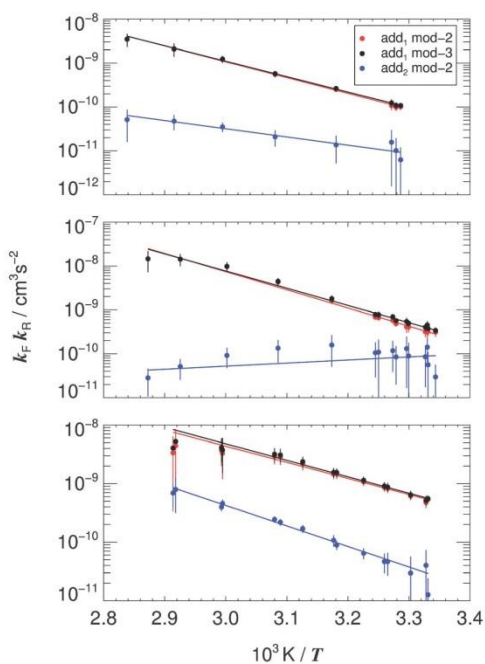


Fig. 4 Arrhenius plots of forward and reverse rate constant products $k_{\text{F}} k_{\text{R}}$ for 14-DMB (upper panel), 135-TMB (middle panel), and 1245-TeMB (lower panel). Black: $[k_{11a}k_{-11a}]$ of model-3, red: $[k_{11a}k_{-11a}]$ of model-2, and blue: $[k_{12a}k_{-12a}]$ of model-2.

The remaining two fit parameters correspond to the total loss rate constants of add_1 ($k_{-11a} + k_{12} + k_{31}$) and add_2 ($k_{-12a} + k_{21} + k_{32}$).

Table 2 Arrhenius parameters A and B of products of rate constants of forward and reverse reactions according to the equation: $k_{\text{F}} \times k_{\text{R}} = A \times \exp(-B/T)$. Error limits do not include potential systematic effects caused by deficiencies of reaction models

	$\ln(A/\text{cm}^3 \text{ s}^{-2})$	$B/10^3 \text{ K}$	$\ln(A/\text{cm}^3 \text{ s}^{-2}),$ $\ln(A/\text{s}^{-2})$	$B/10^3 \text{ K}$
Model-2	$k_{11a}k_{-11a}$		$k_{12a}k_{-12a}$	
14-DMB	4.2 ± 0.6	8.3 ± 0.2	-11.2 ± 1.3	4.3 ± 0.4
135-TMB	9.8 ± 1.6	9.5 ± 0.5	-28.5 ± 2.0	-1.6 ± 0.6
1245-TeMB	-0.3 ± 0.9	6.3 ± 0.3	2.7 ± 1.1	8.1 ± 0.3
Model-3	$k_{11a}k_{-11a}$		$k_{12}k_{21}$	
14-DMB	3.6 ± 0.6	8.1 ± 0.2	42.9 ± 1.7	12.3 ± 0.5
135-TMB	8.4 ± 1.4	9.0 ± 0.4	27.0 ± 2.0	7.3 ± 0.6
1245-TeMB	0.3 ± 0.9	6.5 ± 0.3	51.7 ± 1.5	14.4 ± 0.5
Model-1	$k_{11a}k_{-11a}$			
HMB	6.4 ± 0.2	9.45 ± 0.08	—	—

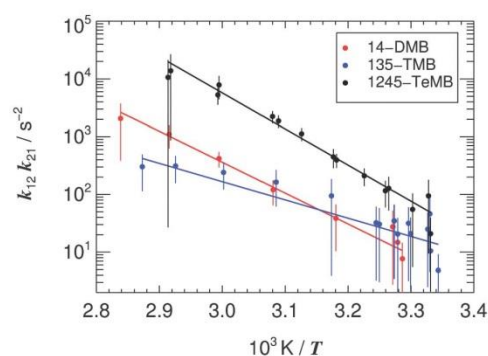


Fig. 5 Arrhenius plots of rate constant products $[k_{12}k_{21}]$ of model-3 for 14-DMB (red), 135-TMB (blue), and 1245-TeMB (black).

They represent a sum of two or three first-order rate constants, dependent on model assumptions. For all investigated compounds it was found that the loss rate constants of add_2 were much smaller than those of add_1 (Fig. 6). Model-2 and model-3 fits gave rather similar results for the two loss rate constants. The differences were not significant for add_1 within estimated uncertainties. Loss rate constants are listed in Tables S3 and S4 (ESI[†]). Note that eqn (4) indicates that the sum of all loss rate constants also has to be constant, independent of the reaction model.

The temperature dependence of the adduct-loss rate constants $k_{\text{L}1}$ (add_1) and $k_{\text{L}2}$ (add_2) can be described by a modified Arrhenius equation: $k_{\text{L}} = A \times \exp(-B/T) + C$. The parameters A , B and C are given in Table 3. Because the dependence of A and B on C is pronounced, in particular for add_2 , the C were kept fixed at values that will be derived in the next section, based on OH budget considerations.

For model-2, the C should correspond to the background loss rate constants k_{31} and k_{32} that are assumed to be independent of temperature for convenience, *i.e.* $k_{\text{L}1} = [k_{-11a} + k_{31}]$ and

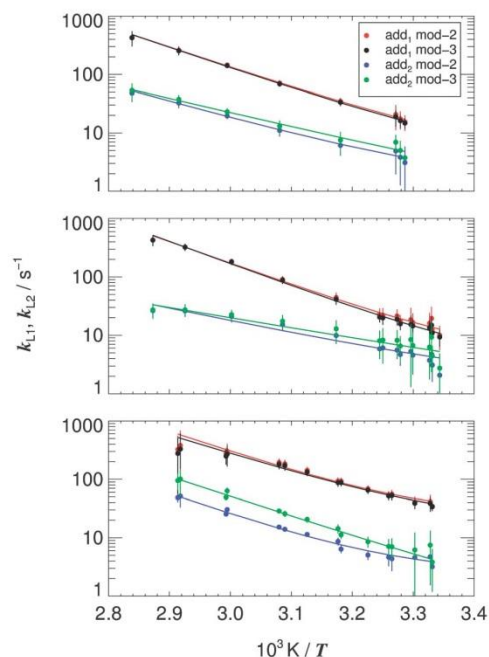


Fig. 6 Arrhenius plots of loss rate constants k_{L1} and k_{L2} of add_1 and add_2 for 14-DMB (upper panel), 135-TMB (middle panel), and 1245-TeMB (lower panel). Red: k_{L1} of model-2, black: k_{L1} of model-3, blue: k_{L2} of model-2, and green: k_{L2} of model-3.

Table 3 Arrhenius parameters A and B of total adduct loss rate constants according to the equation: $k_L = A \times \exp(-B/T) + C$ of add_1 (left), and add_2 (right). The C parameters were held fixed. They correspond to optimized values according to eqn (6) and (7) for model-2 and model-3, respectively. Error limits do not include potential systematic effects caused by deficiencies of reaction models

	add ₁			add ₂		
	ln(A/s ⁻¹)	B/10 ³ K	C/s ⁻¹	ln(A/s ⁻¹)	B/10 ³ K	C/s ⁻¹
Model-2						
14-DMB	29.0 ± 0.5	8.0 ± 0.2	4.1	23.0 ± 0.8	6.7 ± 0.3	1.3
135-TMB	31.0 ± 0.9	8.6 ± 0.3	3.9	18.3 ± 1.4	5.1 ± 0.4	1.2
1245-TeMB	30.1 ± 1.5	8.2 ± 0.5	22.8	28.5 ± 1.5	8.4 ± 0.5	2.5
Model-3						
14-DMB	29.3 ± 0.5	8.2 ± 0.2	3.5	20.1 ± 1.1	5.7 ± 0.3	0.5
135-TMB	31.7 ± 0.8	8.9 ± 0.2	2.8	15.3 ± 1.3	4.1 ± 0.4	0.5
1245-TeMB	28.2 ± 1.2	7.5 ± 0.4	16.3	27.5 ± 1.3	7.9 ± 0.4	0.5
Model-1						
Benzene ^a	29.8 ± 0.8	8.6 ± 0.3	0.0	—	—	—
HMB	32.3 ± 0.5	10.4 ± 0.2	8.7	—	—	—

^a Evaluated from k_R data by Knispel *et al.*,⁴ $k_L = k_R + \text{adduct background loss rate constant}$.

$k_{L2} = [k_{-12a} + k_{32}]$. The temperature coefficients B multiplied by R correspond to the activation energies of adduct decompositions.

They all range around 67–72 kJ mol⁻¹ for add_1 , dependent on compound, in good agreement with results for benzene by Perry *et al.*,²⁰ and Knispel *et al.*,⁴ of (78 ± 8) kJ mol⁻¹ and (72 ± 2) kJ mol⁻¹, respectively. Similar results exist for other aromatic compounds^{4,11,20} but they may be affected by the use of the wrong reaction model.¹¹ In contrast, the activation energy for the OH–HMB adduct is greater (89 kJ mol⁻¹). In recent work on 135-TMB,¹¹ a slightly greater activation energy for the decomposition of add_1 of 135-TMB of (81 ± 9) kJ mol⁻¹ was obtained, but still in the range of combined error estimates compared to the result of this work.

With one exception (1245-TeMB), the corresponding activation energies for add_2 are smaller, in particular for 135-TMB where it is unrealistically small for the decomposition reaction (43 kJ mol⁻¹). This has already been noted in earlier work¹¹ where a similar value was obtained and model-2 was therefore questioned for 135-TMB. However, it should be noted that because of the limited temperature range and the dependence on k_{32} , the parameters A and B for add_2 are particularly uncertain.

The only theoretical study on the investigated compounds that addressed the properties of *ortho* and *ipso* adducts was made by Fan and Zhang²⁷ on the OH+14-DMB reaction based on reaction model-2. Although calculated decomposition rate constants at 300 K were greater by two orders of magnitude, the authors predicted that the *ortho* adduct decomposes a factor of 3.5 more rapidly than the *ipso* adduct. This is in qualitative agreement with this work if we identify add_1 and add_2 as *ortho* and *ipso* adducts, respectively.

For model-3 the situation is more complicated for add_1 and different for add_2 : $k_{L1} = [k_{-11a} + k_{12} + k_{31}]$ and $k_{L2} = [k_{21} + k_{32}]$. A clear assignment of C to k_{31} is difficult here unless k_{-11a} and k_{12} accidentally have the same T -dependencies. However, the contribution of k_{12} to the total loss rate constant of add_1 is small, as will be shown in the next section, *i.e.* back decomposition remains the main loss process for add_1 also for model-3. Generally, similar A and B were obtained as for model-2 but the loss rate constants of add_2 now correspond to the sum [$k_{21} + k_{32}$]. Therefore, the temperature dependence of k_{L2} reflects that of the isomerization rather than of a decomposition reaction which could explain the unexpectedly low value of the activation energy obtained for 135-TMB.

Adduct yields and background losses

The yields of add_1 and add_2 according to model-2, $\phi_1 = k_{11a}/k_{OH}$ and $\phi_2 = k_{12a}/k_{OH}$, can be determined from the obtained fit parameters by utilizing the following equation:¹¹

$$k_{OH} - k_{1b} = k_{11a} + k_{12a} = \frac{[k_{11a}k_{-11a}]}{k_{L1} - k_{31}} + \frac{[k_{12a}k_{-12a}]}{k_{L2} - k_{32}} \quad (6)$$

For the k_{1b} , a recommendation by Atkinson² was used (temperature dependent abstraction rate constant per CH₃ substituent), and background loss rate constants k_{31} and k_{32} were fitted using eqn (6) (Table 3). The fits ensure that the OH budget is closed at least towards lower temperatures where k_{31} and k_{32} have significant influence. The background rate constants obtained this way compare reasonably with the empirical

parameters C introduced in the last section but are preferred for the calculation of adduct yields for consistency reasons.

Correspondingly, the yield of add_1 according to model-3 can be determined using the following relation:¹¹

$$k_{\text{OH}} - k_{1\text{b}} = k_{11\text{a}} = \frac{[k_{11\text{a}}k_{-11\text{a}}]}{k_{\text{L}1} - k_{12} - k_{31}} \quad (7)$$

$$= \frac{[k_{11\text{a}}k_{-11\text{a}}] \times (k_{12} - k_{32})}{(k_{\text{L}1} - k_{31}) \times (k_{12} - k_{32}) - [k_{12}k_{21}]}$$

Again the k_{31} and k_{32} for model-3 were fitted using eqn (7). They were slightly smaller than those of model-2 (Table 3), but generally all adduct background loss rate constants ranged below 4 s^{-1} which is typical for the experimental setup used. The only exception is add_1 of 1245-TeMB where the k_{31} were 23 s^{-1} and 16 s^{-1} for model-2 and model-3, respectively. The reason for this increased background loss is unknown. It could be caused by an exceptionally large rate constant of a reaction of this adduct with traces of O_2 or by a specific unimolecular loss reaction.

Adduct yields, the contribution of H-abstraction and corresponding total yields as a function of temperature are shown in Fig. 7. Total yields are close to unity in all cases, as expected. The ϕ_1 range between lower limits defined by model-2 and upper limits close to 0.9 according to model-3 ($\phi_2 = 0$) while upper limits of ϕ_2 are defined by model-2. Unfortunately, the experimental OH decay data alone do not allow us to further confine these ranges. However, the 14-DMB results of model-2 are in reasonable agreement with a theoretically predicted 0.8 to 0.2 *ortho* to *ipso* branching ratio by Fan and Zhang²⁷ if we again assign add_1 and add_2 as *ortho* and *ipso* adducts, respectively. Regarding the model-2 temperature effect on adduct yields, only 135-TMB exhibits a strong dependence. The exponential decrease of ϕ_2 with temperature corresponds to the aforementioned unusually large negative temperature coefficient of add_2 formation by OH addition, also explaining the negative temperature coefficient of the product $[k_{12\text{a}}k_{-12\text{a}}]$ for 135-TMB.

Equilibrium constants and thermodynamic quantities

Ratios of rate constants of forward and reverse reactions were used to calculate equilibrium constants of reversible reactions involved in the different mechanisms. From the temperature dependencies of the equilibrium constants, standard reaction enthalpies $\Delta H_{\text{r,m}}^\circ$ and entropies $\Delta S_{\text{r,m}}^\circ$ can be estimated. For the equilibrium constants K_c of OH addition and decomposition reactions of model-2 and model-3, the following equation applies:

$$K_c = \frac{k_{\text{F}}}{k_{\text{R}}} = \frac{k_{\text{B}}T}{p^\circ} \times \exp\left(\frac{-\Delta H_{\text{r,m}}^\circ}{RT} + \frac{\Delta S_{\text{r,m}}^\circ}{R}\right) \quad (8)$$

where k_{B} is the Boltzmann constant and p° the standard pressure. Because of a simpler stoichiometry, the expression for the isomerization reactions of model-3 is simpler, and the K_i are dimensionless:

$$K_i = \frac{k_{\text{F}}}{k_{\text{R}}} = \frac{k_{12}}{k_{21}} = \exp\left(\frac{-\Delta H_{\text{r,m}}^\circ}{RT} + \frac{\Delta S_{\text{r,m}}^\circ}{R}\right) \quad (9)$$

Correspondingly, the following simplified functions were fitted to the K_c and K_i , respectively: $K_c = A \times T \times \exp(-B/T)$

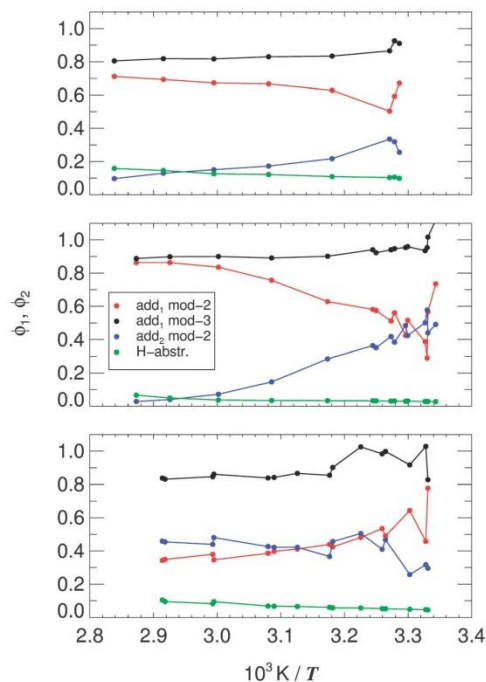


Fig. 7 Yields of add_1 (red) and add_2 (blue) of model-2, add_1 of model-3 (black), and the contribution of H-abstraction (green) following the OH + aromatics reaction for 14-DMB (upper panel), 135-TMB (middle panel), and 1245-TeMB (lower panel).

and $K_i = A \times \exp(-B/T)$. The ratios $k_{\text{F}}/k_{\text{R}}$ can be calculated from the fit parameters as shown previously¹¹ for model-2:

$$K_{\text{c}1} = \frac{[k_{11\text{a}}k_{-11\text{a}}]}{(k_{\text{L}1} - k_{31})^2} \quad (10)$$

$$K_{\text{c}2} = \frac{[k_{12\text{a}}k_{-12\text{a}}]}{(k_{12} - k_{32})^2} \quad (11)$$

For model-3, the following equations apply (k_{12} is determined by solving the right hand side of eqn (7)):

$$K_{\text{c}1} = \frac{[k_{11\text{a}}k_{-11\text{a}}]}{(k_{\text{L}1} - k_{12} - k_{31})^2} \quad (12)$$

$$K_i = \frac{[k_{12}k_{21}]}{(k_{12} - k_{32})^2} \quad (13)$$

For the K_c and K_i calculations, the rate constants k_{31} and k_{32} (that were determined in the previous section) were used. However, instead of using eqn (10)–(13) we followed a slightly different approach and adapted our fit routines to directly return the equilibrium constants. The results are obviously the same but the advantage is that uncertainty estimates for

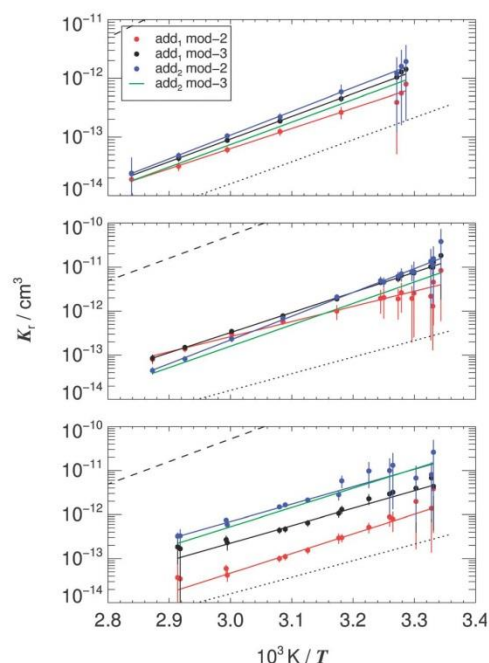


Fig. 8 Van't Hoff plots of equilibrium constants of reversible OH + aromatics reactions for 14-DMB (upper panel), 135-TMB (middle panel) and 1245-TeMB (lower panel). Red: $K_{c1} = k_{11a}/k_{-11a}$ of model-2, blue: $K_{c2} = k_{12a}/k_{-12a}$ of model-2, and black: $K_{c1} = k_{11a}/k_{-11a}$ of model-3. Green lines show the limiting $K_{c,2}$ of model-3 according to eqn (14), dotted and dashed lines show model-1 results for benzene and HMB for comparison.

the K_c and K_i can be determined directly by the method described in the data evaluation section. Also in this case, these estimates are not considered absolute but suitable to weight the data points in fits of the parameters A and B and their uncertainties with the bootstrap method. However, the uncertainties of the parameters A and B are again lower limits, because the background loss rate constants k_{31} and k_{32} (whose influence is significant at lower temperatures) were held fixed in the analysis. The K_c of model-2 and model-3, and the K_i of model-3 are listed in Table S6 (ESI[†]) and shown in Fig. 8 and 9, respectively. Parameters A and B and corresponding thermodynamic data are listed in Table 4 including those obtained in the re-evaluation of HMB data⁹ and those calculated from k_F and k_R results of benzene by Knispel *et al.*⁴ For comparison, the K_c functions for benzene and HMB were also included in Fig. 8 as dotted and dashed lines, respectively. Benzene and HMB are compounds for which the underlying mechanism of OH addition is not questioned (model-1). They represent the formation of prototype non-*ipso* adducts with no methylation and *ipso* adducts with full methylation of the aromatic ring, respectively.

The thermodynamic quantities of benzene and HMB clearly show that while reaction entropies are expectedly similar and in

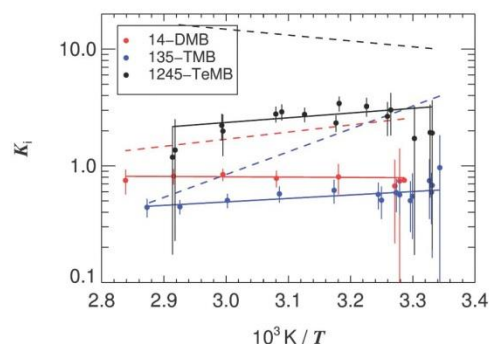


Fig. 9 Van't Hoff plots of equilibrium constants for isomerization $K_i = k_{12}/k_{21}$ of model-3 for 14-DMB (red), 135-TMB (blue), and 1245-TeMB (black). The dashed curves show the calculated, limiting K_i of model-2 according to eqn (14).

a reasonable range for an association reaction, the OH-HMB adduct formation is more exothermic by about -25 kJ mol^{-1} . This is in line with a recently calculated value of the zero-point reaction energy of the OH + HMB addition of -102 kJ mol^{-1} by Loison *et al.*¹⁰ Moreover, the activation energies of the decomposition reactions of the OH-benzene and OH-HMB adducts (Table 3) are in accord with the reaction enthalpies of the forward reactions.

The K_c of all other investigated compounds range between the minimum and maximum values of benzene and HMB. Model differences regarding add_1 are significant, with minimum and maximum K_c corresponding to model-2 and model-3, respectively. On the other hand, model-2 defines the maximum K_c of add_2 that all exceed those of add_1 , except for 135-TMB where K_c functions of add_1 and add_2 cross each other. In contrast to the K_c in Fig. 8, the K_i in Fig. 9 show weak, insignificant temperature dependencies for all compounds, indicating comparatively small reaction enthalpies for potential isomerization reactions. Despite these differences between model-2 and model-3, a decision which model is more realistic turns out to be difficult. In the previous investigation on 135-TMB,¹¹ model-3 was favored based on the obtained reaction enthalpies and entropies, in particular because add_2 formation of model-2 was strongly exothermic while the reverse decomposition had a low activation energy. Moreover, the reaction entropy of add_2 formation was much lower than expected.¹¹ These findings are confirmed in this work for 135-TMB. However, no such inconsistencies of model-2 are evident for 14-DMB and 1245-TeMB. On the other hand, the same is true for model-3: enthalpies and entropies of add_1 formations and isomerization reactions are in a reasonable range for these compounds, at least considering the range spanned by benzene and HMB.

Available theoretical work on OH + aromatics reactions in the literature is based on model-2, *i.e.* isomerization reactions have not been considered so far. Theoretical studies on the OH + toluene reaction show that adduct isomers benefit energetically

Table 4 Parameters A and B and corresponding molar reaction enthalpies $\Delta H_{r,m}^\circ$ and entropies $\Delta S_{r,m}^\circ$ describing equilibrium constants of reversible OH + aromatics reactions according to the equation: $K_c = A \times T \times \exp(-B/T)$ and of adduct isomerization according to the equation: $K_i = A \times \exp(-B/T)$. Error limits do not include potential systematic effects caused by deficiencies of reaction models

	$\ln(A/K^{-1} \text{ cm}^3)$	$B/10^3 \text{ K}$	$\Delta S_{r,m}^\circ/\text{J K}^{-1} \text{ mol}^{-1}$	$\Delta H_{r,m}^\circ/\text{kJ mol}^{-1}$	$\ln(A/K^{-1} \text{ cm}^3), \ln(A)$	$B/10^3 \text{ K}$	$\Delta S_{r,m}^\circ/\text{J K}^{-1} \text{ mol}^{-1}$	$\Delta H_{r,m}^\circ/\text{kJ mol}^{-1}$
Model-2	OH + aromatic \rightarrow add ₁				OH + aromatic \rightarrow add ₂			
14-DMB	-60.9 ± 0.6	-8.2 ± 0.2	-88 ± 5	-68 ± 2	-64.6 ± 0.6	-9.6 ± 0.2	-119 ± 5	-80 ± 2
135-TMB	-59.6 ± 1.3	-8.3 ± 0.4	-77 ± 11	-69 ± 4	-73.3 ± 0.7	-12.8 ± 0.2	-191 ± 6	-106 ± 2
1245-TeMB	-68.3 ± 2.2	-10.6 ± 0.7	-149 ± 18	-88 ± 6	-62.1 ± 1.8	-9.4 ± 0.6	-98 ± 15	-78 ± 5
Model-3	OH + aromatic \rightarrow add ₁				add ₁ \rightarrow add ₂			
14-DMB	-63.5 ± 0.4	-9.2 ± 0.1	-109 ± 4	-77 ± 1	-0.03 ± 0.65	0.1 ± 0.2	-0.2 ± 5.4	0.5 ± 1.8
135-TMB	-67.1 ± 0.3	-10.8 ± 0.1	-139 ± 3	-90 ± 1	-2.8 ± 0.6	-0.7 ± 0.2	-23 ± 5	-6 ± 2
1245-TeMB	-63.3 ± 1.9	-9.5 ± 0.6	-108 ± 16	-79 ± 5	-1.95 ± 1.3	-0.9 ± 0.4	-16 ± 11	-8 ± 3
Model-1	OH + aromatic \rightarrow add							
Benzene ^a	-64.5 ± 1.4	-9.0 ± 0.4	-118 ± 11	-75 ± 4	—	—	—	—
HMB	-65.9 ± 1.1	-12.1 ± 0.4	-130 ± 9	-101 ± 3	—	—	—	—

^a Evaluated from k_F and k_R data by Knispel *et al.*,⁴ $K_c = k_F/k_R$.

from CH₃ substituents in *ortho* and to a lesser extent in *para* position with respect to OH attack.^{43,44} Regarding the *ipso* adduct of toluene, predictions are discordant ranging slightly below the *para* or above the *ortho* adduct, but in any case within 10 kJ mol⁻¹.^{43,44} Studies by Fan and Zhang on 14-DMB²⁷ and 13-DMB²⁸ (four adducts) also report stabilizing effects of CH₃ substituents in *ortho* and *para*, but not in *ipso* positions. This is confirmed qualitatively in work by Huang *et al.* on 12-DMB⁴⁵ and 13-DMB,⁴⁶ and in recent work by Pan and Wang on 13-DMB,⁴⁷ as well as on *p*-cymene (except for the *ipso* adduct with respect to the C₃H₇ substituent).¹² These theoretical studies also imply that generally *ortho* adducts are formed with greater yields and typically decompose more quickly than *ipso* adducts, despite more exothermic formation enthalpies, *i.e.* for the compounds studied here add₁ = *ortho* and add₂ = *ipso* is implicated.

If this concept is transferred qualitatively to the selected compounds, one would expect reaction enthalpies *ortho* \leq *ipso* for 14-DMB, *ortho* < *ipso* for 135-TMB, and *ortho* \leq *ipso* for 1245-TeMB. Moreover, the *ortho* and *ipso* adduct formation of 135-TMB should be the most and the least exothermic among the six reactions studied. It can also be inferred that the formation of the *ortho* adduct of 135-TMB should be similarly exothermic than that of the *ipso* adduct of HMB that is also stabilized by two CH₃ substituents in *ortho* position and one in *para* position.

$$K_i = \frac{(\sqrt{[k_{12a}k_{-12a}]} \times k_{L1} + \sqrt{[k_{11a}k_{-11a}]} \times [k_{12}k_{21}] - k_{31} \times \sqrt{[k_{12a}k_{-12a}]})^2}{(\sqrt{[k_{11a}k_{-11a}]} \times k_{L2} + \sqrt{[k_{12a}k_{-12a}]} \times [k_{12}k_{21}] - k_{32} \times \sqrt{[k_{11a}k_{-11a}]})^2} \quad (15)$$

In reasonable agreement with these considerations we find relatively high model-2 yields of add₁ and similar reaction enthalpies for add₁ and add₂ formations in the case of 14-DMB and 1245-TeMB. On the other hand, the 135-TMB result of model-2 again does not fit because the formation of the alleged *ipso* adduct add₂ would be more exothermic by -40 kJ mol⁻¹ than that of the *ortho* adduct add₁. For model-3, reaction enthalpies of add₁ formations are in the expected range and order for all three compounds with 135-TMB being the most exothermic.

However, for 135-TMB the reaction enthalpy of the add₁ \rightarrow add₂ isomerization is negative by -6 kJ mol⁻¹, again indicating an at least slightly more stable *ipso* adduct. An even more exothermic enthalpy for the add₁ \rightarrow add₂ reaction was estimated before, albeit with a high uncertainty (-35 ± 22 kJ mol⁻¹).¹¹ Obviously, neither model-2 nor model-3 leads to an overall picture that is fully consistent with available theoretical work.

The question remains whether or not the thermodynamic quantities of intermediate cases lie in between those of the limiting models discussed so far or if other results are possible. Because of the degeneracy problem (more fit parameters than parameters describing the decay curves), intermediate cases between model-2 and model-3 are difficult to assess quantitatively. However, a relationship between the three equilibrium constants exists following the detailed balancing applied previously to derive the analytical solutions for the general mechanism:¹¹

$$K_i = \frac{K_{c2}}{K_{c1}} = \frac{[k_{12a}k_{-12a}] \times (k_{L1} - k_{12} - k_{31})^2}{[k_{11a}k_{-11a}] \times (k_{L2} - k_{21} - k_{32})^2} \quad (14)$$

Note that in terms of eqn (8) and (9), the left hand side of eqn (14) corresponds to a path-independence of the state-function changes ΔH and ΔS . Inserting $k_{12} = \sqrt{K_i \times [k_{12}k_{21}]}$ and $k_{21} = \sqrt{[k_{12}k_{21}]/K_i}$, a general equation for K_i was obtained:

The range of possible K_i was determined in a number of further fits to OH decay curve arrays, taking 135-TMB as an example, where the parameter $[k_{12a}k_{-12a}]$ was increased stepwise from zero to the maximum value obtained for model-2. Alternatively, the parameter $[k_{12}k_{21}]$ could have been decreased from its model-3 maximum down to zero. During these fits, the rate constants k_{31} and k_{32} were held fixed at averaged values, based on the optimized model-2 and model-3 results. It turned out that the K_i indeed change smoothly and that eqn (14) also

applies to the limiting cases, *i.e.* a maximum K_1 can be calculated for model-2 as well as a minimum K_{c2} for model-3, as indicated by the green and dashed lines in Fig. 8 and 9, respectively. The true equilibrium constants and corresponding thermodynamic data should in any case range within these limits. Accordingly, the true mechanism could lie somewhere between model-2 and model-3.

Conclusions

For seven aromatic compounds, slightly negative temperature coefficients were obtained for the total OH rate constants as well as a general tendency towards greater rate constants with increasing methylation. Both findings are complementary with previous studies. Temperature dependent OH rate constants for the three TeMBs and PMB were determined for the first time. Room temperature rate constants for 1245-TeMB and PMB previously reported in only study³² were confirmed. All OH rate constants are applicable under atmospheric conditions. Furthermore, a detailed analysis of OH decay curves for three selected compounds revealed insight into the reaction mechanism involving adduct formation, decomposition and possible isomerizations. 14-DMB, 135-TMB and 1245-TeMB were selected because they can form only two adduct isomers: an *ortho* and an *ipso* adduct each. The analysis was based on analytical solutions from a previous study on 135-TMB.¹¹ The general problem with these solutions is that different mechanisms can lead to the same OH decay curves. Therefore, limiting cases of a more general reaction mechanism were examined and the outcome was checked for consistency and qualitative agreement with theoretical predictions from the literature. In summary, adduct yields, reaction entropies and enthalpies obtained in the analysis lie in reasonable ranges for all three compounds. However, the open questions regarding the correct reaction mechanism raised in the previous work on 135-TMB¹¹ could not be answered here conclusively, based on results from two more compounds for which a qualitatively similar mechanism was generally expected. Overall, the reaction model including isomerization led to more conclusive results. Moreover, it was inferred that the *ortho* adducts are those that are formed with higher yields and decompose more quickly back to OH. To further elucidate the importance of different adduct isomers and the potential role of isomerizations, theoretical studies including the investigated compounds would be helpful. In any case, the rate constants derived for potential isomerization reactions are too slow to be of importance for the atmospheric degradation of the aromatics where a fast reaction of the primarily formed adducts with O₂ is expected. For the same reason, the primary yields of adduct isomers are expected to determine the further atmospheric degradation. On the other hand, isomerizations could play a role in laboratory studies at reduced O₂ concentrations or in the absence of O₂.

Acknowledgements

This work was supported by the Deutsche Forschungsgemeinschaft under grant ZE 792/6-1 and BO 1580/3-1 within

the French-German CNRS-INSU/DFG bilateral program ATMO-CHEM. We thank MSc Johannes Kaldun and Prof. Matthias Breuning from the Organic Chemistry Department of the University of Bayreuth for the synthesis of isodurene and the GC-FID analysis of the studied compounds.

Notes and references

- J. G. Calvert, R. Atkinson, K. H. Becker, R. M. Kamens, J. H. Seinfeld, T. J. Wallington and G. Yarwood, *The Mechanism of Atmospheric Oxidation of Aromatic Hydrocarbons*, Oxford University Press, New York, 2002.
- R. Atkinson, *J. Phys. Chem. Ref. Data*, 1989, **Monograph 1**, 204.
- R. Atkinson and J. Arey, *Chem. Rev.*, 2003, **103**, 4605–4638.
- R. Knispel, R. Koch, M. Siese and C. Zetzsch, *Ber. Bunsen-Ges.*, 1990, **94**, 1375–1379.
- R. Koch, R. Knispel, M. Elend, M. Siese and C. Zetzsch, *Atmos. Chem. Phys.*, 2007, **7**, 2057–2071.
- A. Wahner and C. Zetzsch, *J. Phys. Chem.*, 1983, **87**, 4945–4951.
- R. Koch, C. Zetzsch, First experimental evidence of *ipso*-addition of OH to methyl-substituted aromatics and O₂ reactivity of hexamethylbenzene-OH, Bunsentagung Erlangen, 2006.
- T. Berndt and O. Böge, *Int. J. Chem. Kinet.*, 2001, **33**, 124–129.
- J. von Buttler, R. Koch, M. Siese and C. Zetzsch, *Geophysical Research Abstracts*, 2008, **10**, EGU2008-A-10576.
- J.-C. Loison, M.-T. Rayez, J.-C. Rayez, A. Gratien, P. Morajkar, C. Fittschen and E. Villenave, *J. Phys. Chem. A*, 2012, **116**, 12189–12197.
- B. Bohn and C. Zetzsch, *Phys. Chem. Chem. Phys.*, 2012, **14**, 13933–13948.
- P. Alarcon, B. Bohn, C. Zetzsch, M. T. Rayez and J. C. Rayez, *Phys. Chem. Chem. Phys.*, 2014, **16**, 17315–17326.
- P. Alarcon, R. Strekowski and C. Zetzsch, *Phys. Chem. Chem. Phys.*, 2013, **15**, 20105–20114.
- S. Zhang, R. Strekowski, L. Bosland, A. Monod and C. Zetzsch, *Phys. Chem. Chem. Phys.*, 2011, **13**, 11671–11677.
- S. Zhang and C. Zetzsch, 21st International Symposium on Gas Kinetics 2010, Leuven, Belgium.
- A. Bolovinos, J. Philis, E. Pantos, P. Tsekeris and G. Andritsopoulos, *J. Chem. Phys.*, 1981, **75**, 4343–4349.
- A. Bolovinos, J. Philis, E. Pantos, P. Tsekeris and G. Andritsopoulos, *J. Mol. Spectrosc.*, 1982, **94**, 55–68.
- S. P. Sander, J. Abbatt, J. R. Barker, J. B. Burkholder, R. R. Friedl, D. M. Golden, R. E. Huie, C. E. Kolb, M. J. Kurylo, G. K. Moortgat, V. L. Orkin and P. H. Wine, *Chemical kinetics and photochemical data for use in atmospheric studies*, Evaluation No. 17, Jet Propulsion Laboratory, Pasadena, 2011, <http://jpldataeval.jpl.nasa.gov>.
- L. I. Smith, *Org. Synth.*, 1931, **11**, 66–69.
- R. A. Perry, R. Atkinson and J. N. Pitts, *J. Phys. Chem.*, 1977, **81**, 296–304.
- F. Witte, E. Urbanik and C. Zetzsch, *J. Phys. Chem.*, 1986, **90**, 3251–3259.

- 22 H. Geiger, I. Barnes, K. Becker, B. Bohn, T. Brauers, B. Donner, H.-P. Dorn, M. Elend, C. Freitas Dinis, D. Grossmann, H. Hass, H. Hein, A. Hoffmann, L. Hoppe, F. Hülsemann, D. Kley, B. Klotz, H. Libuda, T. Maurer, D. Mihelcic, G. Moortgat, R. Olariu, P. Neeb, D. Poppe, L. Ruppert, C. Sauer, O. Shestakov, H. Somnitz, W. Stockwell, L. Thüner, A. Wahner, P. Wiesen, F. Zabel, R. Zellner and C. Zetzsch, *J. Atmos. Chem.*, 2002, **42**, 323–357.
- 23 A. C. Davison and D. V. Hinkley, *Bootstrap methods and their application*, Cambridge University Press, Cambridge, New York, NY, USA, 1997.
- 24 I. Suh, D. Zhang, R. Zhang, L. T. Molina and M. J. Molina, *Chem. Phys. Lett.*, 2002, **364**, 454–462.
- 25 L. J. Bartolotti and E. O. Edney, *Chem. Phys. Lett.*, 1995, **245**, 119–122.
- 26 V. H. Uc, I. García-Cruz, A. Hernández-Laguna and A. Vivier-Bunge, *J. Phys. Chem. A*, 2000, **104**, 7847–7855.
- 27 J. Fan and R. Zhang, *J. Phys. Chem. A*, 2006, **110**, 7728–7737.
- 28 J. Fan and R. Zhang, *J. Phys. Chem. A*, 2008, **112**, 4314–4323.
- 29 J. M. Andino, J. N. Smith, R. C. Flagan, W. A. Goddard and J. H. Seinfeld, *J. Phys. Chem.*, 1996, **100**, 10967–10980.
- 30 D. Mehta, A. Nguyen, A. Montenegro and Z. Li, *J. Phys. Chem. A*, 2009, **113**, 12942–12951.
- 31 S. M. Aschmann, W. D. Long and R. Atkinson, *J. Phys. Chem. A*, 2006, **110**, 7393–7400.
- 32 S. M. Aschmann, J. Arey and R. Atkinson, *J. Phys. Chem. A*, 2013, **117**, 2556–2568.
- 33 D. A. Hansen, R. Atkinson and J. N. Pitts, *J. Phys. Chem.*, 1975, **79**, 1763–1766.
- 34 G. J. Doyle, A. C. Lloyd, K. R. Darnall, A. M. Winer and J. N. Pitts, *Environ. Sci. Technol.*, 1975, **9**, 237–241.
- 35 A. R. Ravishankara, S. Wagner, S. Fischer, G. Smith, R. Schiff, R. T. Watson, G. Tesi and D. D. Davis, *Int. J. Chem. Kinet.*, 1978, **10**, 783–804.
- 36 J. M. Nicovich, R. L. Thompson and A. R. Ravishankara, *J. Phys. Chem.*, 1981, **85**, 2913–2916.
- 37 T. Ohta and T. Ohshima, *Bull. Chem. Soc. Jpn.*, 1985, **58**, 3029–3030.
- 38 E. O. Edney, T. E. Kleindienst and E. W. Corse, *Int. J. Chem. Kinet.*, 1986, **18**, 1355–1371.
- 39 R. Atkinson and S. M. Aschmann, *Int. J. Chem. Kinet.*, 1989, **21**, 355–365.
- 40 R. Sommerlade, H. Parlar, D. Wrobel and P. Kochs, *Environ. Sci. Technol.*, 1993, **27**, 2435–2440.
- 41 F. Kramp and S. E. Paulson, *J. Phys. Chem. A*, 1998, **102**, 2685–2690.
- 42 S. M. Aschmann, E. C. Tuazon and R. Atkinson, *J. Phys. Chem. A*, 2005, **109**, 2282–2291.
- 43 J. M. Andino and A. Vivier-Bunge, *Adv. Quantum Chem.*, 2008, **55**, 297–310.
- 44 R. Wu, S. Pan, Y. Li and L. Wang, *J. Phys. Chem. A*, 2014, **118**, 4533–4547.
- 45 M. Huang, W. Zhang, Z. Wang, L. Hao, W. Zhao, X. Liu, B. Long and L. Fang, *Int. J. Quantum Chem.*, 2008, **108**, 954–966.
- 46 M. Q. Huang, Z. Y. Wang, L. Q. Hao and W. J. Zhang, *Comput. Theor. Chem.*, 2011, **965**, 285–290.
- 47 S. Pan and L. Wang, *J. Phys. Chem. A*, 2014, **118**, 10778–10787.

Electronic Supplementary Material (ESI) for Physical Chemistry Chemical Physics.
This journal is © the Owner Societies 2015

Electronic Supplementary Information (ESI) for Physical Chemistry Chemical Physics

Kinetic and mechanistic study of the reaction of OH radicals with methylated benzenes: 1,4-dimethyl-, 1,3,5-trimethyl-, 1,2,4,5-, 1,2,3,5- and 1,2,3,4-tetramethyl-, pentamethyl-, and hexamethylbenzene

Paulo Alarcón^a, Birger Bohn^{*b}, Cornelius Zetzsch^{a,c}

^a Atmospheric Chemistry Research Laboratory, University of Bayreuth, 95448, Germany.

^b Institut für Energie- und Klimaforschung IEK-8: Troposphäre, Forschungszentrum Jülich, 52425 Jülich, Germany.

^c Fraunhofer Institute for Toxicology and Experimental Medicine, 30625 Hannover, Germany.

E-mail: b.bohn@fz-juelich.de

S1 Experimental conditions

Table S1. Experimental conditions for 1,4-dimethylbenzene (14-DMB), 1,3,5-trimethylbenzene (135-TMB) and 1,2,4,5-tetramethylbenzene (1245-TeMB).

Exp #	14-DMB ^a				135-TMB ^b				1245-TeMB ^c			
	T / K	N ^d	min. conc. ^e	max. conc. ^e	T / K	N ^d	min. conc. ^e	max. conc. ^e	T / K	N ^d	min. conc. ^e	max. conc. ^e
1	304.3	12	10.0	63	299.1	21	0.85	17	300.2	10	4.9	20
2	305.0	27	8.5	66	300.2	7	0.88	11	300.5	11	4.7	20
3	305.7	26	10.0	71	300.3	9	0.88	12	302.8	11	4.9	19
4	314.4	26	9.8	67	300.8	29	0.87	13	306.3	12	4.7	19
5	324.6	26	6.7	70	303.1	29	0.89	13	306.8	14	4.8	19
6	333.9	11	10.0	52	303.4	23	0.82	13	310.0	14	4.7	19
7	343.0	27	8.7	68	305.0	29	0.90	13	314.3	14	4.5	20
8	352.3	27	8.4	74	305.5	10	0.86	13	314.8	13	4.7	19
9					307.7	21	0.86	13	319.9	7	4.6	19
10					308.2	29	0.87	13	323.7	14	4.8	19
11					315.1	21	0.84	13	324.7	14	4.6	19
12					324.1	21	0.82	13	333.9	13	5.1	20
13					333.1	29	0.81	13	334.1	14	4.6	20
14					341.8	29	0.93	13	342.7	12	4.8	20
15					348.1	27	1.7	13	343.2	12	4.9	19

Total pressure of He: ^a 230 mbar, ^b 200 mbar and ^c 246 mbar (except for experiments 4, 7, 10 and 11: 360 mbar). ^d Number of decay curves. ^e Concentrations in 10¹²cm⁻³.

Table S2. Experimental conditions for 1,2,3,4-tetramethylbenzene (1234-TeMB), 1,2,3,5-tetramethylbenzene (1235-TeMB) and pentamethylbenzene (PMB).

Exp #	1234-TeMB ^a				1235-TeMB ^b				PMB ^a			
	T / K	N ^c	min. conc. ^d	max. conc. ^d	T / K	N ^c	min. conc. ^d	max. conc. ^d	T / K	N ^c	min. conc. ^d	max. conc. ^d
1	298.8	17	0.50	3.1	297.6	51	0.88	17	299.8	12	1.00	7.7
2	303.8	17	0.50	3.1	302.8	35	0.92	17	300.9	31	0.43	7.5
3	305.6	27	0.49	3.1	304.2	30	0.88	17	303.4	15	0.80	8.1
4	313.2	16	0.80	3.1	305.2	31	0.87	17	305.4	15	0.91	7.6
5	324.6	14	1.10	3.1	308.8	36	0.91	17	311.4	15	1.00	8.0
6	334.0	13	0.80	3.2	312.5	39	0.86	17	313.3	15	0.77	7.6
7	343.3	18	0.47	3.1	316.8	38	0.86	17	314.0	15	0.79	7.1
8	352.3	12	1.50	3.1	320.9	28	0.80	17	323.2	15	0.82	8.0
9	361.8	18	0.49	3.1	326.1	33	0.80	17	324.4	15	0.95	7.6
10					330.2	39	0.80	17	328.3	15	0.99	7.1
11					335.4	36	0.80	17	332.2	15	0.98	7.1
12									337.9	15	1.00	7.5
13									342.1	15	0.89	6.9
14									357.6	15	0.94	7.5
15									362.3	15	0.96	7.6

Total pressure of He: ^a 230 mbar, ^b 200 mbar. ^c Number of decay curves. ^d Concentrations in 10¹²cm⁻³.

S2 Fit results

S2.1 Example plots

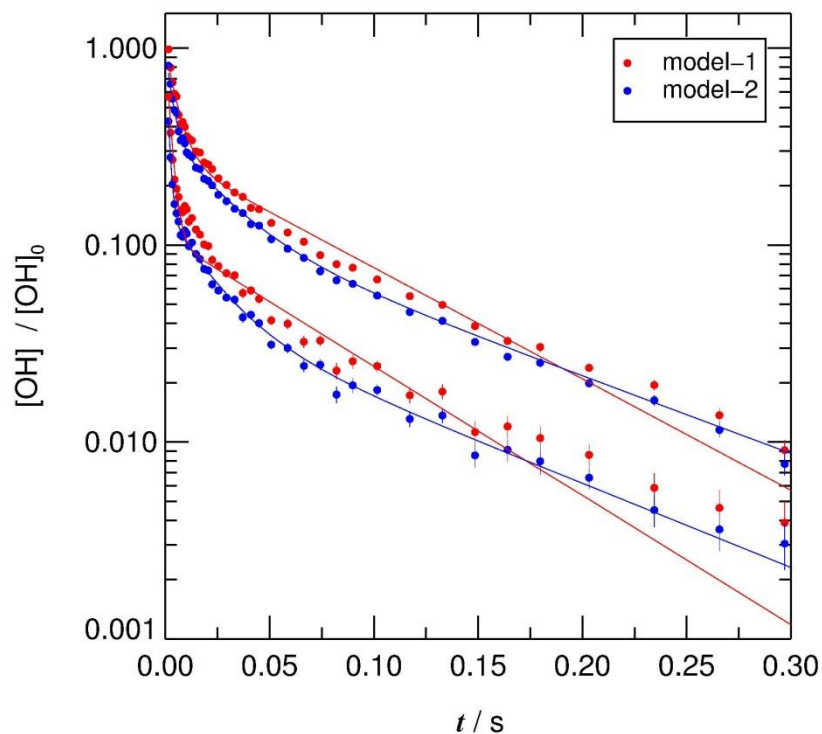


Fig S1. Examples of OH decay curves in a semi-logarithmic plot. Two from a total of eleven decay curves of the experiments with 14-DMB at 334 K are shown. At this temperature a maximum difference in fit qualities is apparent in Fig. 2 of the main paper. 14-DMB concentrations were $1.7 \times 10^{13} \text{cm}^{-3}$ (top) and $5.0 \times 10^{13} \text{cm}^{-3}$ (bottom). Full lines show the results of fits to all eleven decay curves simultaneously according to model-1 (red) and model-2 (blue). The data points were calculated from photon counts divided by interval widths and assigned to the middle of the intervals. Fitted backgrounds were subtracted and data then normalized to the fitted starting count rates. For that reason model-1 and model-2 data points are different even though they represent the same experimental decay curve. Only a small fraction of the total measurement time of 4 s is shown.

Electronic Supplementary Information (ESI) for Physical Chemistry Chemical Physics

S2.2 Model-2

Table S3. Model-2 fit parameters for 14-DMB, 135-TMB and 1245-TeMB. Uncertainties are mean differences to upper and lower limit estimates.

Exp #	k_2 / s ⁻¹	k_{OH} = $k_{11a}+k_{12a}+k_{1b}$ /10 ⁻¹² cm ³ s ⁻¹	$k_{11a} k_{-11a}$ /10 ⁻⁹ cm ³ s ⁻²	$k_{-11a}+k_{31}$ / s ⁻¹	$k_{12a} k_{-12a}$ /10 ⁻¹² cm ³ s ⁻²	$k_{-12a}+k_{32}$ / s ⁻¹
14-DMB						
1	14 ± 9	13.3 ± 0.8	0.102 ± 0.016	15 ± 5	6 ± 13	3.1 ± 2.7
2	19 ± 7	12.5 ± 0.7	0.099 ± 0.017	17 ± 6	10 ± 15	3.8 ± 2.6
3	13 ± 10	12.9 ± 1.0	0.11 ± 0.02	21 ± 10	16 ± 21	4.9 ± 3.0
4	3.5 ± 3.9	12.9 ± 0.8	0.25 ± 0.03	35 ± 5	14 ± 8	6.1 ± 2.0
5	3.8 ± 1.7	12.4 ± 0.9	0.55 ± 0.08	71 ± 9	21 ± 8	11.0 ± 2.3
6	0.5 ± 1.0	12.7 ± 1.1	1.2 ± 0.2	145 ± 13	35 ± 8	19.6 ± 2.4
7	1.8 ± 1.6	11.6 ± 2.1	2.1 ± 0.7	259 ± 43	47 ± 18	32.6 ± 5.9
8	2.0 ± 2.0	11.4 ± 2.9	3.4 ± 1.2	430 ± 120	51 ± 35	48 ± 14
135-TMB						
1	22 ± 9	70.0 ± 8.0	0.31 ± 0.07	10.0 ± 4.4	30 ± 55	2.1 ± 2.1
2	20 ± 4	68.0 ± 4.0	0.32 ± 0.06	12.3 ± 3.7	56 ± 53	3.1 ± 1.5
3	26 ± 4	69.8 ± 4.2	0.31 ± 0.10	19 ± 11	140 ± 80	4.7 ± 1.5
4	8 ± 12	68.5 ± 6.2	0.32 ± 0.08	16.0 ± 8.1	86 ± 69	3.7 ± 1.6
5	25 ± 5	62.9 ± 3.8	0.41 ± 0.10	16.6 ± 7.2	89 ± 89	4.6 ± 2.2
6	22 ± 3	67.1 ± 4.0	0.41 ± 0.11	18 ± 11	130 ± 120	5.3 ± 2.2
7	16 ± 3	64.1 ± 3.8	0.49 ± 0.07	17.5 ± 4.7	85 ± 65	4.7 ± 1.7
8	18 ± 3	65.2 ± 3.9	0.58 ± 0.09	21.4 ± 6.4	120 ± 80	5.6 ± 1.6
9	14 ± 2	64.4 ± 3.9	0.67 ± 0.10	22.1 ± 7.1	110 ± 100	6.1 ± 2.3
10	17 ± 2	63.1 ± 3.8	0.69 ± 0.08	22.6 ± 6.1	110 ± 80	5.8 ± 1.9
11	13 ± 2	64.5 ± 5.8	1.6 ± 0.3	44.3 ± 9.6	160 ± 110	9.9 ± 2.8
12	7.4 ± 0.8	66.0 ± 7.9	4.3 ± 0.8	90 ± 12	135 ± 71	15.2 ± 3.4
13	5.2 ± 0.5	64.5 ± 9.7	9.7 ± 2.3	183 ± 22	92 ± 45	21.0 ± 4.4
14	4.6 ± 0.4	51.4 ± 9.3	14.2 ± 4.3	325 ± 45	51 ± 25	26.2 ± 5.5
15	4.8 ± 0.8	39.6 ± 12.0	14.5 ± 7.3	430 ± 90	28 ± 18	26.4 ± 7.2
1245-TeMB						
1	-22 ± 1	57.8 ± 5.2	0.54 ± 0.07	34.8 ± 5.8	13 ± 24	3.2 ± 4.6
2	-4.4 ± 0.1	55.5 ± 5.0	0.48 ± 0.09	42 ± 12	40 ± 34	4.7 ± 3.2
3	12 ± 17	53.6 ± 4.8	0.61 ± 0.09	41 ± 10	30 ± 37	4.6 ± 4.1
4	32 ± 22	51.7 ± 4.7	0.83 ± 0.14	55 ± 10	46 ± 19	4.4 ± 1.7
5	11 ± 14	51.4 ± 4.6	0.86 ± 0.13	54.2 ± 8.1	46 ± 17	4.7 ± 1.4
6	29 ± 16	48.7 ± 4.4	1.07 ± 0.16	68.6 ± 9.4	64 ± 14	5.1 ± 0.9
7	23 ± 15	49.2 ± 4.4	1.46 ± 0.26	93 ± 13	89 ± 16	6.4 ± 1.0
8	16 ± 14	47.1 ± 4.2	1.45 ± 0.26	93 ± 14	107 ± 24	8.7 ± 1.3
9	25 ± 10	44.9 ± 4.0	2.21 ± 0.51	142 ± 21	170 ± 30	11.4 ± 1.0
10	23 ± 10	44.9 ± 5.4	2.87 ± 0.78	184 ± 33	220 ± 30	14.0 ± 1.3
11	8.7 ± 6.7	44.5 ± 4.7	2.94 ± 0.80	194 ± 32	240 ± 30	15.3 ± 1.1
12	25 ± 6	34.1 ± 6.2	3.3 ± 2.1	300 ± 100	460 ± 70	30.4 ± 2.3
13	17 ± 5	39.2 ± 5.9	3.7 ± 1.7	270 ± 70	400 ± 60	25.5 ± 1.5
14	10 ± 6	35.6 ± 14.1	4.4 ± 6.7	380 ± 310	790 ± 480	51 ± 18
15	18 ± 4	32.6 ± 10.5	3.4 ± 4.6	320 ± 230	690 ± 300	49 ± 8

Electronic Supplementary Information (ESI) for Physical Chemistry Chemical Physics

S2.3 Model-3

Table S4. Model-3 fit parameters for 14-DMB, 135-TMB and 1245-TeMB. Parameters k_2 and k_{0H} are the same as for model-2. Uncertainties are mean differences to upper and lower limit estimates.

Exp #	$k_{11a} k_{-11a}$ / $10^{-9} \text{ cm}^3 \text{ s}^{-2}$	$k_{-11a} + k_{12} + k_{31}$ / s^{-1}	$k_{12} k_{21}$ / s^{-2}	$k_{21} + k_{32}$ / s^{-1}
14-DMB				
1	0.108 ± 0.015	14.7 ± 3.0	8 ± 18	3.8 ± 4.4
2	0.109 ± 0.018	16.2 ± 4.1	15 ± 31	5.0 ± 2.3
3	0.124 ± 0.025	18.9 ± 6.1	27 ± 71	6.9 ± 2.3
4	0.264 ± 0.032	33.5 ± 4.6	38 ± 28	7.5 ± 2.9
5	0.57 ± 0.09	68.9 ± 7.3	120 ± 56	13.1 ± 3.2
6	1.24 ± 0.21	141 ± 13	420 ± 130	23.0 ± 3.5
7	2.1 ± 0.7	254 ± 43	1100 ± 470	37.6 ± 6.8
8	3.5 ± 1.1	420 ± 120	2100 ± 1700	54 ± 17
135-TMB				
1	0.34 ± 0.06	9.3 ± 3.0	5 ± 12	2.8 ± 2.1
2	0.38 ± 0.06	11.0 ± 2.5	11 ± 15	4.4 ± 2.2
3	0.45 ± 0.10	14.9 ± 6.6	46 ± 98	9.3 ± 6.9
4	0.41 ± 0.08	13.5 ± 4.8	25 ± 50	6.3 ± 4.5
5	0.50 ± 0.08	14.5 ± 4.3	21 ± 42	6.7 ± 4.5
6	0.54 ± 0.12	15.3 ± 6.5	32 ± 87	8.4 ± 7.1
7	0.57 ± 0.08	15.7 ± 3.4	21 ± 25	6.5 ± 3.1
8	0.70 ± 0.11	18.8 ± 4.1	35 ± 39	8.2 ± 4.1
9	0.78 ± 0.13	19.9 ± 4.7	30 ± 46	8.3 ± 5.0
10	0.79 ± 0.11	20.4 ± 3.8	32 ± 36	8.0 ± 3.9
11	1.80 ± 0.32	41.3 ± 8.2	94 ± 90	12.9 ± 5.1
12	4.5 ± 0.8	88 ± 12	160 ± 100	17.5 ± 4.8
13	9.8 ± 2.4	182 ± 22	240 ± 120	22.5 ± 4.8
14	14.3 ± 4.3	324 ± 44	310 ± 150	27.3 ± 6.6
15	14.6 ± 7.3	428 ± 90	300 ± 190	27.2 ± 7.7
1245-TeMB				
1	0.55 ± 0.08	34.1 ± 5.3	21 ± 36	3.8 ± 2.6
2	0.52 ± 0.10	38.8 ± 11	94 ± 120	7.5 ± 5.8
3	0.64 ± 0.11	39.0 ± 7.7	55 ± 79	6.2 ± 6.1
4	0.87 ± 0.15	52.7 ± 8.8	127 ± 75	7.0 ± 2.8
5	0.91 ± 0.14	51.8 ± 7.8	116 ± 56	7.1 ± 2.4
6	1.14 ± 0.17	65.1 ± 8.9	210 ± 70	8.6 ± 1.8
7	1.55 ± 0.26	88 ± 12	400 ± 110	11.3 ± 1.7
8	1.56 ± 0.28	87 ± 13	450 ± 160	14.4 ± 2.6
9	2.38 ± 0.50	133 ± 20	1120 ± 280	20.6 ± 2.5
10	2.90 ± 0.78	172 ± 31	1870 ± 450	25.9 ± 3.1
11	3.09 ± 0.84	180 ± 33	2230 ± 540	28.8 ± 2.6
12	3.2 ± 0.9	270 ± 100	7900 ± 3400	63.3 ± 8.7
13	3.8 ± 2.2	248 ± 71	5300 ± 1700	49.2 ± 5.2
14	4.1 ± 1.8	330 ± 290	14000 ± 13000	101 ± 50
15	5.2 ± 7.3	280 ± 220	11000 ± 11000	95 ± 30

Electronic Supplementary Information (ESI) for Physical Chemistry Chemical Physics

S2.4 Model-2/model-3 k_{OH} results for 1234-TeMB, 1235-TeMB and PMB

Because the number of possible adducts is greater than two for these compounds, model-2 and model-3 fits are regarded as approximations and only the presumably robust, common quantity k_{OH} is reported here.

Table S5. Rate constants of the reactions of OH with 1234-TeMB, 1235-TeMB and PMB. Uncertainties are mean differences to upper and lower limit estimates.

Exp #	1234-TeMB	1235-TeMB	PMB
	k_{OH} / $10^{-12} \text{ cm}^3\text{s}^{-1}$	k_{OH} / $10^{-12} \text{ cm}^3\text{s}^{-1}$	k_{OH} / $10^{-12} \text{ cm}^3\text{s}^{-1}$
1	65.5 ± 2.6	62.6 ± 2.2	110.2 ± 6.6 ^a
2	61.9 ± 2.5	62.6 ± 3.7	109.7 ± 4.4 ^a
3	64.3 ± 3.6	60.4 ± 3.7	95.1 ± 3.8 ^a
4	61.0 ± 4.0	58.9 ± 3.5	91.7 ± 7.9
5	57.0 ± 7.6	62.6 ± 3.7	107.0 ± 7.6
6	45.7 ± 4.2	58.3 ± 3.5	97.0 ± 7.3
7	46.2 ± 5.2	60.1 ± 4.2	95.9 ± 6.3
8	43.1 ± 6.5	57.7 ± 4.6	96 ± 12
9	46 ± 10	53.3 ± 5.1	97 ± 11
10		61.9 ± 7.5	94 ± 14
11		53.3 ± 8.3	88 ± 12
12			96 ± 25
13			71.3 ± 3.6
14			59.1 ± 3.5
15			62.3 ± 4.2

^a Model-1 result.

Electronic Supplementary Information (ESI) for Physical Chemistry Chemical Physics

S2.5 Model-2 and model-3 equilibrium constants

Table S6. Equilibrium constants and estimated uncertainties for the direct formation of add₁ (K_{c1}) and add₂ (K_{c2}) and indirect formation of add₂ via isomerization (K_i).

Exp #	$K_{c1} = k_{11a}/k_{-11a}$ / 10^{-13} cm ³ model-2	$K_{c2} = k_{12a}/k_{-12a}$ / 10^{-13} cm ³ model-2	$K_{c1} = k_{11a}/k_{-11a}$ / 10^{-13} cm ³ model-3	$K_i = k_{12}/k_{c1}$ model-3
14-DMB				
1	8.0 ± 4.7	19 ± 26	14.2 ± 6.0	0.75 ± 1.00
2	5.6 ± 3.9	16 ± 20	12.7 ± 4.0	0.74 ± 0.67
3	3.9 ± 3.4	12 ± 15	10.4 ± 3.2	0.67 ± 0.46
4	2.6 ± 0.6	5.9 ± 1.9	4.51 ± 0.54	0.80 ± 0.23
5	1.24 ± 0.19	2.2 ± 0.3	1.87 ± 0.17	0.78 ± 0.13
6	0.61 ± 0.07	1.05 ± 0.09	0.88 ± 0.08	0.84 ± 0.10
7	0.32 ± 0.05	0.48 ± 0.06	0.43 ± 0.05	0.81 ± 0.12
8	0.19 ± 0.05	0.24 ± 0.27	0.24 ± 0.05	0.75 ± 0.18
135-TMB				
1	84 ± 78	380 ± 530	180 ± 220	0.96 ± 1.29
2	46 ± 41	160 ± 190	128 ± 44	0.68 ± 0.52
3	13 ± 18	113 ± 39	99 ± 32	0.59 ± 0.28
4	22 ± 27	140 ± 120	103 ± 36	0.75 ± 0.40
5	26 ± 26	79 ± 54	74 ± 19	0.55 ± 0.31
6	19 ± 26	80 ± 32	76 ± 21	0.50 ± 0.23
7	26 ± 17	70 ± 23	65 ± 10	0.56 ± 0.19
8	19 ± 13	62 ± 15	54.3 ± 8.7	0.59 ± 0.19
9	20 ± 14	46 ± 12	45.8 ± 7.3	0.51 ± 0.16
10	20 ± 11	49 ± 11	44.9 ± 6.3	0.57 ± 0.15
11	10.0 ± 3.7	21.0 ± 3.2	18.9 ± 2.3	0.62 ± 0.14
12	5.8 ± 0.9	6.9 ± 1.0	7.81 ± 0.78	0.57 ± 0.09
13	3.0 ± 0.4	2.3 ± 0.4	3.46 ± 0.42	0.51 ± 0.07
14	1.38 ± 0.21	0.82 ± 0.12	1.49 ± 0.21	0.45 ± 0.06
15	0.81 ± 0.18	0.45 ± 0.08	0.85 ± 0.17	0.44 ± 0.08
1245-TeMB				
1	39 ± 35	260 ± 360	44 ± 54	1.9 ± 2.6
2	14 ± 19	80 ± 110	68 ± 89	1.9 ± 1.4
3	20 ± 18	67 ± 94	40 ± 40	1.7 ± 2.0
4	7.9 ± 3.8	130 ± 180	32 ± 18	3.0 ± 1.2
5	8.9 ± 3.5	100 ± 130	29 ± 11	2.7 ± 0.9
6	5.2 ± 1.4	98 ± 57	22.8 ± 6.3	3.2 ± 0.6
7	3.0 ± 0.6	58 ± 18	13.1 ± 2.7	3.4 ± 0.5
8	3.0 ± 0.8	28.2 ± 7.3	10.6 ± 2.1	2.3 ± 0.4
9	1.55 ± 0.28	21.3 ± 2.6	6.5 ± 1.1	2.8 ± 0.4
10	1.11 ± 0.19	16.5 ± 1.8	4.7 ± 0.8	2.9 ± 0.5
11	1.00 ± 0.17	14.9 ± 1.3	4.4 ± 0.7	2.8 ± 0.4
12	0.42 ± 0.12	5.9 ± 0.5	2.3 ± 0.8	2.0 ± 0.8
13	0.60 ± 0.12	7.5 ± 0.6	2.7 ± 0.6	2.2 ± 0.6
14	0.35 ± 0.42	3.3 ± 1.3	1.7 ± 1.6	1.4 ± 1.1
15	0.37 ± 0.42	3.2 ± 0.7	1.9 ± 1.1	1.2 ± 1.0

Electronic Supplementary Information (ESI) for Physical Chemistry Chemical Physics

S3 Hexamethylbenzene

Experiments with hexamethylbenzene (HMB) made by von Buttler et al.¹ were extensively re-evaluated in this work for direct comparison with the other investigated compounds using meanwhile developed software tools. Fit results are based on model-1. Von Buttler et al.¹ typically recorded seven OH decay curves at different HMB concentrations in a range $(4-10) \times 10^{11} \text{ cm}^{-3}$ at a total pressure of 260 mbar of He. At temperatures below 330 K biexponential decay behaviour was not distinct enough to derive equilibrium constants. Some of the original experiments with suspected technical problems (298 K, 355 K) were rejected in the reanalysis.

Table S7. Model-1 fit parameters for HMB obtained in a re-evaluation of experiments by von Buttler et al.¹

T / K	k_2 / s^{-1}	$k_{\text{OH}} = k_{11a} + k_{1b} / 10^{-12} \text{ cm}^3 \text{ s}^{-1}$	$k_{11a} k_{-11a} / 10^{-9} \text{ cm}^3 \text{ s}^{-2}$	$k_{-11a} + k_{31} / \text{s}^{-1}$	$K_c^a = k_{11a} / k_{-11a} / 10^{-13} \text{ cm}^3$
311.0	14.7 ± 2.5	139.7 ± 5.6	0.067 ± 0.040	9.7 ± 6.9	-
319.4	10.4 ± 2.3	136.0 ± 5.4	0.102 ± 0.027	8.3 ± 2.3	-
325.1	9.3 ± 2.5	129.8 ± 5.2	0.151 ± 0.040	11.2 ± 2.9	-
330.8	12.7 ± 1.9	126.6 ± 5.1	0.256 ± 0.031	11.1 ± 1.3	440 ± 650
334.9	9.5 ± 1.7	123.4 ± 4.9	0.347 ± 0.028	11.7 ± 0.9	380 ± 200
339.5	9.8 ± 1.7	119.7 ± 4.8	0.504 ± 0.040	13.0 ± 0.8	278 ± 80
345.0	8.4 ± 1.9	118.1 ± 4.7	0.792 ± 0.063	16.1 ± 1.0	144 ± 26
349.8	7.5 ± 1.1	117.3 ± 4.7	1.195 ± 0.072	20.0 ± 0.8	94.3 ± 6.7
360.3	8.0 ± 1.0	111.7 ± 4.5	2.56 ± 0.21	35.0 ± 1.4	37.1 ± 1.5
365.1	6.8 ± 0.7	104.4 ± 6.3	3.54 ± 0.35	46.9 ± 1.9	24.3 ± 1.0
370.3	7.2 ± 0.7	99.8 ± 10.0	5.25 ± 0.84	69.8 ± 5.6	14.1 ± 0.8

^a Results for a fixed background loss rate constant $k_{31} = 8.7 \text{ s}^{-1}$.

S4 Reactant vapour pressures

OH rate constants determined in this work rely on correct aromatic reactant concentrations. These concentrations were calculated from gas-flow rates and saturation vapour pressures of the compounds at the employed saturator temperatures (270-330 K, dependent on compound; accuracy: $\pm 1 \text{ K}$). Reliable vapour pressure data from the literature are therefore critical for the determination of reactant concentrations.

In Table S8 available studies and their temperature range are summarised for the investigated aromatic compounds in the indicated phase (l = liquid, s = solid). The temperature of the saturator, the corresponding vapour pressures at saturator temperatures and coefficients for Antoine parameterisations that were applied are also listed. Vapour pressures for 14-DMB and 135-TMB have been reported in several publications with good agreement in a wide temperature range, including the saturator temperatures. For these compounds we used Antoine coefficients recommended by Stephenson et al.² In the case of 14-DMB the saturator temperature was accidentally set 2 K below the melting point at 286 K. No freezing was positively observed, so we are not sure about the phase during these experiments and Antoine coefficients for liquid 14-DMB were finally applied. In case the sample was solid, the vapour pressure would be lower by 5% (Tab. S8) and OH rate constants would increase accordingly by 5%.

No vapour pressure data were reported so far for 1245-TeMB(s), 1234-TeMB(l) and 1235-TeMB(l) at the saturator temperatures. For 1245-TeMB(s) we fitted Antoine coefficients to the low temperature data of Colomina et al.³ and extrapolated to the saturator temperature. The resulting vapour pressure is in good agreement with a recommendation of Ruzicka Jr. et al.⁴ that is based on an analysis of vapour pressures at higher temperatures and thermodynamic data. Vapour pressure measurements for the other two tetramethylbenzenes are only available in the form of parameterisations for temperatures much higher than the ones used in this study. An extrapolation of these data down to

Electronic Supplementary Information (ESI) for Physical Chemistry Chemical Physics

the saturator temperatures is uncertain. Therefore, we preferred the recommendations of Ruzicka Jr. et al.⁴ to fit Antoine coefficients.

For PMB, Colomina et al.³ reported direct measurements covering the saturator temperature that were used to determine Antoine parameters. The measured data are also in good agreement with the recommendation by Ruzicka Jr. et al.⁴. For HMB, a large number of consistent vapour pressure data have been reported. In this case, the compilation published by Stephenson et al.² was used. In summary, we estimate maximum uncertainties of reactant concentrations of around 10% for 14-DMB, 135-TMB, PMB and HMB, and 20% for the three tetramethylbenzenes.

Table S8. Temperature range of literature studies on vapour pressures, saturator temperatures T_{sat} and corresponding vapour pressures P_{sat} of investigated compounds. Vapour pressures were calculated using parameterisations recommended in the various studies unless indicated otherwise. The Antoine equation: $\log_{10}[P_{\text{sat}}/\text{mbar}] = A - B / (T_{\text{sat}}/K + C)$ was applied in this work using the listed parameters.

Compound	T -range / K	A	B	C	T_{sat} / K	P_{sat} / mbar
14-DMB (l, s)	263–272 ⁵					– (s) ^a
	286–348 ⁶					5.01 (l)
	273–286 ⁷					4.70 (s)
	286–333 ⁷					5.00 (l)
	247–286 ⁸					4.69 (s)
	286–453 ⁸					4.98 (l)
	273–353 ⁹					4.38 (l)
	247–286 ²	16.501	6327.0	115.72		4.70 (s)
286–453 ²	7.1478	1475.8	–55.24	284	4.97 (l)	
135-TMB (l)	271–276 ⁵					– ^a
	273–373 ⁹					0.985
	255–268 ¹⁰					0.959 ^b
	223–323 ⁴					0.940
	273–348 ⁶					0.942
	249–356 ²	7.6231	1810.7	–43.31	280	0.940
1245-TeMB (s)	271–275 ⁵					– ^a
	223–323 ⁴					0.812
	263–277 ³	10.704	3028	–32.8	313	0.790 ^{a, b, c}
1234-TeMB (l)	333–478 ¹¹					0.048 ^b
	393–478 ¹²					– ^a
	223–323 ⁴					0.087
	223–323 ⁴	7.836	2083	–41.81	276	0.087 ^c
1235-TeMB (l)	328–468 ¹¹					0.573 ^b
	223–323 ⁴					0.969
	223–323 ⁴	7.761	2007	–44.74	303	0.977 ^c
PMB (s)	223–323 ⁴					0.091
	296–313 ³	2.973	333	–215.6	300	0.107 ^{a, c}
HMB (s)	314–363 ¹³					– ^a
	303–343 ¹⁴					– ^a
	289–304 ³					– ^a
	223–323 ⁴					0.028
	303–343 ²	9.622	2966	–59.6	325	0.028

^a No parameterisation given in the literature. ^b Extrapolated value, T_{sat} outside the studied range. ^c Antoine parameters from a fit to published data.

Electronic Supplementary Information (ESI) for Physical Chemistry Chemical Physics

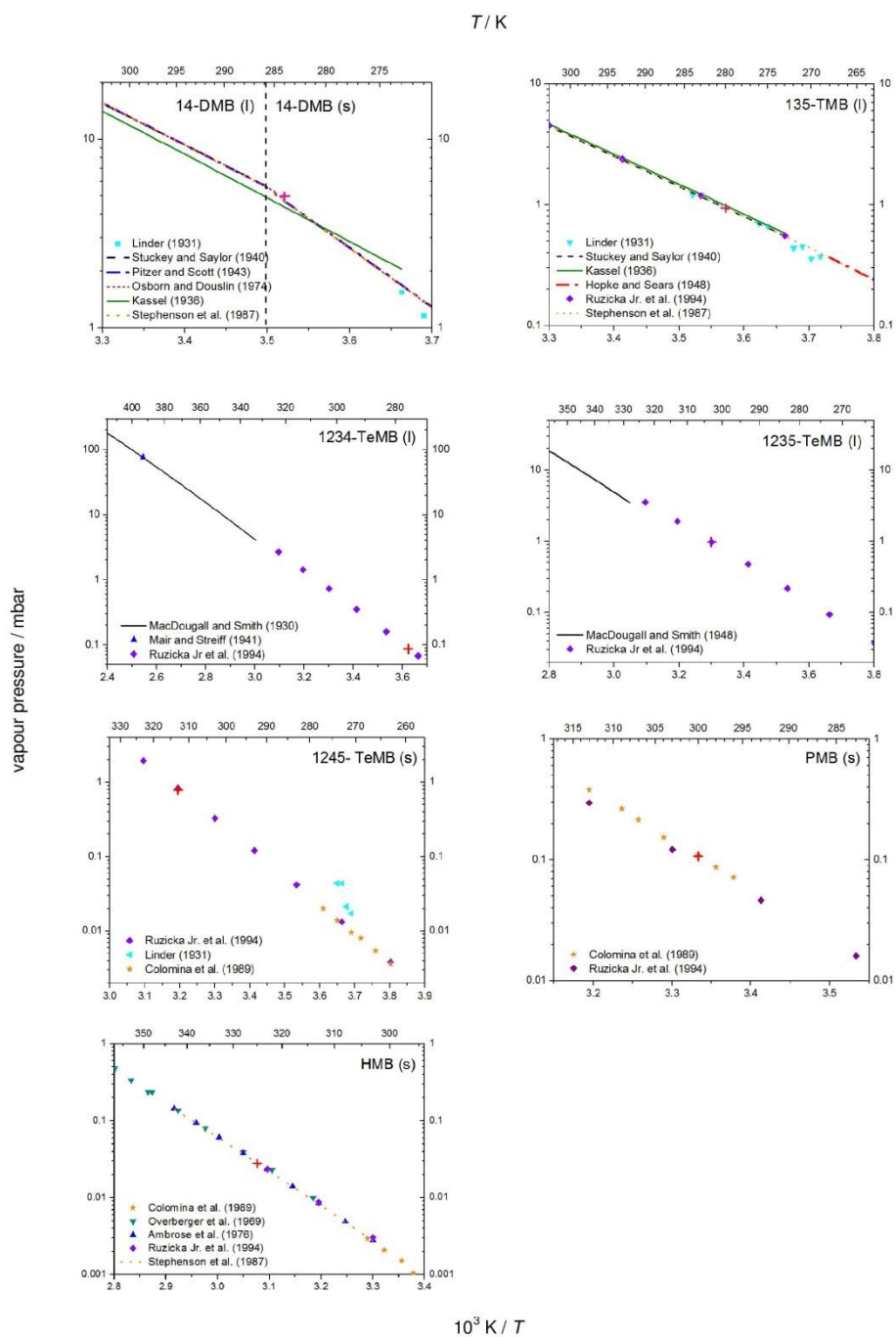


Fig S2. Vapour pressure data from the literature for the studied compounds. Crosses show the vapour pressures used for the determination of the aromatic concentrations in this study. For 14-DMB the vertical dashed line indicates the melting point.

Electronic Supplementary Information (ESI) for Physical Chemistry Chemical Physics

References

1. J. von Buttlar, R. Koch, M. Siese and C. Zetzsch, *Geophysical Research Abstracts*, 2008, **10**, EGU2008-A-10576.
2. R. M. Stephenson, S. Malanowski and D. Ambrose, *Handbook of the thermodynamics of organic compounds*, Elsevier Science Publishing, New York, 1987.
3. M. Colomina, P. Jiménez, M. V. Roux and C. Turrión, *J. Chem. Thermodyn.*, 1989, **21**, 275-281.
4. V. Ruzicka Jr, M. Zabransky, K. Ruzicka and V. Majer, *Thermochim. Acta*, 1994, **245**, 121-144.
5. E. G. Linder, *J. Phys. Chem.*, 1931, **35**, 531-535.
6. J. M. Stuckey and J. H. Saylor, *J. Am. Chem. Soc.*, 1940, **62**, 2922-2925.
7. K. S. Pitzer and D. W. Scott, *J. Am. Chem. Soc.*, 1943, **65**, 803-829.
8. A. G. Osborn and D. R. Douslin, *J. Chem. Eng. Data*, 1974, **19**, 114-117.
9. L. S. Kassel, *J. Am. Chem. Soc.*, 1936, **58**, 670-671.
10. E. R. Hopke and G. W. Sears, *J. Am. Chem. Soc.*, 1948, **70**, 3801-3803.
11. F. H. MacDougall and L. I. Smith, *J. Am. Chem. Soc.*, 1930, **52**, 1998-2001.
12. B. J. Mair and A. J. Streiff, *J. Res. Nat. Bur. Stand.*, 1941, **27**, 343-359.
13. J. E. Overberger, W. A. Steele and J. G. Aston, *J. Chem. Thermodyn.*, 1969, **1**, 535-542.
14. D. Ambrose, I. J. Lawrenson and C. H. S. Sprake, *J. Chem. Thermodyn.*, 1976, **8**, 503-504.

ERKLÄRUNG

Hiermit erkläre ich, dass ich diese Arbeit selbständig verfasst habe und keine anderen als die angegebenen Quellen und Hilfsmittel verwendet habe.

Ferner erkläre ich, dass ich nicht anderweitig mit oder ohne Erfolg versucht habe, eine Dissertation einzureichen oder mich einer Doktorprüfung zu unterziehen.

Bayreuth, den 8. Juni 2015

Paulo Cesar Alarcón García